NTNU – Trondheim
Norwegian University of
Science and Technology

Characterization and Thermal/Catalytic Upgrading of Kerogen in a Green River Oil Shale

Isaac Yeboah

Chemical Engineering
Submission date: June 2015
Supervisor: De Chen, IKP

Norwegian University of Science and Technology
Department of Chemical Engineering

NTNU

Norwegian University of Science and Technology

Faculty of Natural Science and Technology

Department of Chemical Engineering

A thesis submitted in partial fulfillment of the requirements for the award of MSc. Chemical Engineering

Characterization and Thermal/Catalytic Upgrading of Kerogen in a Green River Oil Shale

by

Isaac Yeboah

Under the kind tutelage of

Prof. De Chen & Dr. Xuezhi Duan

June 10, 2015

Abstract

Comprehensive structural characterization of oil shale (kerogen) and subsequent upgrading to fuels are of paramount scientific and industrial importance, calling for a better understanding. In this work, an oil shale from Green River formation was employed and characterized by multiple techniques such as Rock-Eval pyrolysis, TOC, XRD, FTIR and TGA-MS. It is found that the inorganic matter were mainly calcite, dolomite and Fe-doped quartz, while the organic matter consists of soluble bitumen and insoluble kerogen. The kerogen belongs to Type I, and locates in the oil window with excellent maturity. Subsequently CH_2Cl_2 was used as extractant to separate bitumen, and the as-extracted oil shale was treated with HCl to remove carbonates which might interfere with the subsequent analysis for the thermal upgrading of kerogen to fuel. The contents of bitumen and kerogen are 3.67% and 27.56%, respectively. TGA measurements showed that bitumen and kerogen have overlapping thermal behaviors, strongly indicating the necessity of bitumen pre-extraction. Thermally produced fuel yields of bitumen and kerogen are 96% and 79% respectively. The H/C ratios of bitumen and kerogen were aliphatic in nature and have a linear hydrocarbon pyrolyzates within the range of C_3-C_{35}. Furthermore, various catalysts such as mineral acids, in-situ formed metal oxides and metal chlorides were tested for the kerogen conversion. Among them, $CuCl_2 \circ 2H_2O$ is the most active. Its fuel produced is shifted towards diesel yield and slightly higher than bitumen diesel yield. Its apparent activation energy and pre-exponential factor are ca.78 kJ/mol and 3.6e+19 sec^{-1} respectively whereas those of un-catalyzed reaction of kerogen are ca. 98 kJ/mol and 1.4e+24 sec^{-1} respectively.

Keywords: Oil shale; Kerogen utilization; Characterization; Thermal upgrading; Catalytic upgrading; Fuels; Activation energy

Declaration

"I, Isaac Yeboah, hereby declare that this is an independent work according to the exam regulations of the Norwegian University of Science and Technology (NTNU)."

Student	**Signature**	**Date**
ISAAC YEBOAH	……..	……

Supervisor

Prof. DE CHEN	……	…….

Co-supervisor

Dr. XUEZHI DUAN	…….	……..

Acknowledgement

I express my heartfelt gratitude to Prof. De Chen, my supervisor for his meticulous supervision and counsel throughout my MSc thesis and studies. His dedication and warranted support has broadened my scope in this novel area of research.

Also, much thanks to Dr. Xuezhi Duan for his kind tutelage in guiding me to understand the entire project, the use of equipment as well as the writing and presentation for this thesis.

Abundance of gratitude and appreciation to Statoil for funding this project (VISTA); as well as Prof. Erling Rytter for his kind contributions and suggestions during the monthly presentation sections and entire Statoil collaborative staff.

I further express my appreciation to the Department of Chemical Engineering for the analytical facilities provided and especially Karin Dragster for organizing equipment training.

All what I can say is much thanks to you all and to whom much is given much is expected as I pledge to conform to standards to raise the bar in this novel area of energy research now and beyond.

Dedication

I dedicate this work to Miss Racheal Yaa Yeboah and the entire Yeboah family.

Table of Contents

Abstract i

Declaration ii

Acknowledgement iii

Dedication iv

Table of Contents v

List of Figures viii

List of Tables xii

Abbreviations xiii

Physical constants xiii

1. Introduction 1

1.1 Motivation 1

1.2 Utilization of kerogen as a future substitute energy source 2

1.3 Subsurface conversion of kerogen 3

1.4 Objectives 4

2. Literature Survey and Theory 6

2.1 Oil shale 6

2.1.1 Oil shale reserves 7

2.1.2 Shale oil production 9

2.1.4 Environmental issues with shale oil production 13

2.2 Kerogen 14

2.2.1 Kerogen origin and formation 14

2.2.2 Kerogen evolution 16

2.2.3 Kerogen types 17

2.2.4 Green River Formation kerogen model 19

2.2.5 Kerogen pyrolysis 20

2.2.6 Kerogen catalytic and/or hydro pyrolysis 21

2.3 Organic matter separation 22

2.3.1 Bitumen separation 22
2.3.2 Kerogen concentration via chemical methods 23
2.3.3 Kerogen storage 24
2.4 Characterization 24
2.4.1 Elemental analysis 25
2.4.2 Rock- Eval pyrolysis 25
2.4.3 X-ray diffraction (XRD) 26
2.4.4 SEM 27
2.4.5 FTIR 28
2.4.6 TGA-MS 28
2.4.7 Py-GC/MS 29
3. Material and Methods 31
3.1 Pretreatment/Comminution 31
3.2 TOC/Rock-Eval pyrolysis 32
3.3 Soxhlet extraction 32
3.4 Demineralization 33
3.5 Characterization 34
3.5.1 SEM 34
3.5.2 XRD 35
3.5.3 FTIR 35
3.5.4 Thermal behavior/ TGA-MS 36
3.6 Py-GC/MS 36
3.7 Catalyst preparation, screening and optimization. 36
4. Results and Discussion 37
4.1 Petroleum generating potential of Green River oil shale 37
4.1.1 TOC/Rock-Eval pyrolysis 37
4.2 Characterization of model oil shale 39
4.2.1 Elemental analysis 39

4.2.2 Physico-chemical properties of model oil shale 40
4.3 Separation and Characterization of Organic Matters in Oil Shale 43
4.3.1 Bitumen 43
4.3.2 Decarbonated kerogen characterization 46
4.3.3 Energy release and weight loss profile of organic matters in oil shale 49
4.3.4 Deconvolution /$NaHCO_3$ decomposition 53
4.3.5 H/C ratio of bitumen and decarbonated-kerogen 53
4.4 Thermal upgrading of bitumen and kerogen to fuels (TGA/DSC) 55
4.4.1 Pyrolysis-GC/MS of bitumen and kerogen 57
4.5 Catalytic thermal upgrading of kerogen 64
4.5.1 Active phase identification 64
4.5.2 Optimization 72
4.5.3 Synergistic effect 76
4.6 Fuel produced from 5 wt % Cu^{2+} catalysts 79
4.7 Kinetic parameters 81
4.8 Design of fixed bed reactor 90
5. Conclusions 92
6. Perspectives 94
References 95
Appendix 99
A) XRD pattern for oil shale 99
B) XRD pattern for HCl treated sample 99
C) Calculation of HCl concentration used in decarbonate experiment 99
D) Calculation of catalyst loading 100

List of Figures

Figure 1 Petroleum source rock (oil shale)[18] 6
Figure 2 Countries with Oil Shale Resource in the world [23, 24] 7
Figure 3 Location of the Green River Formation Oil Shale and its Main Basins, adopted from Smith, 1980. 8
Figure 4 Oil Shale production approaches adopted from USA DOE, 2004 9
Figure 5 Enefit 280 retort process flow diagram,1-oil shale cyclone, 2-heat carrier cyclone, 3-dust chamber cyclone, 4-ash recycle cyclone, ESP-electrostatic precipitator, BFW-boiler feed water, CFB-circulating fluidized bed [4] 10
Figure 6 Major process steps in mining and surface retorting [27] 11
Figure 7 Shell process of extracting crude oil from oil shale [29] 12
Figure 8 Chevron's technology for in situ conversion of oil shale [30] 13
Figure 9 Comparison of amounts of dispersed kerogen and ultimate resources of fossil fuels, adapted from Durand (1980). 14
Figure 10 General scheme of evolution of the organic matter from the freshly deposited sediment to the metamorphic zone. CH: carbohydrates, AA: amino acids, FA: fulvic acids, HA: humic acids, L: lipids, HC: hydrocarbons N, S,O: N,S,O (non-hydrocarbons) [10] 16
Figure 11 Thermal maturation of kerogen and oil window formation [24] 17
Figure 12 Kerogen maturation and types [42] 18
Figure 13 2D (left) and 3D (Right) Siskin model of Green River oil shale C, gray; O, red; N, blue; S, yellow; H, white [42] 20
Figure 14 TGA curves for the Huadian oil shale [52] 22
Figure 15 Soxhlet extractor model from Royal society of chemistry world/issues/2007 23
Figure 16 Schematic diagram of Rock Eval pyrolysis[59] 26
Figure 17 Schematic view of the principles of SEM operations[61] 27
Figure 18 Schematic view of TGA[63] 29
Figure 19 Py-GC/MS instrument schematic view[64] 29
Figure 20 Oil shale samples from Green River Formation, USA. 31
Figure 21 Laboratory disk milling machine 32
Figure 22 Soxhlet extraction set-up 33
Figure 23 Decarbonation setup 34
Figure 24 Proposed experimental steps for decarbonated-kerogen isolation 34
Figure 25 SEM image of the milled oil shale sample 35
Figure 26 EDS spectrum of fine oil shale 40

Figure 27 XRD pattern (left) and FTIR spectrum (right) of milled oil shale. Note: ▲, dolomite ($Ca_{1.17}Mg_{0.83}$ $(CO_3)_2$, PDF 04-011-9829); ∆, calcite (CaCO3, PDF 04-012-0489); ■, analcime ($Na8Al8Si16O48{\cdot}(H_2O)_8$, PDF 04-011-6233); □,Fe-doped quartz (SiO2,PDF 04-007-0522) 41
Figure 28 TGA/DSC curves of fine oil shale in air (A) and Ar (B) atmosphere at a ramping rate of 10 ^oC/min. 42
Figure 29 Nitrogen BET for surface area (left) and pore diameter (right) of the milled oil shale sample 43
Figure 30 TGA/DSC-MS profiles of bitumen in air atmosphere at 10 ^oC/min 44
Figure 31 FTIR (left) and Raman (right) spectra of bitumen 45
Figure 32 XRD spectra (A) of raw oil shale (red, up curve) and decarbonated oil shale (black, down curve). 46
Figure 33 FTIR spectra of raw oil shale (red, up curve) and decarbonated oil shale (blue, down curve (A=CH_2:2930 and 2850, B=CH_3:2960 and 2870 stretching vibration, C=O: 1697, D= O-Si-O (quartz), 775-800 symmetric stretching vibration and E=745 Carbonates) 47
Figure 34 Compared FTIR analysis of the organic matters in an oil shale (A=CH_2:2930 and 2850, B=CH_3:2960 and 2870 stretching vibration, C=O: 1697, D= O-Si-O (quartz), 775-800 symmetric stretching vibration and E=Carbonates 48
Figure 35 TGA/DSC curves of extracted oil shale (red) and decarbonated oil shale (blue) in air atmosphere at a ramping rate of 10 ^oC/min. 49
Figure 36 Comparative TGA profiles of the organic matters in oil shale: air atmosphere at a ramp rate of 10 ^oC/min 50
Figure 37 DSC curve of the compared organic matters in oil shale under air atmosphere, 10 ^oC/min. 52
Figure 38 TGA/DSC-MS for pure $NaHCO_3$ used as standard for deconvolution analysis at air atm., heating rate 10 ^oC/min 53
Figure 39 TGA-MS peak for bitumen and kerogen in air atm., heating rate 10 ^oC/min 54
Figure 40 TGA- pyrolysis of bitumen (left) and decarbonated-kerogen (right) in Air and Ar atm. 10 ^oC/min to show fuel yield. 56
Figure 41 EGA-MS results of decarbonated oil shale. 58
Figure 42 Two-dimensional-display of EGA thermograms obtained by F-Search. It is shown that the EGA TIC peak consists of major hydrocarbon fragment ions (m/z = 41, 43, 55, 57, 69 and 71) and some characteristic fragment ions (m/z=91, 119, 121, and 191). 58
Figure 43 Product distribution of extracted bitumen 59
Figure 44 Typical structure of C_{17} and C_{28} and their characteristics fragments ions 60
Figure 45 Fuel produced from the pyrolyzates of bitumen from Py-GC/MS at 20 ^oC/ min for 550 ^oC in Helium atm. 60

Figure 46 Pyrograme of decarbonated oil shale at 550 ^{o}C 61
Figure 47 Magnified pyrograms of Figure 44 62
Figure 48 Peak area fraction (up chat), fuel yield (down chat) of kerogen pyrolyzates: Py-GC/MS at 20 ^{o}C/ min for 550 ^{o}C in Helium atm : the gasoline(C_4-C_{12}), Jet A(C_8-C_{18}), diesel(C_8-C_{24}) 63
Figure 49 TGA/DSC curve for Phosphoric acid catalyzed decarbonated-kerogen sample: ar atm. 10 ^{o}C/min 65
Figure 50 TGA/DSC curve for sulphuric acid catalyzed decarbonated-kerogen sample: ar atm. 10 ^{o}C/min 66
Figure 51 TGA/DSC curve for cobalt oxide (CoO) catalyzed decarbonated-kerogen sample: ar atm. 10 ^{o}C/min 67
Figure 52 TGA/DSC curve for Nickel (IV) oxide catalyzed decarbonated-kerogen sample: ar atm. 10 ^{o}C/min 69
Figure 53 TGA/DSC curve for Tetralin catalyzed decarbonated-kerogen sample: ar atm. 10 ^{o}C/min. 69
Figure 54 TGA curve for metal chlorides catalyzed decarbonated-kerogen sample 70
Figure 55 DSC curve for metal chlorides catalyzed decarbonated-kerogen sample, (A= point of crystalline water decomposition) 72
Figure 56 TGA/DSC curve for potassium chloride (KCl) catalyzed decarbonated-kerogen sample ... 72
Figure 57 TGA/DSC profile for optimization of $CuCl_2 \circ 2H_2O$ catalyzed pyrolysis of kerogen 73
Figure 58 EGA pyrograms of the lowest Cu^{2+} catalyst loading 74
Figure 59 Optimized loading of 5 wt% Cu^{2+}: Ar atm. 25^{o}C/min 75
Figure 60 (TGA profile) effects of variable ramping rate on selected catalyst: 10 ^{o}C/min in Ar atmosphere for sample 76
Figure 61 Synergistic effects from H_2SO_4 and Cu^{2+} catalyst: TGA profile at 10 ^{o}C/min in Ar atmosphere 77
Figure 62 Synergistic effects from H_3PO_4 and Cu^{2+} catalyst: TGA profile at 10 ^{o}C/min in Ar atmosphere 78
Figure 63 Synergistic effects from tetralin and Cu^{2+} catalyst: TGA profile at 10 ^{o}C/min in Ar atmosphere 79
Figure 64 Fuel products from Cu^{2+} catalyst impregnated on Kerogen sample: Py-GC/MS 10 ^{o}C/min in Helium atmosphere 80
Figure 65 Compared fuel products [(gasoline (C_4-C_{12}), jet A (C_8-C_{18}), diesel (C_8-C_{24})] produced from the Cu^{2+} catalyst + kerogen sample: Py-GC/MS 20 ^{o}C/min in Helium atmosphere 81
Figure 66 Arrhenius plot for original oil shale pyrolysis at 10^{o}C/min with its corresponding linear regression data plot: temperature range (250 -500 ^{o}C) 83
Figure 67 TGA for decarbonated-kerogen pyrolysis at different heating rates 84

Figure 68 Arrhenius plot for decarbonated-kerogen pyrolysis at different heating rate with their corresponding linear regression plot: temperature range 250-380 ^{o}C/min..... 85
Figure 69 TGA for kerogen pyrolysis at same heating rates (10 ^{o}C/min) for Cu^{2+} catalyst and un-catalyst kerogen sample 87
Figure 70 Arrhenius plot for catalytic-kerogen and bitumen pyrolysis at10 ^{o}C/min: temperature range (290-350^{o}C)..... 88
Figure 71 Proposed reactor scheme for fixed bed reactor for catalytic pyrolysis of kerogen..... 91

List of Tables

Table 1 Simplified petrographic classification of kerogen constituents after (Robert, 1979; Alpern, 1980) 15
Table 2 Types of kerogen and their depositional environment[43] 18
Table 3 FTIR peak assignment adopted from Robin et al., [10, 25] 28
Table 4 Rock-Eval pyrolysis data of fine oil shale HC# (hydrocarbon). 38
Table 5 Petroleum potential (quantity) of an immature source rock (Peters and Cassa, 1994) (TOC =total organic carbon, S1=volatized existing hydrocarbon, S2=kerogen decomposition) [48] 38
Table 6 Mass percentages of elements in raw oil shale. 40
Table 7 Bitumen contents in the oil shale from three experiments 43
Table 8 Summary of relative weight loss profile of organic matters TGA,MTO (moderate temperature oxidation, HTO (high temperature oxidation): air atmosphere at a ramp rate of 10 ^{o}C/min 51
Table 9 H/C ratio of bitumen and decarbonated-kerogen from Deconvolution analysis after MS peak splitting 54
Table 10 Percentage of fuel produced by thermal process within the temperature range of 200-550 ^{o}C 56
Table 11 Kinetic parameters (apparent E_a and A) for pyrolysis of kerogen at various heating rates using direct Arrhenius plot method: temperature range (250- 380^{o}C) 86
Table 12 Kinetic parameters (apparent E_a and A) for 5 wt % Cu^{2+} catalytic pyrolysis of kerogen at 10 ^{o}C/min using direct Arrhenius plot method: temperature range (290-350^{o}C) 89
Table 13 Results of standard error of estimate for the kinetic method 90

Abbreviations

OPEC	Organization of Petroleum Exporting Countries
PY-GC/MS	Pyrolysis- Gas Chromatography -Mass Spectrometer
TGA/DSC	Thermal Gravimetric Analysis/ Differential Scanning Calorimetry
XRD	X-Ray Diffraction
ATR-FTIR	Attenuated Total Reflection Fourier -transform infrared
DCM	Dichloromethane
ICP	Inductively Coupled Plasma

Physical constants

$\rho_{HCl} = density\ of\ HCl = 1.19 g/cm\text{^}3$

$\%purity\ HCl = 37\%$

1. Introduction

1.1 Motivation

Global energy demand in 2030 has been projected to be 36% higher than the current trend and emerging economies (China and India etc.) will contribute mostly to the growth [1] as they contributed for ca. 80% of the global increase in energy consumption in 2013[1]. Sustainability and security of supply in energy production depends hugely on efficiency in manufacturing of goods and services in these highly manufacturing countries. The high energy consumption in the world is predominately caused by increase in human population, urbanization and industrialization, and their associated needs such as electricity and transport fuel. The global increased in oil demand was seen in 2014 with world consumption of about 600,000 barrels per day oil in third quarter [1].

This energy demand has become a major challenge of our time since it has outpaced the discovery of conventional fossil fuel sources [1]. The proposed reserves for conventional sources in the world is about 1.490 trillion barrels of crude as of 2013 with 81% from the OPEC countries[2, 3] however 66% of the OPEC reserves are located in the Middle East[2]. The OPEC reserves geopolitical influence has many implications on other smaller countries that do not belong to OPEC for accessibility of energy. In 2014, a record reduction in oil prices has been observed[1]. The reduction has its own geopolitical factors, but contribution from unconventional US shale oil and gas is a factor that cannot be underestimated. This has called for recent attention into alternative unconventional resource that is evenly distributed around the world and among them is kerogen (oil shale).

Other unconventional hydrocarbon sources are shale gas/oil, tight oil, heavy oil, coal bed methane, methane hydrate biomass. They are widely distributed all over the world and in most especially oil shale is found in almost all continents in the globe [4]. Shale gas and/or oil produced from fracking have increasingly transformed the energy balance in the world especially in the USA. US Shale development is capable of providing the global net growth in oil supply to 2020, and over 70% of its growth to 2030 and thus USA will be 99% independent in net energy[5]. Hence there is a need, to explore other unconventional alternative sources of crude oil such as kerogen (oil shale).

The hydrocarbon product from oil shale (kerogen) can be easily upgraded to transport fuel as it fits into existing refinery configurations. Among the various sources and applications of energy, the aspect of transportation fuel has raised ultimate concern in recent times. At present, about 80% of the world's demand for transportation fuels; road, rail, air and sea are products from fossil fuel[6]. The inflow of shale gas and oil as a fuel for the transport sector is influencing the energy dynamics of this sector due to the relatively cheap price of this fuel. The fuel from oil shale is still one of the viable alternatives for the current transport fuel challenge although Bartis et al. proposed $70-95 per barrel as the cost of fuel from oil shale surface retort processing in large scale from detailed 2005 cost estimates[7]. However, the current trend of fuel prices of around $60.32 per barrel for Brent crude[8] has called for further and better research for an energy efficient process for oil shale development.

1.2 Utilization of kerogen as a future substitute energy source

Oil shale contains organic matter that is dispersed in a sedimentary rock. The rock is made up of predominantly inorganic/mineral component such as calcite, dolomite, quartz[9] etc. while the organic matter is made up of bitumen and kerogen. Oil shale is unconventional reserves not to be confused with shale oil and contains hydrocarbon called kerogen that is immature organic matter in the transition from biomass to conventional oil and gas. Petroleum geochemists described kerogen as the main source of petroleum compounds and its derivatives[10]. Kerogen is found in many countries and has raised recent attention as a supplement to conventional sources of fossil fuel[10]. With gradual depletion of conventional petroleum sources (fossil) and increase in oil consumption, there is a focus on the usage of oil shale as a future alternative energy source for the transport sector.

Kerogen is an insoluble, complex carbonaceous macromolecular organic matter (OM) spread in sedimentary rocks that has undergone severe cementation and compaction. The kerogen can be produced as a crude-like liquid, i.e. shale oil and natural gas, when the rock (oil shale) is heated to elevated temperatures and kerogen thus is converted through the chemical process of pyrolysis. When kerogen resides in shale, the whole material is often referred to as oil shale[11]. The most abundant form of organic matter (OM) on earth[12] is kerogen. Kerogen has high hydrogen-to-carbon ratio that makes it potentially superior to heavy oil, biomass and coal as a source for liquid fuel[13].

Production of shale oil (fuel) from the organic matter (kerogen and bitumen) in oil shale requires a considerable amount of heats, and therefore a challenge to energy-efficiency. The

shale has low permeability and porosity as well as poor conductivity[14] and hence makes heat transfer challenging. The major techniques applied in production of shale oil are in situ and ex-situ pyrolysis. The ex-situ process has issues with high energy-intensive operations as high temperature retorting of ca. 500 ^{o}C is often applied. The material-handling involved in the mining of oil shale, transportation to a central processing unit and retorting as well as spent rock disposal is also a challenge[15]. In addition, the oil shale ex-situ process also enforces severe environmental constraints as the kerogen contains significant amounts of sulfur and nitrogen[16]. Other encounters are water contamination as well as post production costs and land reclamation [14] However, as in the case with extra heavy oil such as oil sands, there is an option for in situ pyrolysis of oil shale. Using in situ conversion processes at pilot scale, Shell (ICP), Electrofrac^{TM}, Chevron's technology and Occidental Modified in-situ (MIS) have produced a good quality, middle-distillate refinery feedstock that requires little or no further upgrading[14, 17]. This fuel produced from the subsurface process has made the process more viable alternative to the surface process as the later has a lot of environmental challenges.

1.3 Subsurface conversion of kerogen

The process occurs underground without mining the oil shale. In this technology, wells are drilled, and the oil shale reservoir is slowly heated to about 200-350 °C, at which point kerogen is converted to oil and gas on a time scale of months to years. Development of in situ conversion is in progress and has caught the industry's attention. Since in situ conversion technologies are just emerging, it is not obvious which specific technologies can promote state of the art over the coming years. The main challenge is to increase energy efficiency of the process, with enhanced reaction at temperatures as low as possible. Another task is to control the product quality. An issue is to stabilize the product towards polymerization and gum formation. Among the explored in situ processes the common trait is high temperatures. Both Shell (ICP) and Electrofrac^{TM} used electricity to heat the surrounding shale deposit combined with long production times. Shell (ICP) used almost 2 to 3 years to produce crude oil for subsequent upgrading. Chevron's used heated and pressurized CO_2 to heat the oil shale underground. This requires significant amount of water and is environmentally less benign[14]. These and many other challenges such as product selectivity and long residence times of the reaction have called for research into catalytic subsurface conversion of organic matters (kerogen) in the oil shale. Catalytic thermal (pyrolysis) upgrading of kerogen appears to be in a formidable position to arrest these challenges in the in-situ (subsurface) conversion.

Therefore, a fundamental understanding of the reactions involved in in situ conversion (subsurface) of kerogen is highly desired to develop this novel technology and as such a better understanding of the physico-chemical features of the oil shale is required for its subsequent upgrading.

The main goal of this thesis is to gain better understanding of the fuel potential of the source rock (oil shale) and chemistry of depolymerization of separated bitumen from oil shale, HCl treatment of oil shale to give decarbonated-kerogen as well as bitumen and kerogen characterization and thermal upgrading. The **decarbonated-kerogen** is a notation for **bitumen and carbonates freed oil shale,** would be subsequently subject to several catalysts testing under thermal conditions. The catalytic effects of mineral acids, transitional metal oxides and chlorides salts on kerogen conversion would be investigated. In summary, the thesis covers characterization of oil shale, separated bitumen, decarbonated-kerogen and thermal and catalytic upgrading of organic matters to fuels. Also, highlighted are the influence of catalyst loading, variable ramping rate and pre-conditioning of decarbonated-kerogen under acidic and reducing agents to promote kerogen decomposition to fuel. The product distribution of the catalytic and/or decarbonated-kerogen and bitumen will be studied from the Green River formation oil shale. Furthermore, kinetic modeling such as activation energy (E_a) and pre exponential factor (A) for kerogen pyrolysis would be determined.

1.4 Objectives

Our main objectives are to gain insights into physico-chemical properties of organic matters in oil shale and thermal and or catalytic upgrading of kerogen to fuels. In other words, our objectives are to

- characterize oil shale, with Rock-Eval pyrolysis, TOC, XRD, FTIR, Raman, TGA-MS etc and separate bitumen from oil shale and perform HCl treatment to produce decarbonated-kerogen
- study the thermal behavior of bitumen and decarbonated-kerogen with TGA-MS, EGA and Py-GC/MS
- screen and select catalyst(s) for kerogen upgrading to fuel by the use of TGA-MS and EGA
- optimize the selected catalyst(s) for the kerogen upgrading by the use of TGA-DSC and EGA
- quantify the product distribution for catalytic upgrading of kerogen using Py-GC/MS

- determine activation energy and pre-exponential factor for catalyzed and un-catalyzed kerogen pyrolysis

2. Literature Survey and Theory

2.1 Oil shale

The name oil shale is a deceptive term since it contains no liquefied matured oil. In a stern geological point of view may not always be a shale rock but consists of sedimentary rock and organic rich matters[11]. It is a low porous and less permeable rock made up of mineral matrix, soluble-bitumen and insoluble kerogen. Oil shale lies halfway between crude oil and coal or very heavy oil in terms of hydrogen-to-carbon ratio, it has higher hydrogen content and thus makes it more attractive as precursor for fuel than coal, biomass or heavy oil[13]. **Figure 1** is a pictorial view of petroleum source rock which contains organic matters and mineral matrix. The source rock with Total Organic Carbons (TOC) of ca. 4-20 wt% matures to petroleum within ca. 30 ^{o}C/km geothermal gradient. As the temperature and pressure increases in anoxic conditions and at about 60 ^{o}C oil and gas begins to form. Kerogen (oil shale) is a biomass in transition to oil and gas generation that needs longer geothermal time to mature. Kerogen matures to oil at an oil window of 60-120 ^{o}C[12] at which the oil expel from the source rock into the reservoir rock.

Figure 1 Petroleum source rock (oil shale)[18]

Oil shale deposits were formed in many years ago by the co-sedimentation of silt or sand and organic debris, followed by compression, compaction, cementation and heating[19]. Cunningham-Craig defined an oil shale as an algae shale resource from which hydrocarbons can be produced only by thermal process and not by solvents treatments [20]. This illustrates

the fact that oil shale contains organic matter (kerogen) which is a precursor to crude oil and only produced by thermal methods (pyrolysis).

Frequently, the terms shale oil and tight oil are used interchangeably in public dialogue, shale formations are only a subgroup of all low permeable tight formations, which includes sand stones, carbonates and shale. Sand stones and carbonates are conventional sources while oil shale is unconventional source of tight oil production. In the United States, tight oil production is preferred terminology for the oil and natural gas industry rather than shale oil production; because with respect to the geologic formations, it is a more incorporating and accurate term for producing oil in such source rocks. Energy Information Administration (EIA), USA adopted this convention, and develops estimates of tight oil production and resources in the United States that include, but are not limited to, production from shale formations [21] but is however, not clear if oil shale fits into this category.

2.1.1 Oil shale reserves

The known reserves of oil shale in the world are found in every continent with the largest quantities found in the North America. In terms of oil generating potential oil shale amount is very large, leading to its outpacing the amount of crude oil in the world [22, 23].

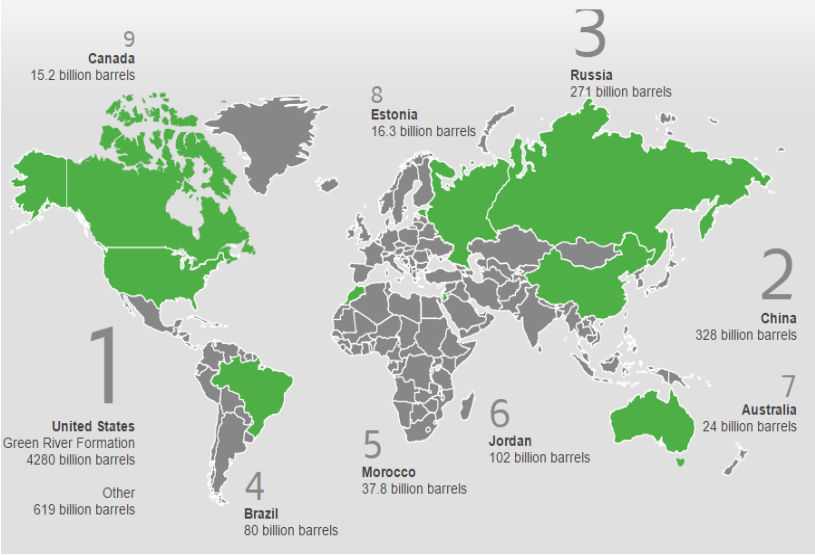

Figure 2 Countries with Oil Shale Resource in the world [23, 24]

Figure 2 illustrates the oil shale resource in the World and the wide spread nature of the resource in global energy pool is seen. Significant deposits of oil shale are located in about 600 different places in more than 30 countries. Among them are western USA, China, Russia, Brazil, Queensland (Australia), Morocco and Estonia, with smaller quantities in many other

countries as showed in **Figure 2**. Oil shale is a widely distributed resource and unlike conventional resource which more than 81.3% (1193 billion barrels) is located in OPEC countries. The recoverable barrels of oil from oil shale reserve are targeted as ca. 2.8-3.3 trillion. This quantity is three times greater than the conventional crude oil reserves (1.2 trillion barrels oil) in the world[23]**.** The distribution of oil shale resource in the world is far and wide and thus makes an oil shale an attractive source of fuel in terms of location preference and oil geopolitical factors.

USA has the world's largest deposit of oil shale, found in Green River formation. It has the largest technically recoverably hydrocarbon generation in the World of ca. 72% and the greatest portion of US resource is held in this chamber[23].

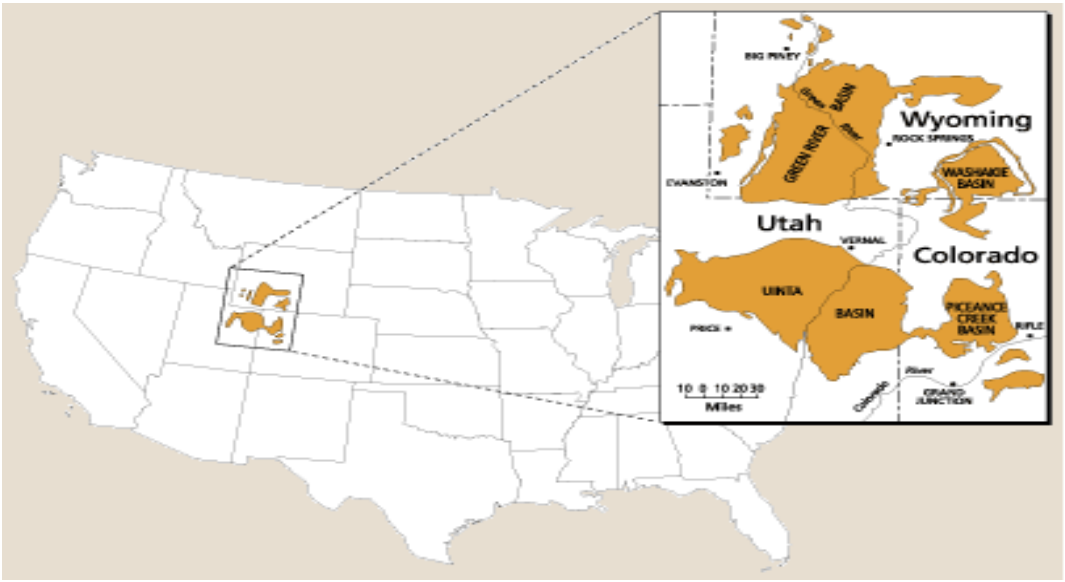

Figure 3 Location of the Green River Formation Oil Shale and its Main Basins, adopted from Smith, 1980.

Figure 3 describes the Green River formation found in Colorado, Utah and Wyoming. The main constituents of green river oil shale are tertiary evaporates, kerogen-rich marls, silicates and carbonates[24]. The organic rich matters in oil shale are bitumen and kerogen which are potential precursors to crude oil. Durand, (1980) studied the overall resources of fossil fuels and compared with the amount of dispersed kerogen in oil shale and concluded that the total kerogen is 10^{16} tons more than oil and gas[25]. It has been determined that one-fifth of the world oil shale resource is technically and economically recoverable and per ton of shale processed about 25 gallons of oil may be recovered on average[26]. Obviously, oil shale is

geographically widespread and a major resource of world petroleum[16] and thus a need to develop a technology to promote its recovery.

2.1.2 Shale oil production

The economic growth of certain countries reached its ultimate between 1930 and the late 1940s from oil shale industry and notable among them is Estonia where direct combustion of oil shale was used to produce electricity. In the 1955-65 a tauter competition from crude oil made oil shale industry unfavorable and most production stopped [20]. However, in spite of the drop in oil prices, Enefit in Estonia produced a record amount of 1.7 million barrels of shale oil in last quarter of 2014 from oil shale. The company paid $102 million of dividend to its owners i.e. the Republic of Estonia with an overall output increase of 24% of 2013 [24]. This growth supports the point that oil shale is economically viable venture and thus a need to develop environmentally safes methods for its processing.

The production of fuel (shale oil) from oil shale needs higher energy and has many environment issues and thus calling for an efficient and dependable technology for the process. **Figure 4** explains the two routes to produce crude oil from oil shale; ex-situ (surface process) and in-situ (subsurface) methods.

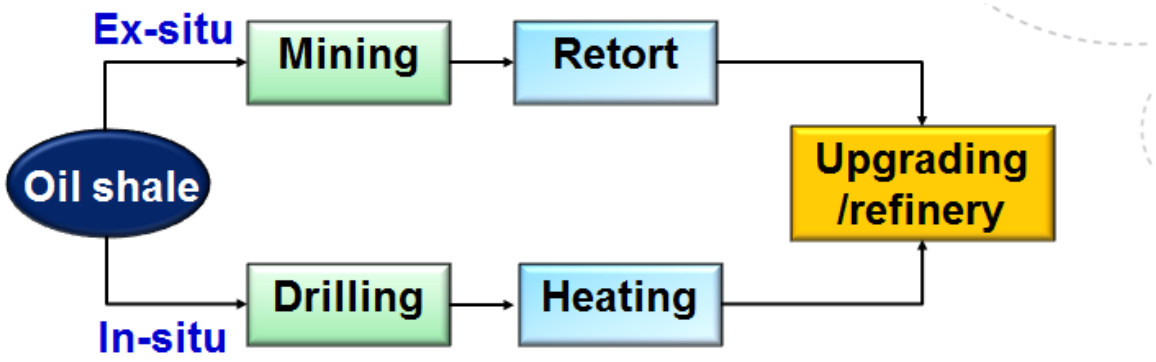

Figure 4 Oil Shale production approaches adopted from USA DOE, 2004

The Enefit 280 project in Estonia applies the ex-situ process in an energy efficient circulating fluidized bed retort chamber as described in **Figure 5**.

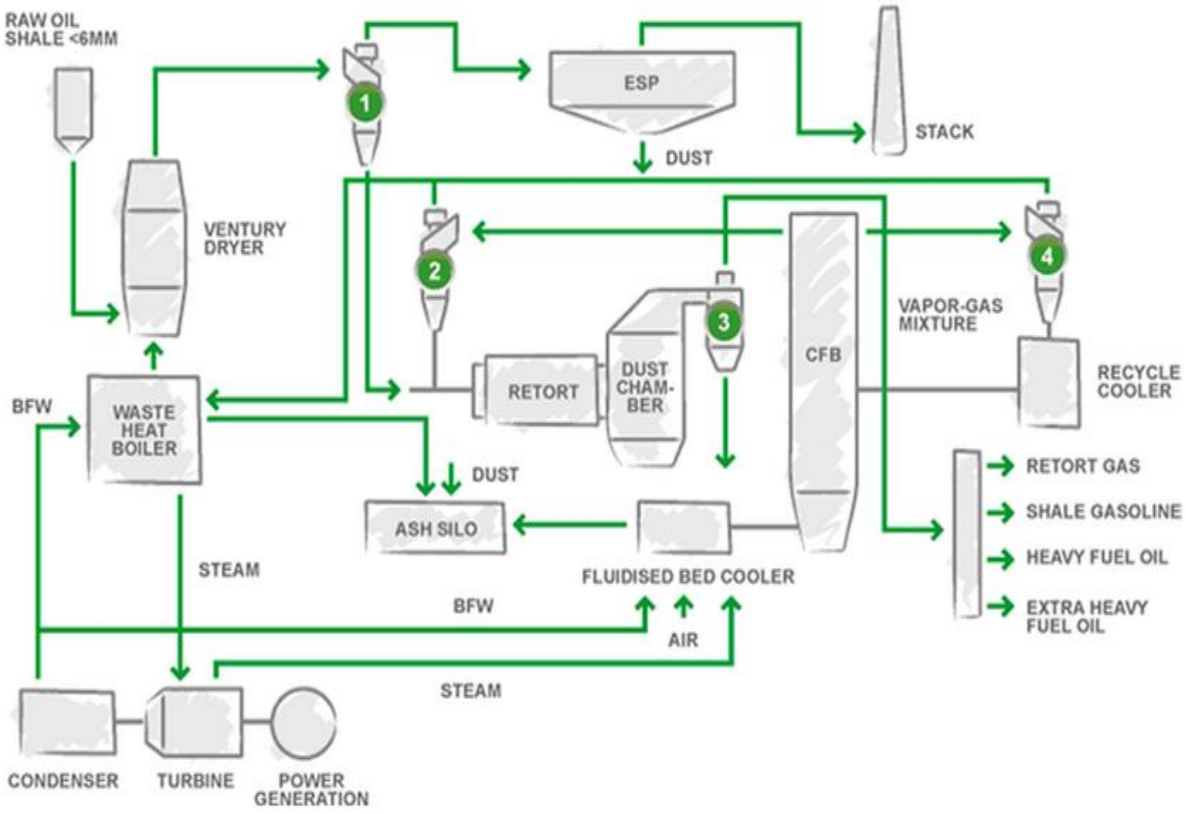

Figure 5 Enefit 280 retort process flow diagram,1-oil shale cyclone, 2-heat carrier cyclone, 3-dust chamber cyclone, 4-ash recycle cyclone, ESP-electrostatic precipitator, BFW-boiler feed water, CFB-circulating fluidized bed[4]

The ***ex-situ process*** includes mining (surface or underground) of oil shale, crushing to a particle size to increase the surface area. The crush rock is decomposed by heat treatment in a surface retorting process. In this, a commonly applied heat treatment method is ***horizontal retort***; the crushed oil shale, larger particle size, is decomposing to free the kerogen and bitumen in the oil shale. In addition to the oil, combustible gas is released and the residual shale ash contains carbonaceous coke or char. These by-products are progressively burnt to assist in heating of the retort. An alternative process is to crush the oil shale to a small size and heat the shale in a ***fluidized bed as applied in circulating fluidized bed retort for the Enefit 280***. The particle size of the raw oil shale is less than 6 millimeters [4, 16]. The ex-situ process has issues with land reclamation, water usage and pollution to the environment as seen in **Figure 6**.

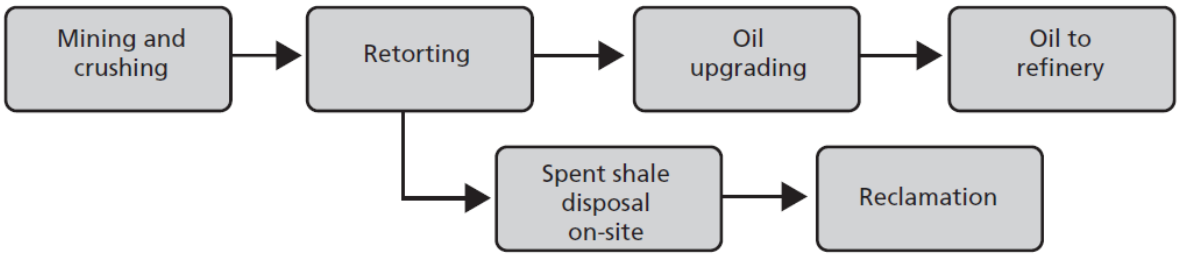

Figure 6 Major process steps in mining and surface retorting [27]

The mining of the oil shale leads to heavy destruction of land, water table and cost associated with water treatment and overburden rock disposal. Also, the topography needs to be restored and thus land reclamation cost is undeniable. This and many other issues have called for an alternate technology.

In situ pyrolysis as applied in oil sand is a possible method for an underground processing of oil shale without mining the oil shale. In this process, wells are drilled and the oil shale (kerogen) is heated in the subsurface. The decomposed kerogen and bitumen is liquefied and pumped back to the surface using the tradition oil recovery process. Several companies such as Shell (ICP), ElectrofracTM, Chevron's technology and Occidental Modified in-situ (MIS) investigated this process using different heating method at the subsurface [26]. Also, Total in 2008 oil shale symposium in Colorado presented a new technology called the geothermal fuel cell design in a pilot scale which has a self-heating system The efficiency of the process was 90% and applies preheating mode as well as the use of surface gas reforming and electricity production as a byproduct[28]. For medium scale production, Shell in Colorado USA, in 2005, produced middle distillate fuel without further upgrading from underground heating of oil shale and called the process as In-situ Conversion Process (ICP) seen in **Figure 7**. It uses a subsurface heater that slowly heats the oil shale to 350-400 ^{o}C. The kerogen oil and gas are released from the shale and captured at the surface by pumps. This ICP has preferably positive impact to the environment as compared with the traditional retorting process. As seen in the figure below a freeze wall of ammonia was applied in the heating zone to prevent the leakage of oil and gas into the water bodies [26].

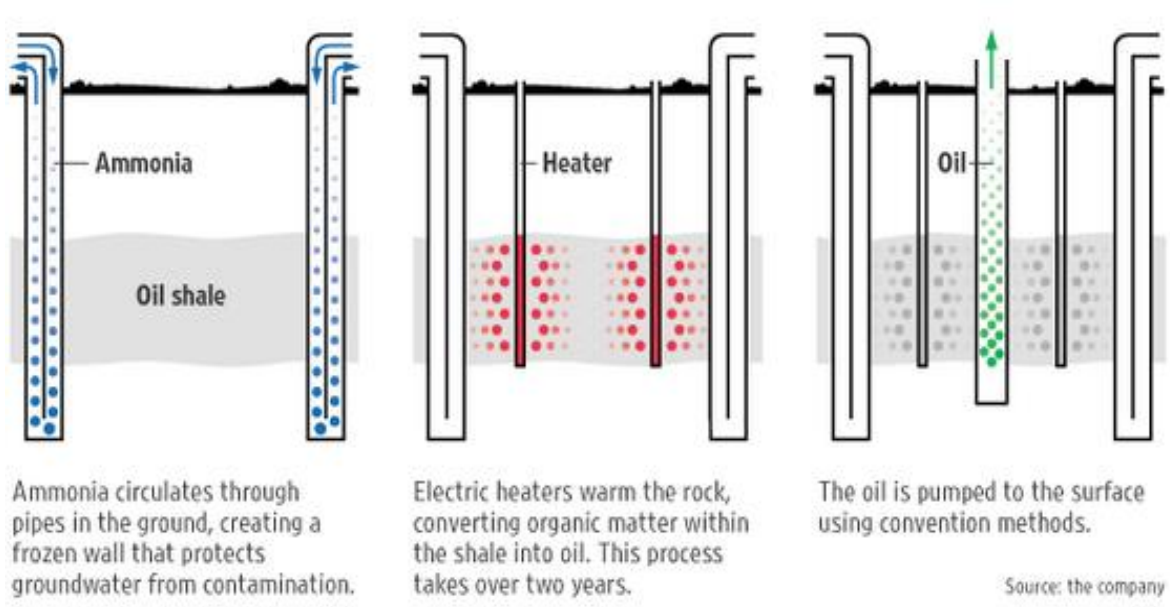

Figure 7 Shell process of extracting crude oil from oil shale [29]

This process involves no open pit or subsurface mining, does not produce tons of shale waste as applied to the surface retorting and avoids ground water contaminations via ammonia freeze wall between oil shale and underground water resources. However, it takes such a long time of two to three years and hence the need to speed the thermal reaction[16].

Figure 8 shows the schematic view of the Chevron's technology which used heated and pressurized carbon dioxide to heat the kerogen in the oil shale at the subsurface. The process captures and re-uses combustion gases and thus has an advantage of preventing greenhouse gas emissions. It uses conventional drilling and fracturing techniques at subsurface formation and as such makes the cost equivalent to any drilling for oil. The viability of the process depends on the cost of fracturing oil shale to produce economic quantities of oil shale through decomposing kerogen at its right temperatures[30]. These processes have no control on product selectivity and stability against gum formation as well as high decomposition temperature and thus the need for catalyst.

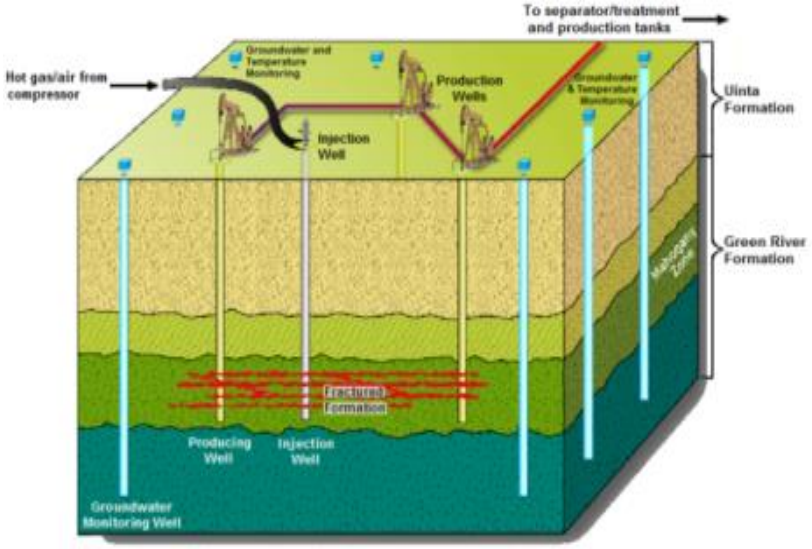

Figure 8 Chevron's technology for in situ conversion of oil shale [30]

2.1.4 Environmental issues with shale oil production

Oil shale usage has severe environmental constraints. The shale often made up of significant amounts of sulfur and nitrogen. Hydrogen sulfide and sulfur dioxide are one of the causal agents for acid rain, is produced through the release of elemental sulfur from the oil shale[31]. Ammonia, a greenhouse gases is produced from the elemental nitrogen found in oil shale. These gases must be sequestered to avoid polluting the atmosphere. In addition, toxic carcinogenic polycyclic aromatic, heavy metal impurities and hydrocarbons are also found in the waste from oil shale processing most significantly from surface retorting[11]. This may leach into surface and ground water if not contained in standard tailing (waste) dams. Also, the in-situ process has a potential for aquifer contamination if not well engineered as in ammonia freeze technology applied by Shell in 2005. Similarly, large amount of water is required for the processing of the shale, for every barrel of oil produced from oil shale 5 barrels of water is required[15] thus impose significant burden to water bodies. Although water usage depends on the technology applied for the shale oil production but research has showed that significant amount of water is required. Furthermore, processed water contamination is factor that could lead to high cost on water treatment plants. Oil shale mining requires material handling that includes the transportation of the mined oil shale to the dedicated processing Unit as well as disposal of spent shale rock as applied in ex-situ process. This process requires the use of heavy duty vehicles leading to high amount of CO_2 release into

the atmosphere. The mining of the rock may also disturb the natural topography and seismic pattern which could contribute to other natural disasters[16]. In-situ process is still in developing stage and refined environmental impact assessment is needed to prove its environmental sustainability.

2.2 Kerogen

The major resource to unlock the global transport energy demand is kerogen: organic matter lock in oil shale, a precursor to crude oil, which is formed from biomass in transition to conventional fossil fuel. Kerogen is the solid organic matter (OM) which generates petroleum and natural gas when heated. It is dispersed in the oil shale (sedimentary rock) and insoluble to organic solvents. Kerogen represent the largest organic matter (OM) pool on Earth in the range of ca. 10^{16} tons of carbon compared to ca. 10^{12} tons in living biomass and the major sink in the global carbon cycle [13]. This dispersed insoluble material accounts for the largest portion of the oil and gas pool from the sedimentary OM as well as other forms of organic matter such as coal, oil and asphalts as seen in **Figure 9**, Durand, (1980).

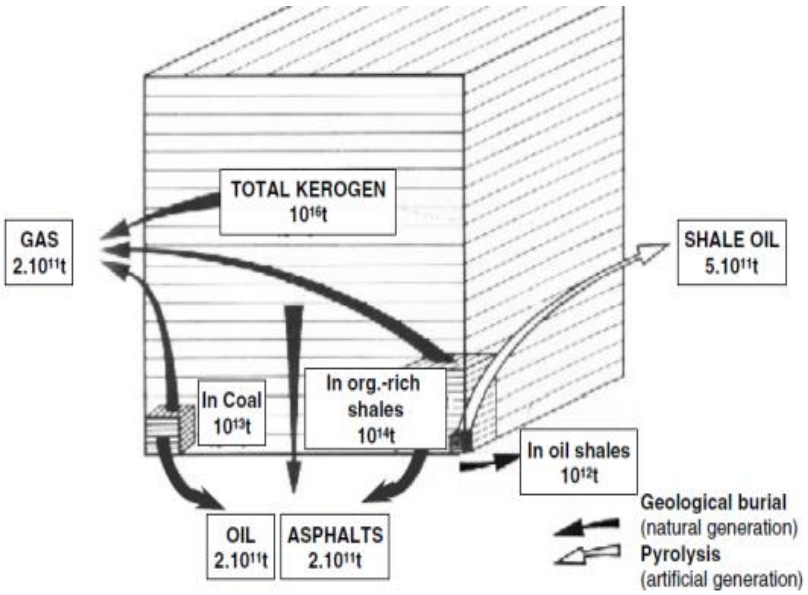

Figure 9 Comparison of amounts of dispersed kerogen and ultimate resources of fossil fuels, adapted from Durand (1980).

2.2.1 Kerogen origin and formation

Kerogen physico-chemical structure, as well as its evolution during sediment burial is required to better predict its oil and gas pools. Peters et al, 2004 [32] stated that the origin and evolution of kerogen is a sedimentary rock that contains organic matter. This organic matter is from two main primary producers' *algae and terrestrial sources.* It has been proposed that

the remains from these primary producers and organism (heterotrophic) like fungi and bacteria. These organisms escape complete mineralization during the entire carbon cycle and the remains are deposited in lacustrine or marine environments.[12] Huc [33] stated that the organism (photoautotrophic) is the first part of the carbon cycle that involves the primary producers which transform CO_2 or inorganic carbon (CO_2, CO_3^{-2}) dissolved in water using sun by photosynthesis into metabolites. Phytoplankton in water and higher plants on earth are the major contributors. Heinrichs et al., [34] stated that the death of autotrophs is the second part of the cycle. The mineralization by heterotrophic organisms in their food chain correspond to their energy from oxidation reactions to synthesis their own metabolites [35]. However, from Heinrichs et al. (1993) stated that OM buried below 1 meter will be well-kept at high sedimentation rates. The depositional environments with large terrestrial organic input relate to high sedimentation. Bacterial degradation of minerals are responsible for Total Organic Carbon (TOC) during sedimentation and cementation times[36]. In marine environments 70 and 30 % of the sedimented material will be particulate OM of detrital rain and living organisms remains near the sediment-water interface of benthic heterotrophs respectively[37].

The source and preservation pathways of the organic matter determine the morphology of the source rock. The remains of source organism are identified in reliable petrographic data in coal studies [38]. **Table 1** shows petrological classification of petroleum source rocks based on two main organic matter sources: aquatic (algae and bacteria) and terrestrial (lignin).

Table 1 Simplified petrographic classification of kerogen constituents after (Robert, 1979; Alpern, 1980)

Maceral	Organic (organic micro constituents , Apern, 1980	Source of constituents (Rober,1973)
Vitrinite	Woody tissues	Primary
Inertinite	Burned organic	Primary
Exinite	High plant protective tissues source pollen grains	Primary
Alginite	Phytoplankton	Primary
Bituminate	Migrated bitumen	Secondary
Faunal relics	Zoobenthos	Primary

2.2.2 Kerogen evolution

Kerogen evolution in sedimentary rocks occurs in four stages. The stages involve thermal cracking, sediment burial and geothermal heating. The direction of increasing maturity of the phases is as follows: The first involves ***early diagenesis*** which includes the loss of Nitrogen, mostly due to biological processes and leads to the production of amino acids and ammonium ion. The second is the loss of oxygen as H_2O, CO_2 in humic and fulvic acids known as ***diagenesis***. The third stage is ***catagenesis***, which involves the major loss of Hydrogen and Carbon (oil and wet gas). In here the kerogen evolution paths fuse into a single path on the van Krevelen diagram, around an H/C atomic ratio of 0.5[12, 13] where oil and gas generation occurs. Finally**,** ***metagenesis*** is the stage where production of CH_4 (dry gas) and non-hydrocarbon gases such as CO_2, H_2S and N_2 occurs. Redistribution of the aromatic network in the residual kerogen also happens at this stage. The mechanisms of kerogen reaction is influenced by minerals, water, pressure, and temperature range after early diagenesis and is often simulated by carrying out pyrolysis experiments [12]. The general scheme of the organic matter evolution into oil and gas via kerogen is expressed in **Figure 10**[10].

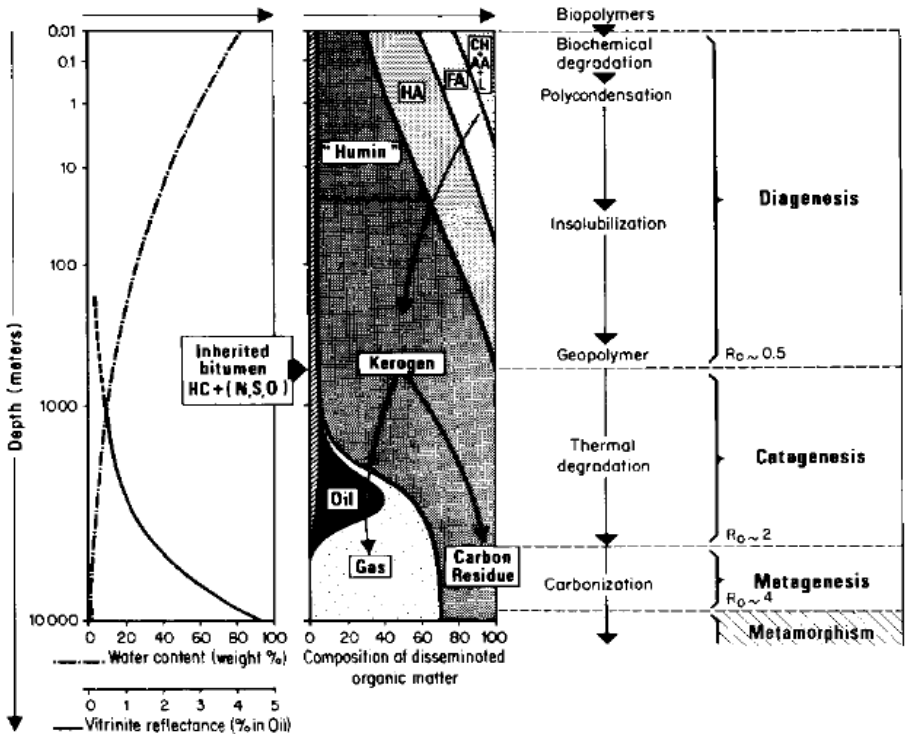

Figure 10 General scheme of evolution of the organic matter from the freshly deposited sediment to the metamorphic zone. CH: carbohydrates, AA: amino acids, FA: fulvic acids, HA: humic acids, L: lipids, HC: hydrocarbons N, S,O: N,S,O (non-hydrocarbons) [10]

Figure 11 illustrates the temperature and pressure profile in a source rock, kerogen, and transition from reactive carbon to dead carbon that determines the generation of hydrocarbons. Early diagenesis involves biologic activities that produce gases while catagenesis produce oil and gas. However, with increasing depth and temperature any remaining oil is cracked to dry gas, suggested by Tissot et al. and the maturation temperature is around 100-160 ^{o}C [39].

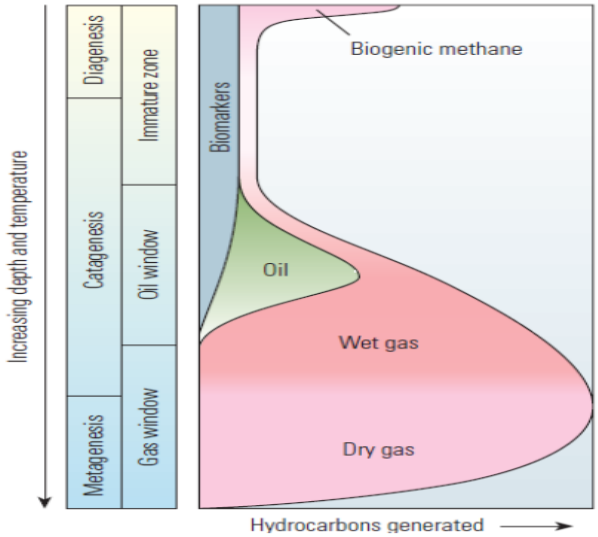

Figure 11 Thermal maturation of kerogen and oil window formation [24]

2.2.3 Kerogen types

Down and Himus, (1941)[40] compared coal and kerogen samples from sedimentary rocks in marine environment. The goal was to determine their organic precursors in controlled oxidation at which Light Microscopy was used to illustrate the presence of an aromatic core. [40] studied kerogen compositional difference and attributed it to variation in plant sources, bacterial reworking based on different techniques and concluded similarly to those of Down and Himus (1941). Two main types of kerogen were observed as indistinguishable kerogen from coal and the other being more aliphatic.

However, Durand and Espitalie´ et al, first proposed generally accepted classification of source rock kerogen into three main types [13]. Paris Basin elemental analysis of kerogen samples and related literature data on various kerogen samples of different age and location, were used and most data from McIver, (1967)[19]**.** The analyses were represented in an atomic H/C vs. O/C diagram, similar to van Krevelen diagram proposed in 1961 for coal studies [41]**.**

The maturity was based on the elemental analysis of kerogen samples from petroleum systems studied at the time by Durand and Espitalie[13, 39] and Tissot et al.[13, 39]. Four kerogen types were defined in van Krevelen diagram in **Figure 12.**

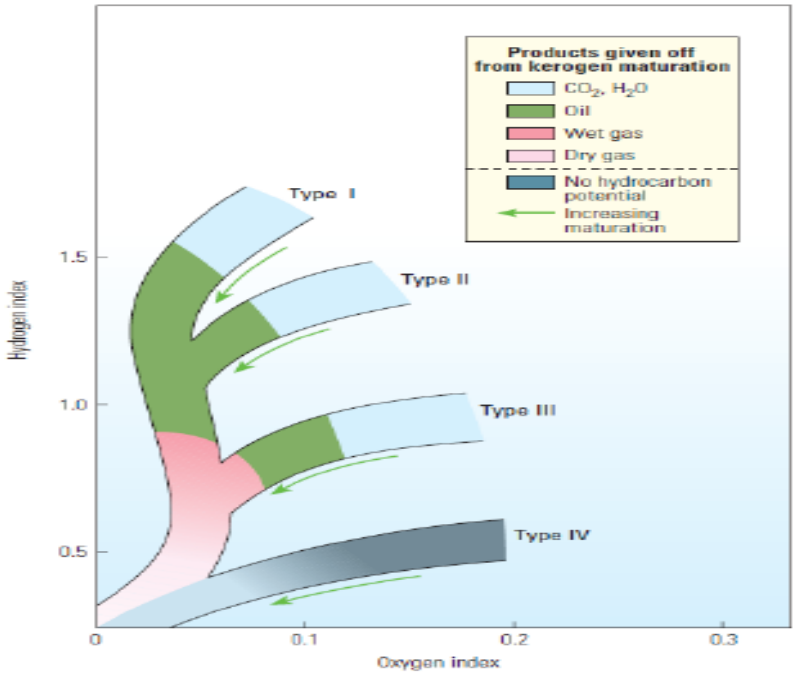

Figure 12 Kerogen maturation and types [42]

The classification of the types of kerogen in terms of origin, H/C and O/C evolution path is summarized in ***Table 2.*** The type 1 is mostly matured form and has high hydrogen to carbon ratio greater than 1.25 and 1.25> O/C<1.05 depending on its origin.

Table 2 Types of kerogen and their depositional environment[43]

Depositional environment	Kerogen type	Kerogen form	Origin	HC Potential	H/C ratio	O/C ratio
Aquatic	I	Alginite	Algal bodies	Oil	>1.25	<1.25
		Amorphous kerogen	Structureless debris of algal origin	Oil		<1.05
			Structureless Planktonic			

	I		material, primary of marine origin			
Terrestrial	II	Exinite	Skins of spore and pollen cuticle of leaves and herbaceous plants	Oil	>1.25	<0.03-0.18
	III	Vitrinite	Fibrous and woody plant fragments and Structureless, Colloidal humic matter	Gas, some oil	<1.0	<0.03-0.3
				Mainly gas		
	IV	Inertinite	Oxidized, recycled woody debris	None	<0.5	<0.13

2.2.4 Green River Formation kerogen model

The largest known oil shale resource in the world is found in the Green River Formation as shown in **Figure 3**.The basin: Piceance, Uinta, Green River and Washakie covers Colorado, Utah and Wyoming in USA. The organic deposit is found over millions years ago and located in sedimentary rock. The rock is marlstone made up of carbonates and silicates. Smith et al, proposed that the total oil resource is ca.1.8 trillion barrels of oil[15].

The chemical structure and the molecular dimension of the kerogen found in Green River formation were proposed by Siskin 2 D and 3 D models **(Figure 13)** as type 1. It has H/C ratio greater than 1.25 and O/C ratio less than 0.15.

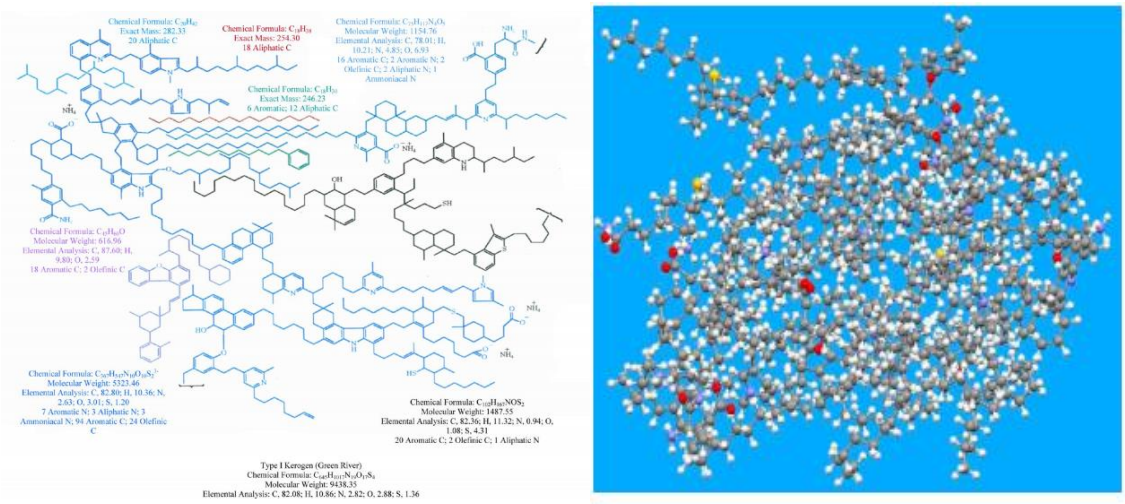

Figure 13 2D (left) and 3D (Right) Siskin model of Green River oil shale C, gray; O, red; N, blue; S, yellow; H, white [42]

Its origin is derived primarily from cyanobacteria (eukaryotic algae) or varied chlorophyta and dinoflagellates (marine plankton)[44].The Green River kerogen is complex macro organic compound of both aliphatic and aromatic groups and has matured oil generation potentials. It is suggested that the chemical formulae is a different based on a specific stratigraphic end and sedimentary core. A typical example was $C_{367}H_{547}N_{10}O_{10}S_2^{-3}$ with the elemental analysis of C=82.80, H=10.36, N=2.63, O=3.01 and S=1.20[44]. The proposed 3D model has 1702 atoms with colors of the elements as follows: C, gray; O, red; N, blue; S, yellow; H, white. The tubes represent the molecule's backbone and the spheres represent the atoms.

2.2.5 Kerogen pyrolysis

Pyrolysis is the process of heating an organic matter (kerogen) in the absence of air. Kerogen decomposes to form a liquid fuel and leaves behind a solid matter. The heat treatment occurs in a closed atmosphere where no oxygen is available; the decomposed organic matter is cooled and upgraded to liquid fuel such as naphtha, diesel and jet fuel. Enefit in Estonia has used ex-situ pyrolysis process to produce over 1.3 million barrels of shale gasoline, heavy fuel oil and extra heavy fuel in 2014[23].

However, topochemical reaction method has been proposed by[3] in the presence of a small amount of air for low energy consumption and high efficiency oil shale cracking. In this process, a chemical heat-enhanced process, partial oxidation of kerogen, occurs in chemical reactions between oil shale and a limited amount of oxygen. The energy produced by

topochemical reaction is used subsequently to promote oil shale cracking into shale oil and gas with great reduction in the external heat-consumption.

[45] used ***gas chromatography-mass spectrometry*** on kerogen pyrolysis at temperature of 410 ^{o}C**.** Aliphatic and aromatic fractions products were observed indicating the petroleum potential of kerogen at this temperature. Also,[46] used ***pyrolysis-gas chromatography*** to examine kerogen thermal decomposition behavior. From all samples examined isoprenoid hydrocarbons were generated at 430 ^{o}C, while majority of 1-alkenes and n-alkanes were generated at 470 ^{o}C and/or 520 ^{o}C.

2.2.6 Kerogen catalytic and/or hydro pyrolysis

As temperature increases, the physical and chemical properties changes and makes the solvent properties of water at 300^{o}C equivalent to those of acetone at 25 ^{o}C as water dissociation constant increases by three orders of magnitude [47]**.** The increase in the dissociation constant will increase the rate of both acid and base catalyzed reactions in water and as such soluble catalyst in hot water may promote kerogen upgrading to fuel. This makes the hydropyrolysis of kerogen a viable alternative.

Speight[11] converted kerogen in Stannous Chloride ($SnCl_2$) acid catalyzed to promote the hydrogenolysis of carbon-carbon bond cleavage mechanism and removal of the heteroatoms. Nitrogen, Oxygen and Sulfur were removed as ammonia, carbon dioxide or water and hydrogen sulfide respectively. Snape et al studied catalytic hydropyrolysis by the use of high H_2 pressure with Mo catalyst pyrolysis for coal liquefaction to increase shale oil production under retorting [48]. Joll et al. investigated yield improvement by using different base strengths such as acetate (TMAAc) or carbonate ($TMACO_3$). Catalytic hydropyrolysis with tetramethylammonium (TMA) salts was also achieved[49]. Catalytic kerogen conversion up to 80 wt% of soluble material has been achieved by the thermal degradation of some *Type II*-S kerogen samples by Schaeffer-Reiss et al,[50] and Hold et al.[51] even though S-rich samples are relatively easy to cleave due to the weaker sulfur bonding with the central carbon core structure under chemical treatments.

H. Jiang et al.,[52] studied catalytic pyrolysis and obtained maximum shale oil yield of 22.17 wt % from $CoCl_2 \circ 6H_2O$ catalysts. The Co ion acts as activation center to speed the breaking of chemical bonds in organic matters.

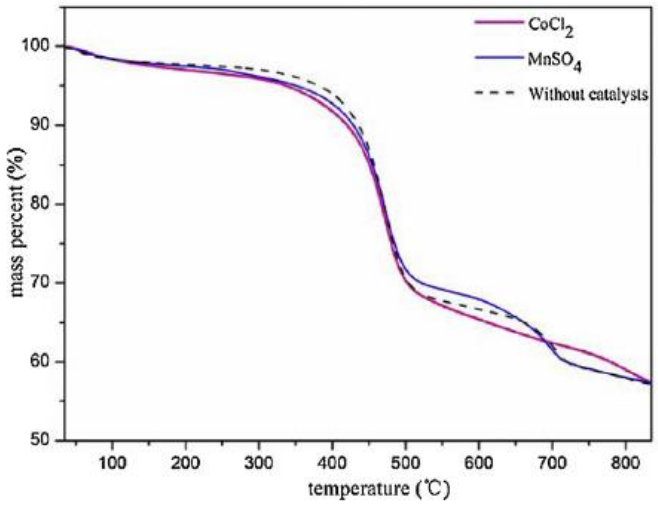

Figure 14 TGA curves for the Huadian oil shale [52]

The TGA curves for the Huadian oil shale with and without catalyst is seen **Figure 14** but clearly not significant shift in low temperature was observed. However, olefin selectivity led to aromatization and thus influenced the production of aromatic hydrocarbons through the addition of $CoCl_2 \cdot 6H_2O$[52]. Advances in the development of new catalyst and more suitable experimental conditions are still needed to obtain acceptable yields from other kerogen types.

2.3 Organic matter separation

2.3.1 Bitumen separation

The study of the thermal behavior and structure of kerogen requires isolation of kerogen [53].

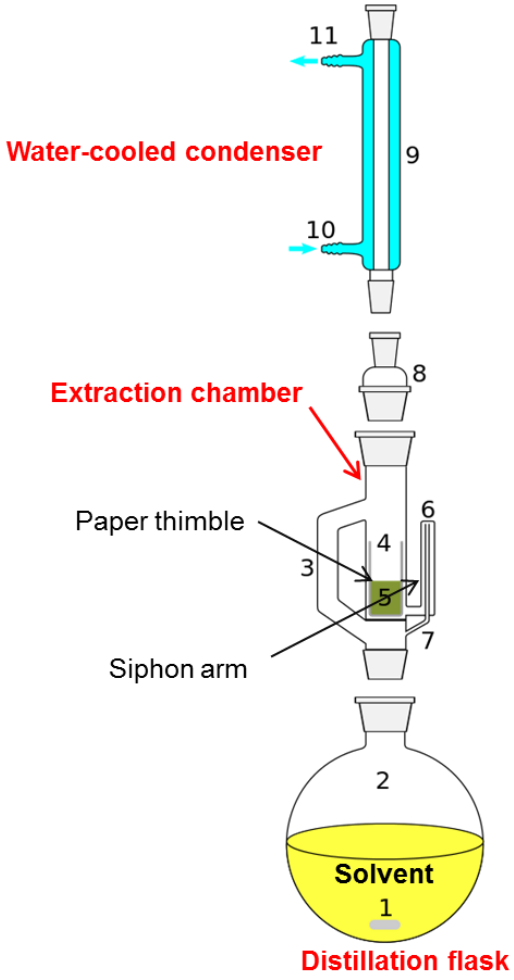

Figure 15 Soxhlet extractor model from Royal society of chemistry world/issues/2007

As seen in **Figure 15** the Soxhlet setup ensure easily removal of the soluble bitumen from the oil shale. The oil shale is place in the thimble chamber while the solvent circulate from the bottom of the flask under heating into vapor phase. The extraction of the soluble organic matter (bitumen) is the first step of kerogen isolation from the oil shale. Suitable organic solvent such as methanol, benzene and dichloromethane $CHCl_3$ or C_6H_6/CH_3OH mixtures are mostly used. Polar solvents like CH_2Cl_2, sometimes mixed with CH_3OH with low boiling point are generally used for their low toxic level [9]. There are various methods of isolation of kerogen that has been studied which can be classified into physical and chemical methods.

2.3.2 Kerogen concentration via chemical methods

The interaction between kerogen and mineral matrices influences its isolation. Demineralization is a chemical method of using acid to remove inorganic matters from the oil

shale thereby facilitating kerogen concentrate. The mineral matrix in an oil shale is dissolved in a series of acid treatments with hydrochloric/hydrofluoric acid mixture and at ca. 65 ^{o}C carbonates and silicates are removed [25]. Also,[54] used base to dissolve silicates and then applied acids treatment to dissolve carbonates. Residual minerals, including pyrite and minor heavy oxides such as zircon, rutile and anatase still remaining after acid treatments, and are removed using oxidizing agents. In addition, ralstonite NaxMgxAl$_2$x (FOH) 6H$_2$O and other complex fluorides can be formed resulting from the HF treatment. Further analysis of kerogen may be interfered by fluorides as they are difficult to redissolve once precipitated and hence need to prevent their formation. The best way to do this is to perform several thorough washing with hot deionized water between the acid steps, without filtering the residue to dryness. Moreover, a second 6 N HCl treatment is performed, after the HF/HCl destruction of silicates, in order to eliminate the ions capable to form these fluorides[12]. The removal of the carbonates creates pores and thereby exposing the kerogen to heat treatment and reaction media.

2.3.3 Kerogen storage

Kerogen is stable when found in its mineral matrix but after isolation it is reported to undergo oxidation and which may leads to alteration in its chemical structure. It is recommended that freshly isolated kerogen samples be stored in an inert atmosphere such as argon or nitrogen medium. Also the storage container could be sealed with Teflon septum and kept in the dark[12].

2.4 Characterization

Spectroscopic and other analytical procedures are mostly used methods to study the physico-chemical properties of isolated kerogen. Atomic constituents of kerogen are revealed by elemental analysis. Van Krevelen diagram is used to elucidate the structure and type of kerogen derived from the elemental analysis on which oil and gas can be traced through the evolution path of kerogen**.** Also, extracted bitumen analysis is used to infer the characteristic nature of kerogen. The bitumen represents units of the oil precursor that did not bound into the insoluble three dimensional macromolecular stable network of the kerogen. Therefore bitumen extract represent units of the kerogen that have been cleaved by the solvents[11].

The bulk structure is studied by TOC and Rock Eval pyrolysis as well as other petrological methods such as Vitrinite reflections [13]. Different compounds types have been identified

from kerogen matrix by extraction, as Anderson et al., [55] discovered paraffins and steranes whiles Anders et al., [56] identified aromatics and polar compounds and Anders and Robinson [57] produced cycloalkanes. The evidence of these compounds in kerogen matrix speculates why kerogen is described as the route to oil and gas generation.

2.4.1 Elemental analysis

The key elements (wt %) in kerogen concentrates are C, H, N, O, S and possibly Fe from pyrite. The sum of all these should be greater than 90 wt% and with an average oxygen value at 11% and often measured directly and not by difference. Gases produced at 1000 ^{o}C by C, H and N is measured by Thermal Conductivity Detector (TCD). Oxygen is determined by kerogen pyrolysis under N_2 flow and transforming oxygen containing gases to CO_2 which is often quantified by coulometry. Elemental analysis data is used to plot the van Krevelen diagram as showed in **Figure 10** [58]**.** Also, spectroscopic techniques such as ICP, EDS, XRF, and NMR are all used to determine the elemental composition of kerogen[25, 44].

2.4.2 Rock- Eval pyrolysis

This technique is a rapid method to characterized kerogen in the whole rock. Programmed temperature is used to heat the rock in a pyrolysis oven under N_2 flow upon which the hydro-carbon effluents are quantified by flame ionization detector (FID). **Figure 16** illustrates the schematic diagram of the Rock Eval pyrolysis. The first peak (**S1: 150-300 ^{o}C**) is due to thermo-vaporized free compounds of the already generated oil in the rock referred as free hydrocarbon [58]. The second peak (**S2: 300-500 ^{o}C**) is hydrocarbon pyrolysis compounds that are similar to those yet to be generated upon source rock burial and maturation. This peak refers to the nonvolatile organic matter decomposition and hence represents kerogen peak. The third (**S3)** peak is the amount of CO_2 formed during OM pyrolysis up to 390 ^{o}C with a specific detector.

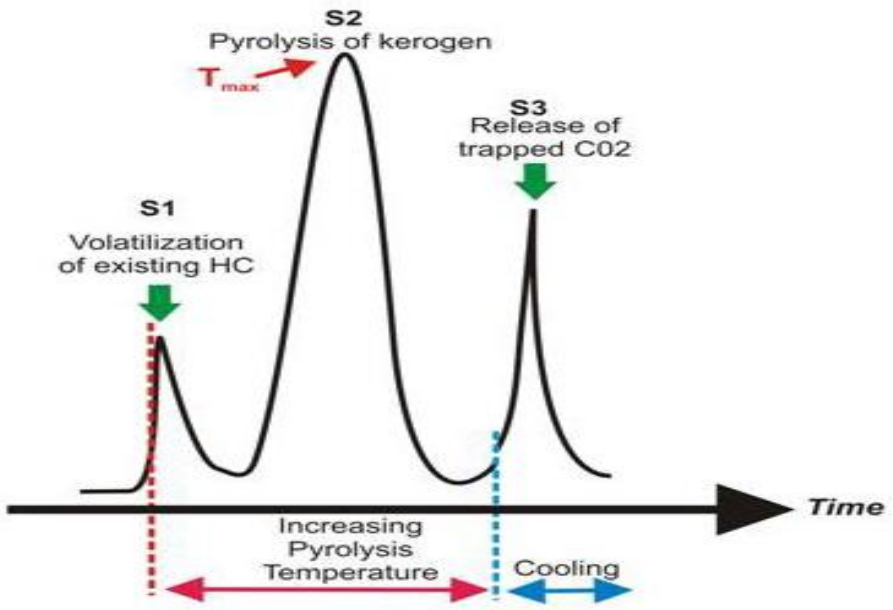

Figure 16 Schematic diagram of Rock Eval pyrolysis[59]

The third (**S3)** peak is the amount of CO_2 formed during OM pyrolysis up to 390^{o}C with a specific detector. In recent times Peters and Moldowan have proposed a variant form of Rock Eval II at which the S3 peak represent the peak that evolves at oxidative atmosphere. The residual organic matter is burned at 850^{o}C under air and the resulting CO_2 is (**S4**) peak. The hydrogen index (HI) represents the oil richness of the source rock and is determined by S2 peak area divided by TOC. PI is the production index=S1/(S1+S2) while S1+S2 is the potential yield. Oxygen index (OI=S3 peak area/TOC) and T_{max} is the pyrolysis temperature at maximum S2 peak for kerogen [12]. The Rock Eval pyrolysis, elemental analysis, TGA and Py-GC-MS are often used to model the type and maturity of kerogen.

2.4.3 X-ray diffraction (XRD)

XRD is often used for phase characterization and detects crystals larger than 3-5 nm in quantities higher than 1% [59]. In this analysis, a crystalline material diffracts X-rays for quantitative and qualitative analysis. The angles of diffraction differ from the various planes within the crystals and hence every compound has its own diffraction pattern which is governed by Bragg's law[60]. The general relationship between the wavelength of the incident X-rays, angle of incidence and spacing between the crystal lattice planes of atoms is known as Bragg's Law, expressed as ***(eqt.1)***.

$$n\lambda = 2dsin\theta \qquad \mathbf{1}$$

Where an integer (n) is the order of reflection, λ is the wavelength of the incident X-rays, d is the interplanar spacing of the crystallites and θ is the angle of incidence. This equation and Scherrer (**eqt.2**) below where L is the size of crystals, B is the breadth at half peak height of an XRD line, λ is the x-ray wavelength, θ is diffraction angle and K= 1 is constant.

$$B = \frac{K\lambda}{LCOS\theta} \qquad \mathbf{2}$$

The (***eqt.1&2)*** are used in XRD experiments to determine the crystalline phase, size and elements presents based on standard XRD patent for compounds identification and characterization[60].

2.4.4 SEM

The ultrastructure and morphology of kerogen is determined by scanning electron microscopy (SEM) high resolution. The SEM is used to generate images of shapes of objects and to show spatial variations in chemical compositions. The higher kinetic energy produced by accelerated electrons in SEM if dissipated on a solid sample produces a variety of signals.

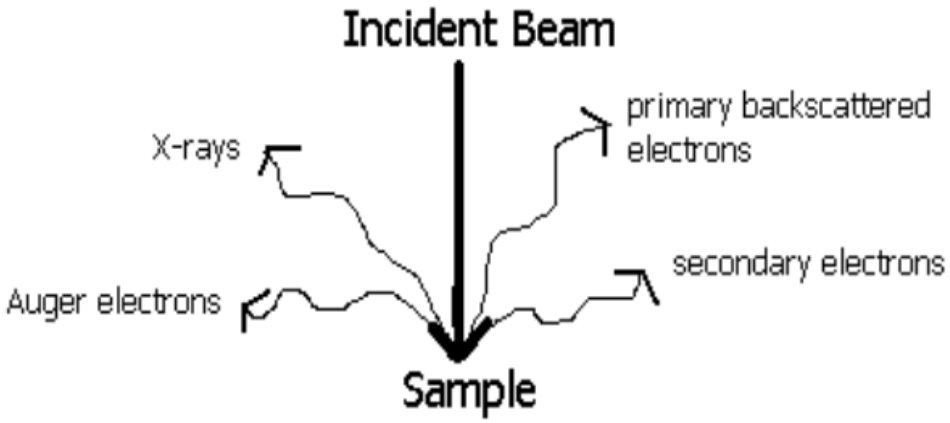

Figure 17 Schematic view of the principles of SEM operations[61]

The sample imaging is determined by secondary electrons and backscattered electrons [61]. The secondary electrons are mostly used to determine morphology and topography of samples. The schematic view of the principles of SEM is showed in **Figure 17.**

2.4.5 FTIR

Infrared Spectroscopy is well established method for qualitative analysis of functional group and most especially aliphatic hydrocarbons. Conventional IR analysis uses electromagnetic radiation in the IR region that spreads from 10 to 13000 cm^{-1} but only the mid-IR region (400-4000 cm^{-1}) is often utilized [61].

Table 3 FTIR peak assignment adopted from Robin et al., [10, 25]

Wavenumber (cm^{-1})	Functional group
3430 wide asymmetric band	OH groups (phenolic, alcoholic, carboxylic OH)
2920 and 2855 strong absorption	two maxima (related to CH_2, and CH_3 aliphatic groups;
1710 wide band	C=O groups (ketone, acids, esters)
1630	mostly related to aromatic C=C, olefinic" C=C, particular types of C=O groups (bridged quinonic carbonyl), and of free water
absorption band at 1455	CH_3 and linear and cyclic CH_2 groups
1375	CH_3 only
1400 to 1040	includes C-O stretching and OH bending
930 to 700	aromatic CH (Bending out of plane)
720	aliphatic chains of 4 or more carbon atoms

The absorption spectra are often analyzed based on beer's lambert law (***eqt.3***). $A = -\log(T) = \varepsilon c l$ **3** , where A is the absorbance of a single or multicomponent system, T is the transmission, ε= molar extinction coefficient (cm^2/mol), c is the concentration (mol/l) and l is the path length (cm). The infrared spectra of compounds has been be recorded by different infrared spectroscopies such as TIR, ATR-FTIR, and DRIFT etc. [62].

The vibrational frequencies of functional groups, such as C–C, C–H, C=C, O–H, C=O and N–H are used to determine their wavenumbers upon which characterization is done. The peaks assignment for kerogen studies is proven much complicated due to its heterogeneity but following the peak allocations proposed by Tissot et al., and adopted from Robin et al.[10] some peaks of kerogen natures has been identified.

2.4.6 TGA-MS

Thermal techniques are used to measure physical property as a function of temperature program (heating, cooling or isothermal). Differential Scanning Calorimetry (DSC) measures energy release per time while TGA as showed in **Figure 18** measures mass loss.

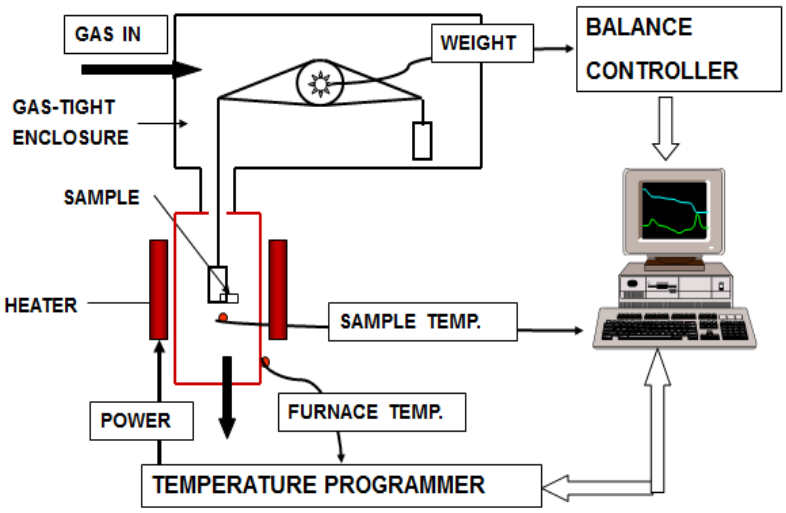

Figure 18 Schematic view of TGA[63]

Thermal properties and kinetics parameters such as activation energy and pre-exponential factor of kerogen decomposition can be identified by the use of TGA. It is a useful tool to obtain thermal characteristics of compounds by microscopic weight loss in few milligrams of the sample at varied atmospheres and temperature conditions. The unit is often couple with Mass spectrometer to determine the off gases from the sample decomposition or oxidation which is measured as a function of temperature[25].

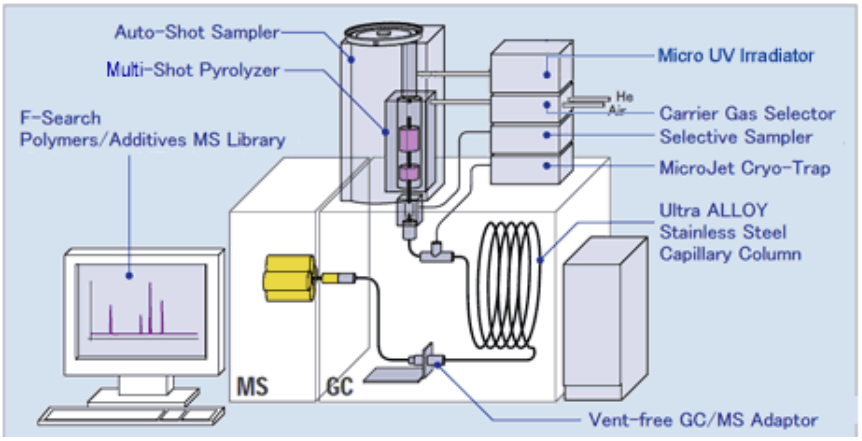

Figure 19 Py-GC/MS instrument schematic view[64]

2.4.7 Py-GC/MS

Higher molecular weights (HMW) polymeric organic matters are classified by temperature resolved pyrolysis mass spectrometry. The PY-GC/MS as shown in **Figure 19** is fantastic equipment for performing multiple analysis of an organic complex polymer molecule such as

kerogen. It works like the normal GC-MS but with a pyrolysis unit that can provide higher temperature program for the compound decomposition.

The kerogen studies require higher temperature decomposition due to its heterogeneity and complex molecular structure[64]. It also has a furnace, GC oven and column and MS. The sample undergoes pyrolysis in a temperature program in the furnace and the volatile molecules are carried by the carrier gas into the GC column in an oven for separation into various components while the ion source in the MS ionizes the molecules into ions to be detected by the MS. The detection is based on scan program such as 29-600 m/z ratio and represented by total ion chromatogram (TIC). The frontier laboratory F searches software and NIST library allows the identification of the pyrograms.

Zhang et al. used Py-GC/MS at 650 ^{o}C to generate hydrocarbon pyrolyzates from Huadian kerogen formations yielded high concentrations of n-alkanes[65]. The high concentration of hydrocarbon products was attributed to microalgae source which produced a wide range of saturated and unsaturated n-aliphatic hydrocarbons from C_5-C_{40}.

3. Material and Methods

In this chapter, various experimental and characterization techniques are described. A short description of the oil shale (kerogen) used for the experiments and the pretreatment procedures including separation of bitumen and carbonates removal are highlighted. Also the experimental procedures for the various characterization techniques as well as catalyst preparation have been elaborated.

3.1 Pretreatment/Comminution

Figure 20 shows the picture of the oil shale sample received from Green River Formation, USA, and herein used in all the experiments and analysis. The bulk Green River oil shale sample was supplied by Statoil. The internal layer is predominately made up of rich organic matters bitumen and kerogen.

Figure 20 Oil shale samples from Green River Formation, USA.

The sample (oil shale) is crushed and milled using the laboratory disk milling machine showed in **Figure 21**. Steel metal balls are used to help in milling of the crush oil shale sample.

The mill machine was cleaned with solvent and run with clean sand pre-washed to avoid contamination. The fine particle size of the oil shale is obtained for subsequent solvent extraction and characterization.

Figure 21 Laboratory disk milling machine

3.2 TOC/Rock-Eval pyrolysis

The TOC was determined using a LECO SC-632 carbon/ sulfur analyzer while the Rock Eval pyrolysis was done with Rock Eval 6. The TOC instrument used followed NIGOGA, 4th Edition protocol. A Rock-Eval 6 instrument is used and diluted HCl is added to the crushed rock sample to remove carbonate. Jet-Rock 1 is run in every tenth sample and checked against the acceptable range given in NIGOGA. The sample is then introduced into the Leco combustion oven, and the amount of carbon in the sample is measured as carbon dioxide by an IR-detector. The temperature programme applied in pyrolysis mode is: 300 °C (3 min.) - 25 °C/min - 650 °C (0 min.)

3.3 Soxhlet extraction

The milled sample is subjected to Soxhlet extraction to remove the bitumen fraction by the use of organic solvent dichloromethane (CH_2Cl_2). It is done for eighteen hours at 60 ^oC to allow a sufficient time to separate the soluble organic matter with a solid to solvent (DCM) ratio of 6.5 grams: 150 mL. The endpoint was determined by the clarity of the solution in the thimble chamber after several recirculation of the solvent. **Figure 22** is the picture of the Soxhlet extraction setup used. This setup is located in a fume hood for safety considerations.

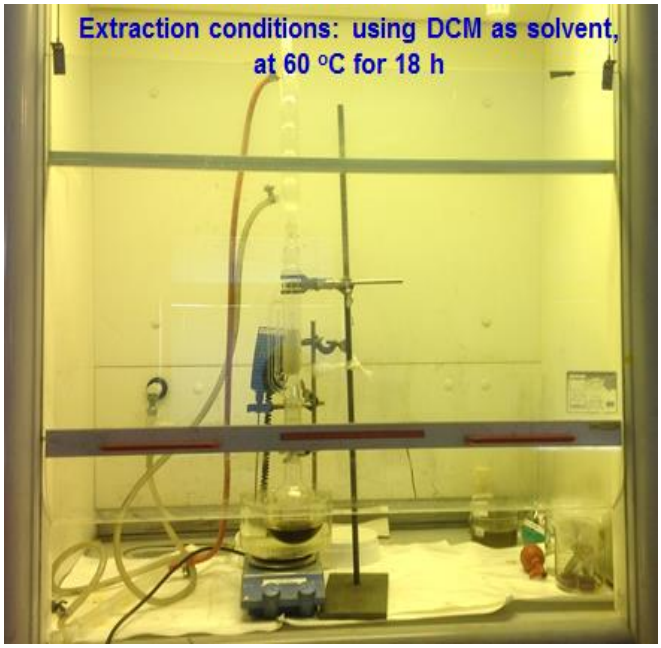

Figure 22 Bitumen extraction setup (Soxhlet)

3.4 Demineralization

The presence of insoluble carbonates and dolomite may affect the catalytic thermal conversion and were removed from the solid residue after Soxhlet extraction. 6 M Hydrochroric (HCl) acid and equal volumes of water and HCl of 75 mL were used. The mass of extracted oil shale residue used is ca. 8 grams for 24 hours. The product after the reaction is washed repeatedly in centrifuge by hot distilled water until pH of 7 is obtained. The as-obtained residue is dried in a vacuum oven for 1 hour at a temperature of 100 ^{o}C before stored in an inert atmosphere. This setup **(Figure 23)** also removes any elemental and/or organic Sulphur in the sample which may persist. **The as-obtained oil shale sample is herein denoted as decarbonated-kerogen which is free from bitumen, calcite and dolomite.**

Figure 23 Decarbonation setup

The complete process flow diagram for decarbonated-kerogen isolation is shown in **Figure 24**.

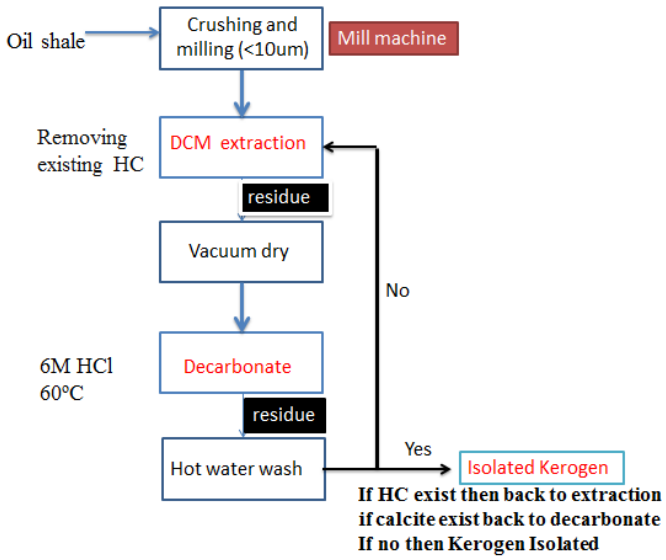

Figure 24 Proposed experimental steps for decarbonated-kerogen isolation

3.5 Characterization

3.5.1 SEM

The morphology and size distribution of samples were studied with scanning electron microscopy. Hitachi S-5500 S(t)EM located at *NTNU Nanolab* was used. The milled oil shale sample was deposited on the carbon tape placed on the holder. The holder together with the

sample was inserted into the SEM. The voltage and current were adjusted to achieve clear view.

The particle size distribution for the fine oil shale sample obtained from the SEM is showed in the **Figure 25.** This typical image of the milled oil shale sample indicates that its size is less than 10 micrometer. Subsequently, N_2-BET (Micrometrics Trister 3000) was carried to determine the surface area and pore diameter of the fine oil shale sample. The sample (0.1g) was degassed at 200 ^{o}C overnight.

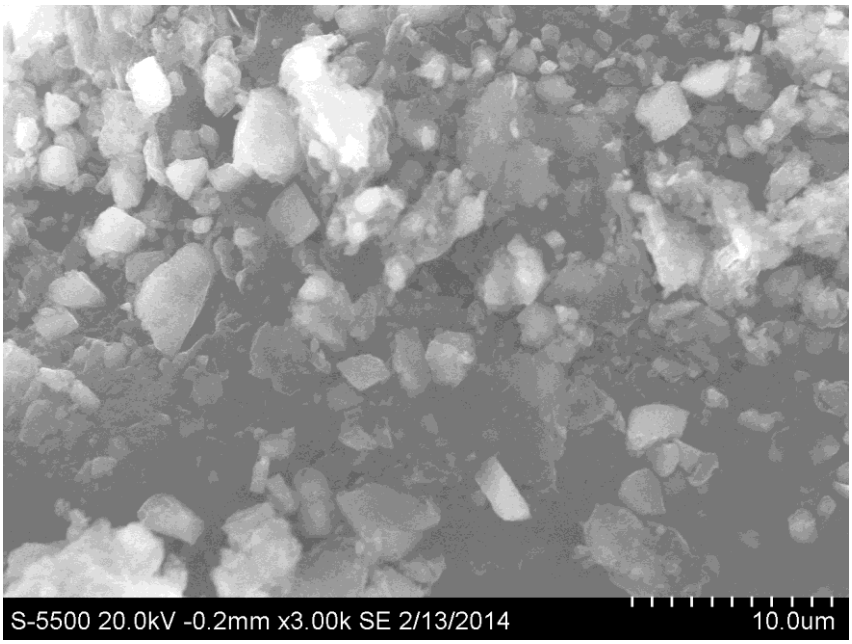

Figure 25 SEM image of the milled oil shale sample

3.5.2 XRD

The XRD was carried out by D8 ADVANCE with the DIFFRAC^{plus} SEARCH software to assign the peaks. The XRD pattern was determined by applying $CuK_{\propto}1$ radiation in the range of 2θ from 15-75^{o}. Automatic background subtraction and smoothing were performed for better qualitative analysis and phase characterization.

3.5.3 FTIR

The infra-red spectra were obtained with a Nicolet iS50 IR spectrometer. All samples for the analysis were prepared and pressed in an evacuated die for 1 min. The data were obtained in an attenuated total reflection mode with a resolution of about 2 cm^{-1}. The functional groups of the organic matters were determined by ATR- FTIR standard pattern data.

3.5.4 Thermal behavior/ TGA-MS

TGA (thermo gravimetric analysis) and DSC (differential scanning calorimetry) were performed using Netzsch STA 4496 **(Figure 26)** thermal analyzer system at a heating rate of 10 $^{o}C\ min^{-1}$ under argon and air atmospheres. In all the TGA/MS experiment correction is done first to calibrate the empty crucible mass to room temperature. The sample mass of ca. 10-15 mg were used in all the analysis. The air and argon atmosphere were applied with the protective gas (argon) flow of 75 mL/min as well as 25 mL/min flow for the purge gas.

3.6 Py-GC/MS

The Py-GC/MS was performed in EGA/PY-3030D with a pyrolyzer temperature of 550 ^{o}C; Agilent GS/MS77780 was used at GC injection temperature of 300 ^{o}C and oven temperature of 340 ^{o}C (20 ^{o}C/min, 13 min hold). The sample mass used is ca. 0.1- 0.5 mg of the treated oil shale samples. The Ultra Alloy capillary column of 5-30M-0.25F was used with a Helium column flow of 1 mL/min. The scan range was from 29-600 (m/z) at a scan speed of 4.87 scans/sec. In order to minimize contamination of pyrolysis residue a blank sample is carried out after every sequence.

3.7 Catalyst preparation, screening and optimization.

The role of transitional metal salts as stated in US patent in [66] provide enough premises for the screening of transitional metal ions as catalyst for the kerogen conversion. Incipient wetness impregnation method was applied. The model calculation procedures are shown in **Appendix D.** The total adsorbed water for the decarbonated kerogen sample was determined and approximated to be the total pore volume of the kerogen sample. Subsequently, variable wt % of the metal ions were calculated and impregnated on the decarbonated-kerogen sample. The metal ions employed are Cu^{2+}, Fe^{2+}, V^{2+}, Mn^{2+} etc. metal chlorides, mineral acid (H_2SO_4 and H_3PO_4) and metal oxides (Ni and Co oxide). The oxide were in-situ formed from the following precursors $Ni(NO_3)_2.6H_2O$ and $Co(NO_3)_2.6H_2O$. Prior to the impregnation, the determined metal loading is dissolve in the adsorbed water volume and impregnated onto the sample and thoroughly stirred by the use of metal rod. The stirring ensures adequate deposition of kerogen on the metal surface. It is then dried in a vacuum at 100^{o}C for 8 hours. The different catalyst prepared samples were screen by the use of EGA and TGA-MS. The active ones were optimized by varying conditions such as loading (wt %) and heating rate.

4. Results and Discussion

It is well-known that the organic matter in an oil shale sample is made up of existing hydrocarbons (bitumen) and kerogen [7, 8, 10] which is a precursor for petroleum generation. The source rock was evaluated based on Rock-Eval pyrolysis and TOC to determine the kerogen and bitumen content as well as petroleum production indexes and parameters. The kerogen is insoluble in organic solvent while bitumen is soluble in organic solvent and thus solvent extraction method was applied to separate the bitumen from the oil shale. The oil shale was further treated with HCl to remove inorganic carbon which might interfere with subsequent thermal and catalytic upgrading of kerogen. The model oil shale, extracted bitumen, and decarbonated kerogen were characterized by multiple techniques. The thermal (pyrolysis) and catalytic upgrading of kerogen to fuels would be investigated as well as kinetic modeling.

4.1 Petroleum generating potential of Green River oil shale

The oil shale is a precursor to crude oil generation [10, 33, 67]. It is often stated that the oil shale is a source of crude oil that has not matured in the geologic process and contains organic matters. The organic matters are bitumen and kerogen [9, 20, 54] while the inorganic matters depends on the organic matters depositional environments, sedimentation and cementation conditions. The Green River Formation oil shale, applied in this analysis is known to contain inorganic components such as calcite, dolomite, analcite, pyrite, illite, feldspar and quartz. The inorganic matter is mostly washed into the geologic formation through the process of erosion and precipitation. The Green River Formation has organic matters in the form of kerogen and bitumen [53]. The petroleum generating potential of the Green River oil shale was determined by TOC and Rock-Eval analysis to ascertain its maturity level.

4.1.1 TOC/Rock-Eval pyrolysis

The TOC and Rock-Eval pyrolysis is applied to classify the organic matter in a source rock into **S1, S2** and **S3** peaks. **Table 4** represents the results from the oil shale sample and clearly an S1 peak of 0.54 wt% is observed. indicates the less volatile organic matter referred to as free hydrocarbon (bitumen) [9].

Table 4 Rock-Eval pyrolysis data of fine oil shale HC[#] (hydrocarbon).

S1 (mg/g)	S2 (mg/g)	S3 (mg/g)	HI (mgHC[#]/g TOC)	OI(mg/g TOC)	T_{max}(°C)	TOC (%)
5.43	152.84	2.06	621	8	433	24.6

The S2 peak indicates the higher boiling point and insoluble kerogen of 15.2% at pyrolysis maximum temperature (T_{max}) of 433° C. The S3 peak is 0.2% and represents the CO_2 formed during OM pyrolysis up to 390°C.

Figure 16 illustrates the schematic view the Rock- Eval analysis. The total organic carbon (TOC) obtained was 24.6 wt % from the **Table 4**. The TOC value indicates that the oil shale has excellent petroleum generation potential according to Peters and Cassa (1984) as shown in **Table 5** as the determined TOC is greater than 4.

Table 5 Petroleum potential (quantity) of an immature source rock (Peters and Cassa, 1994) (TOC =total organic carbon, S1=volatized existing hydrocarbon, S2=kerogen decomposition) [48]

Source Rock	Petroleum potential (quantity) of immature		
Petroleum potential	**Organic matter**		
	TOC	Rock-Eval pyrolysis	
	(Wt %)	**S1**	**S2**
Poor	0-0.5	0-0.5	0-2.5
Fair	0.5-1	0.5-1	2.5-5
Good	1-4	1-2	5-10
Very good	2-4	2-4	10-20
Excellent	**>4**	**>4**	>20

This indicates that the sample is credible to produce oil and gas. The TOC measurement provides a semi quantitative scale of petroleum generation potential and indicates quantity of organic matter but not the quality. It is an initial treatment and screening method and combined with other methods to ascertain the organic matter richness and maturity of the source rock. According to Peters and Cassa, hydrogen index (HI) greater than 600 shows that the oil shale is found in the oil window and type I kerogen. The analysis result in **Table 4**

shows HI of 621 and thus found in oil window and type I. The HI also provides the amount of hydrogen found in the oil shale and the greater this value may predict the oil richness of the source rock and hence it quality.

The T_{max} of 433^{o}C alone suggest that the kerogen is type II according to source rock evaluation criteria (Type I; T_{max} 435-445^{o}C) by peters and Cassa (1994) but the closeness of this value to type I makes it possible to combine T_{max} with the H/C ratio which is discussed in *subchapter 4.3.5* the kerogen may fall into type I. The T_{max} is the maximum temperature for kerogen maturity and oil yield and if considered with HI a type I kerogen is observed which avoids the problems connected with oxygen index (OI) on pseudo van Krevelen plot. In evaluating the source rock richness and maturity a combination of factors is desired to ascertain a complete evaluation criterion. The OI helps to determine the amount of oxygen in the oil shale and is often used to determine the type and maturation of the oil shale. The low oxygen value of 0.8 wt % indicates that the source rock has less oxygen groups and aromatics. The oxygen could also be from inorganic oxygen source such as crystalline water which may also evolve at such high temperatures for S3 peak determination. The production yield (S1+S2) obtained was 158.27 mgHC/g rock and a production index (PI) of 0.034 which are useful for reservoir modeling and subsequent thermal and or catalytic upgrading.

4.2 Characterization of model oil shale

4.2.1 Elemental analysis

ICP and elemental analysis measurements were further performed to quantitatively determine the elemental composition. It was performed with Flash 2000 element analyzer from Thermo Fisher at Statoil Rotvol to know the elemental composition of the kerogen. As shown in **Table 6**, the contents of Al, Ca, Mg, Fe, K and Na are 2.0, 9.7, 4.1, 1.0, 0.88 and 0.76 wt%, respectively. In addition, the evolved gases from high-temperature treatment of fine oil shale contain 20.8 wt% C, 2.7 wt% H, 2.4 wt% O, 0.7 wt% N and 0.5 wt% S, in which the C includes the organic C and the inorganic C from the decomposition of dolomite and calcite. The oxygen analysis was done on the carbonate free sample where the other elements were done on the oil shale sample. The decomposition of $CaCO_3$ produces CaO and CO_2. Since CaO is solid and its oxygen content is not detected it makes the oxygen analysis incorrect if both organic and inorganic oxygen is not well incorporated and as such carbonates free sample is used for analysis of oxygen.

Table 6 Mass percentages of elements in raw oil shale.

Method	Mass percentage (wt %)					
ICP	Al	Ca	Mg	Fe	K	Na
	2.0	9.7	4.1	1.0	0.88	0.76
Elemental analysis*	C	H	O	N	S	
	20.8	2.7	2.4	0.7	0.5	

* Only the evolved gases from high-temperature treatment of oil shale were analyzed.

In terms of elemental composition, the oil shale has less nitrogen and Sulphur. The residual percentage may represent other inorganic and metal constituents. Subsequently, EDS measurement was carried out to qualitatively analyze the composition of fine oil shale, and the results are shown in **Figure 26**. Clearly, the spectra of Al, Ca, Mg, Fe, K, Na, C and O are present.

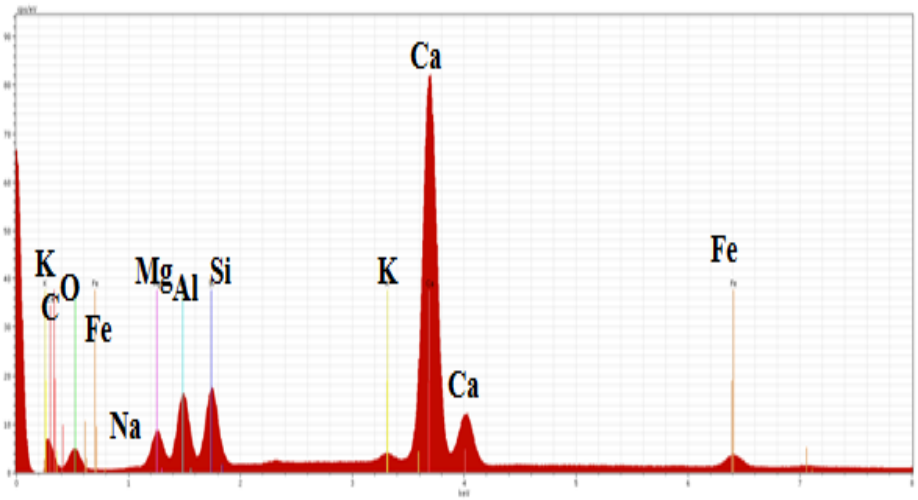

Figure 26 EDS spectrum of fine oil shale

4.2.2 Physico-chemical properties of model oil shale

The organic and inorganic matters found in the source rock were characterized by multiple techniques. The XRD and FTIR are used to predict the inorganic mater while TGA/MS and FTIR are also applied to ascertain the organic matters in the model oil shale. **Figure 27 (left).** Shows the XRD of the milled oil shale from Green River Formation while the **Figure 27 (right)** indicates the FTIR. XRD shows legible characteristic diffraction peaks of dolomite

(PDF 04-011-9829), calcite (PDF 04-012-0489), analcime (PDF 04-011-6233) and Fe-doped quartz (PDF 04-007-0522). Meanwhile it should be pointed out that the organic matters were not identified due to the lack of standard diffraction peaks patterns.

Furthermore, FTIR was used to identify the organic matters functional groups. Clearly as can be seen in **Figure 27 (right),** the fine oil shale exhibits no legible aromatic C-H stretching absorption peaks, but legible aliphatic ones. The two absorption peaks concentrated at ca. 2927 and 2856 cm^{-1} are ascribed to the asymmetric and symmetric stretching vibrations of CH_2, respectively. However, their broad behavior in principle explains the presence of the absorption peak of CH_3.

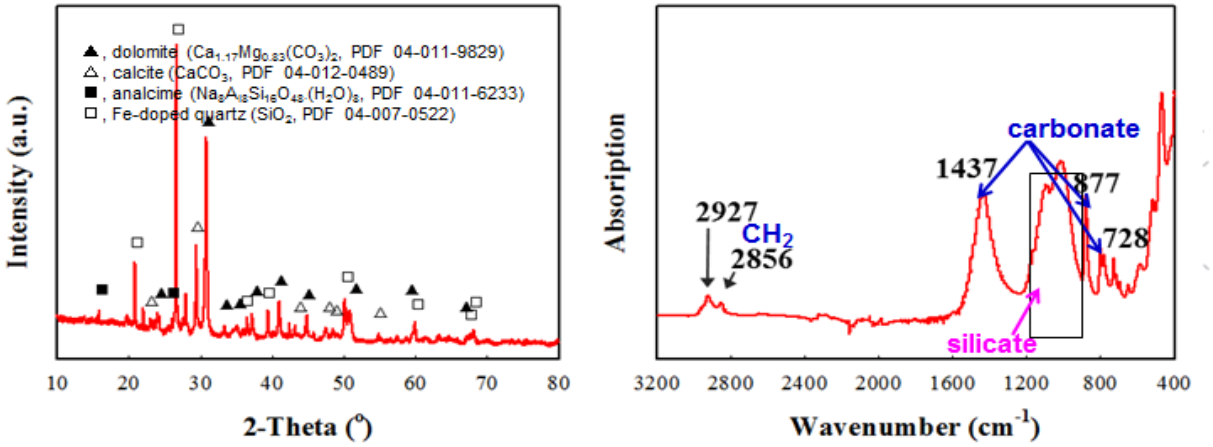

Figure 27 XRD pattern (left) and FTIR spectrum (right) of milled oil shale. Note: ▲, dolomite ($Ca_{1.17}Mg_{0.83}(CO_3)_2$, PDF 04-011-9829); △, calcite (CaCO3, PDF 04-012-0489); ■, analcime ($Na8Al8Si16O48\cdot(H_2O)_8$, PDF 04-011-6233); □,Fe-doped quartz (SiO2,PDF 04-007-0522)

Moreover, there also show three absorption peaks at 1437, 877 and 728 cm^{-1} arising from the vibrations of CO_3^{2-} together with broad peaks in the range of 900-1200 cm^{-1} arising from silicates, which are well consistent with the above results of XRD.

Subsequently, the thermal behavior of the fine oil shale was determined to ascertain the decomposition and conversion of the organic matters by TGA/DSC. **Figure 28 (A)** shows TGA/DSC curves of fine oil shale in air atmosphere at a ramping rate of 10 ^{o}C/min. visibly, there are two kinds of reactions: one is the oxidation reaction mainly arising from the combustion of organic matters; the other is the decomposition reaction mainly arising from the decomposition of carbonates (e.g., dolomite and calcite). Their weight losses were

estimated to 31.23% and 17.95%, respectively. Again, **Figure 28 (B)** shows the decomposition of the organic matters in the fine oil shale determined by TGA/DSC under argon atmosphere at ramp rate of 10 ^{o}C/ min. It can be seen that, there are two main weight loss steps, which show endothermic behaviors. Their weight losses are estimated to 26.58 and 17.69 wt%, for organic and inorganic respectively. Dividing the relative weight loss percent due to pyrolysis atmosphere by oxidative atmosphere gives ca. 85.11 wt% that can be released or converted, mainly by thermal process to yield fuel.

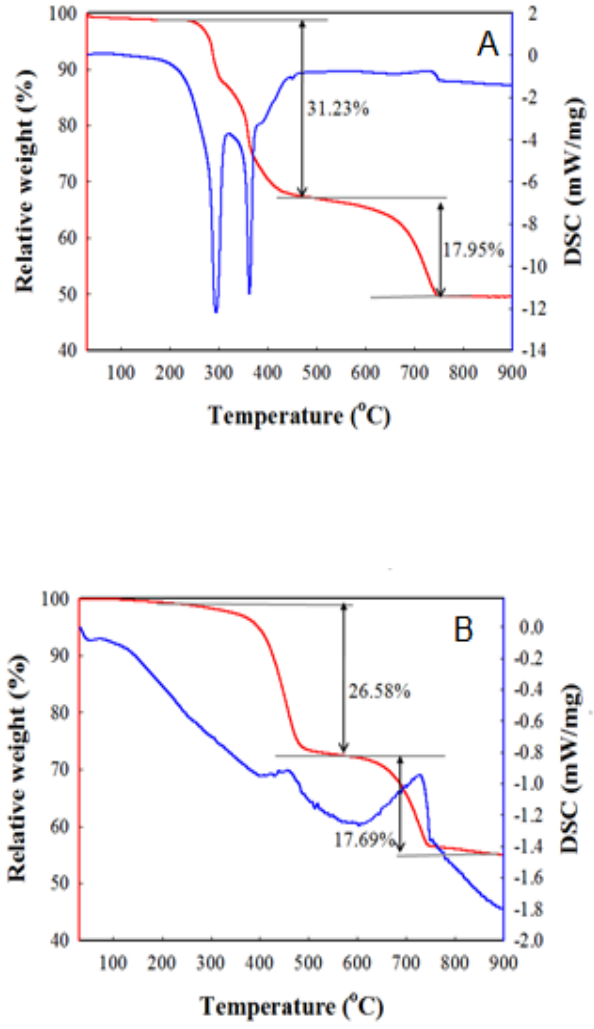

Figure 28 TGA/DSC curves of fine oil shale in air (A) and Ar (B) atmosphere at a heating rate of 10 ^{o}C/min.

Subsequently, in **Figure 29** N_2-physisorption was carried out to study the textual properties of oil shale sample. The results showed that the oil shale sample shows the natures of low-surface-area, non-porous and flaky. The surface area obtained was 3.4 m^2/g with its pore diameter concentrated around 2-10 nm. In these results it was visible that the accessibility of

the kerogen is low and such bitumen extraction and decarbonated experiment was later carried to increase the kerogen exposed surface area to heat treatment and reaction media.

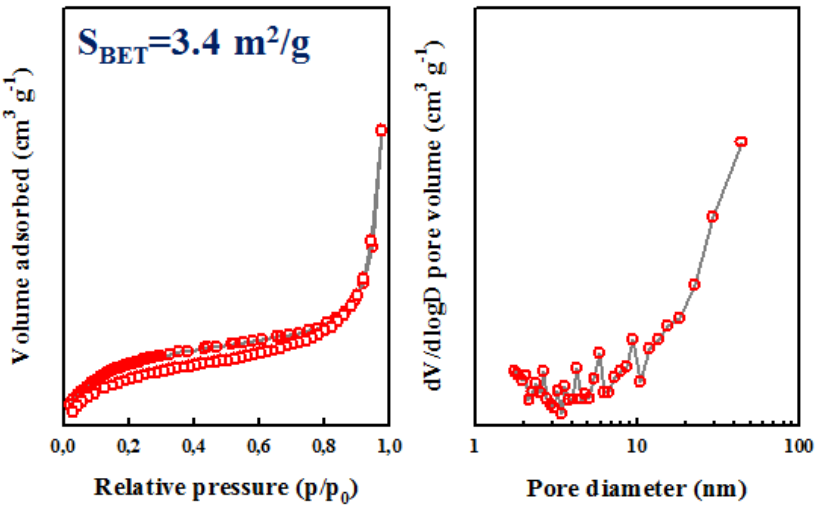

Figure 29 Nitrogen BET for surface area (left) and pore diameter (right) of the milled oil shale sample

4.3 Separation and Characterization of Organic Matters in Oil Shale

4.3.1 Bitumen

The oil shale concurrently contains bitumen and kerogen. In order to study the intrinsic physico-chemical properties of kerogen, it is imperative to separate the bitumen from the oil shale to obtain kerogen-containing samples. Herein, the extraction of bitumen from the fine oil shale was carried out by using dichloromethane (CH_2Cl_2) as the extractant in the Soxhlet extractor. **Table 7** shows the bitumen contents from three extraction experiments of oil shale.

Table 7 Bitumen contents in the oil shale from three experiments

	1	2	3	Average
Bitumen Content (wt %)	3.65	3.70	3.65	3.67

Clearly, the method has good reproducibility, and the average content of bitumen is ca. 3.67 wt%. The wt % is far higher than the Rock Eval pyrolysis, S1 peak 0.54%, of free hydrocarbon (soluble hydrocarbon) but if compared with the extraction data is clearly seen

that the Rock Eval analysis has greater deviation for this analysis. The S1 peak for Rock Eval analysis used a temperature of 300 ^{o}C and hence if the soluble bitumen has higher boiling temperature than 300 ^{o}C all its content cannot be obtained. This great difference may be due to the detector since the detector used in Rock Eval pyrolysis has quench effect and if not well calibrated might have contradicted the results. The S1, S2 and S3 peak represent the organic content in the oil shale sample but if compared with TGA/MS which gave 26.58 wt % the results seem very conflicting.

Figure 30 shows TGA/DSC curves of bitumen in air atmosphere at a ramping rate of 10 ^{o}C/min. It can be seen that the main weight loss peak of bitumen locates at high temperature of 400-500 ^{o}C. However, the corresponding temperature range of the weight loss is very broad, indicating the overlapping with that of kerogen. This again highlights that it is necessary to first separate the bitumen from the oil shale.

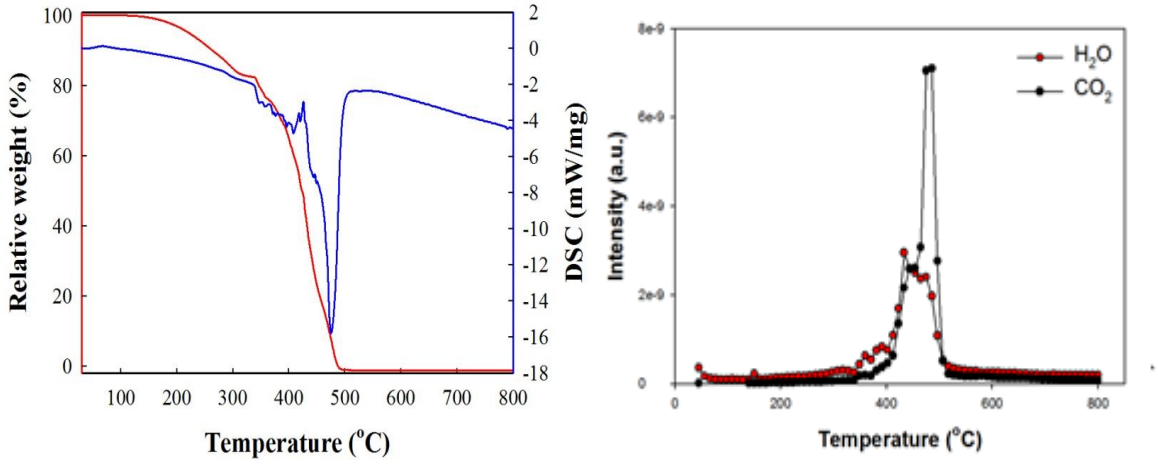

Figure 30 TGA/DSC-MS profiles of bitumen in air atmosphere at 10 ^{o}C/min

The MS curves also confirm that the product was released at higher temperature of 500 ^{o}C and hence the oxidation of oil shale at this temperature may release product due to bitumen and kerogen reaction. The bitumen is expected to decompose at lower temperatures but in this case is found in the T_{max} region which represents the maximum temperature for kerogen pyrolysis. The overlapping nature of kerogen and bitumen in temperature program emphasizes the fact that the catalytic study of kerogen requires the separation of bitumen.

Figure 31 (left) shows FTIR spectrum of the (bitumen) free hydrocarbon. FTIR apply infrared radiation with vibrating dipole moments of molecules. The molecular absorption of

the organic matters with different chemical bonds is reflected in the spectra. Clearly it can be seen that no legible aromatic C-H absorption peak was detected while legible CH_2 asymmetric absorption stretching was detected at 2913 and symmetric CH_2 at 2845 cm^{-1} bridge bands. Moreover, from 1703 cm^{-1} shows C=O carbonyl stretch bands. In addition aliphatic peaks were observed at 1456 to 1372 cm^{-1} represent an absorption band at 1456 cm^{-1} due to CH_3 linear and cyclic CH_2 groups and band at 1372 cm^{-1} related to CH_3 only as can be seen. The FTIR in conjunction with the TGA confirms the bitumen availability in the oil shale.

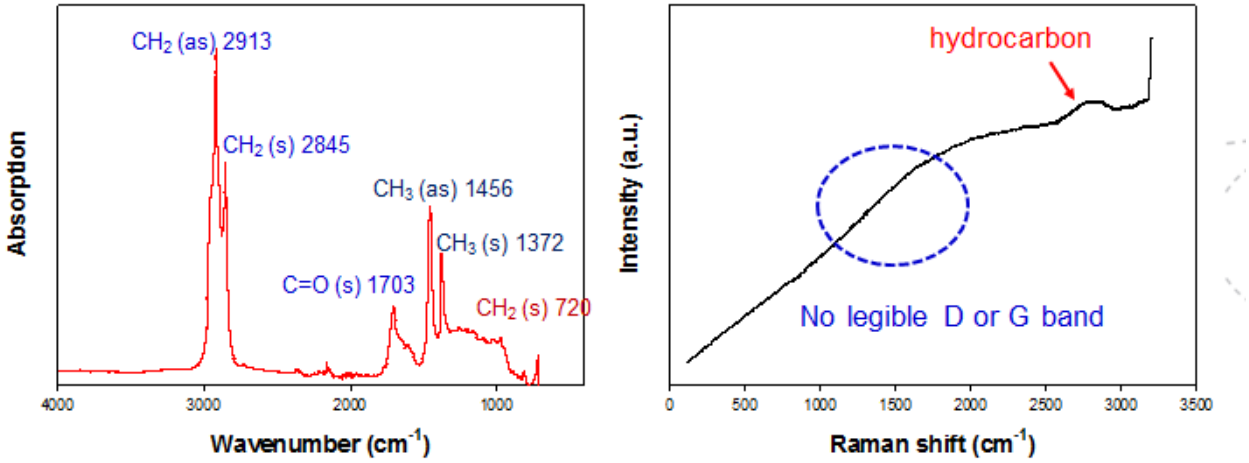

Figure 31 FTIR (left) and Raman (right) spectra of bitumen

The kerogen might have similar properties like the extracted bitumen which originate from the kerogen. The bitumen and kerogen might look similar since the bitumen is a kerogen that has matured by geologic process to yield crude bitumen.

Figure 31 (right) displays the Raman spectra of the bitumen extracted and clearly one can see visible hydrocarbon peak with no aromatics and D and G band. The Raman spectra also confirm that the bitumen has no aromatics as disordered and graphite peak signifies the existence of aromatics and poly-aromatics compounds. This result is also supported by FTIR. It can be seen that the FTIR and Raman model confirms each other. The understanding of the bitumen nature is necessary to probe the characteristics features of the organic rich kerogen, because bitumen was part of kerogen and has cleave into soluble and free hydrocarbon form.

4.3.2 Decarbonated kerogen characterization

The extracted oil shale was further treated with HCl as expressed in **eqt.4** to remove carbonates and thus create additional pores to expose more accessible kerogen surfaces.

$$CaCO_3 + 2HCl = CaCl_2 + H_2O + CO_2 \qquad \mathbf{4}$$

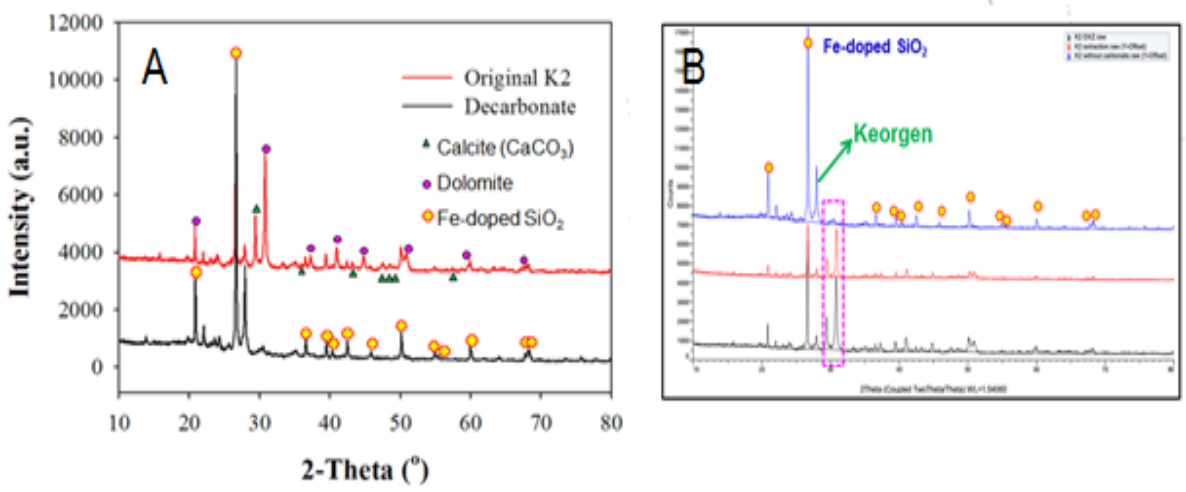

Figure 32 XRD spectra (A) of raw oil shale (red, up curve) and decarbonated oil shale (black, down curve).

The XRD spectrum was used to elucidate whether the carbonates were completely removed, and the results are shown in **Figure 32 (A).** Obviously, the characteristic XRD diffraction peaks and absorption peaks of carbonates disappears, indicating that the HCl treatment guarantees the removal of carbonates in the oil shale. The dominant inorganic compound still available was quartz which was in the form of Fe-doped. Although, the organic matters were not determined but the decarbonate sample has indifferent peak at ca.30 degrees was not visible in the original oil shale due to its high crystallinity. In **Figure 32 (B)** a predicted kerogen peak is seen and this explains that the HCl treated makes the oil shale more accessible for qualitative analysis.

Also, in **Figure 33** the FTIR spectrum of the decarbonated sample and the original oil shale is shown. The blue curve in reference to the peak assignment, clearly no legible aromatic peak was detected. The -CH_2 asymmetric (2913cm^{-1}) and symmetric peak (2845cm^{-1}) are also observed. Also, the C=O functional group is also seen at 1703 cm^{-1} which might represent carbonyl groups The -CH_3 asymmetric and symmetric peaks are also visible at 1459 and 1372 cm^{-1} respectively. This however, confirms that the decarbonated sample contains organic

matter ‘kerogen’ and inorganic component quartz and carbonates which were confirm by FTIR and XRD.

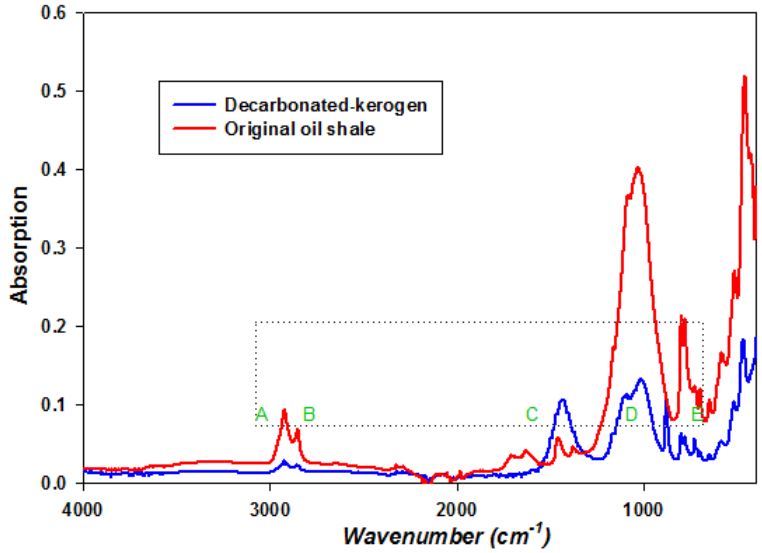

Figure 33 FTIR spectra of raw oil shale (red, up curve) and decarbonated oil shale (blue, down curve (A=CH_2:2930 and 2850, B=CH_3:2960 and 2870 stretching vibration, C=O: 1697, D= O-Si-O (quartz), 775-800 symmetric stretching vibration and E=745 Carbonates).

The organic matters in the oil shale were visible after the bitumen and decarbonated-kerogen were compared with the TGA residue after oxidation in **Figure 34**. The TGA residue after oxidation atmosphere has no peak in the A and B region indicating complete combustion of the organic matters.

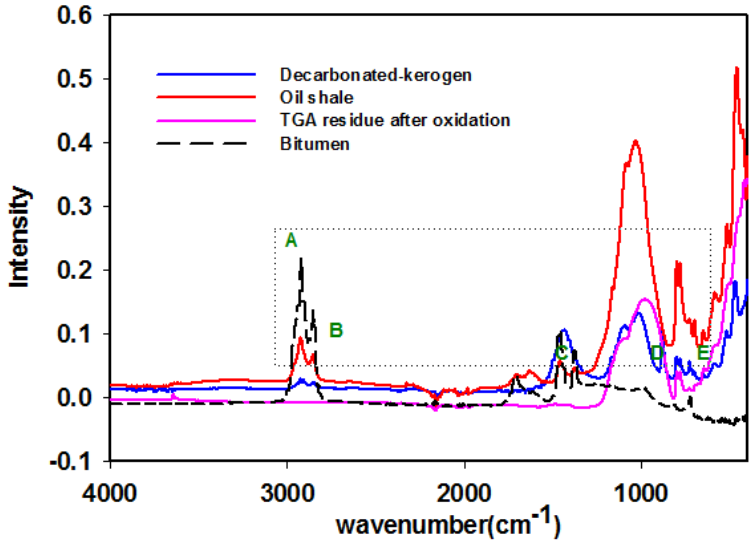

Figure 34 Compared FTIR analysis of the organic matters in an oil shale (A=CH_2:2930 and 2850, B=CH_3:2960 and 2870 stretching vibration, C=O: 1697, D= O-Si-O (quartz), 775-800 symmetric stretching vibration and E=Carbonates

The FTIR spectra according to Ganz and Kalkreuth [68] is used to predict the H/C ratio based on the A factor which is the ratio of aliphatic peak to aliphatic plus carbonyl wavenumber ***(A+B/A+B+C).*** They reported an A factor of ca. 0.86-0.74 for an oil shale type 1 kerogen. The decarbonated-kerogen has an A factor of ca. 0.771 as the aliphatic peaks increases with an increase in maturation while the carbonyl peak decrease. The calculated A factor, further support the fact that the kerogen is type 1. The A factor represent changes in peak intensities due to the aliphatic ends. The A factor is similar to the traditional van Krevelen diagram for H/C ratio. Organic matters when subjected to oxidative atmosphere undergo combustion. The FTIR spectra of the TGA residue in **Figure 34** have no peak at the CH_3 and CH_2 asymmetric and symmetric binding and stretching vibration. This clearly shows that the decarbonated-kerogen and the bitumen were aliphatic in nature and their organic matters have been oxidized to CO_2 and H_2O. Also, from these compared spectra is visible that the inorganic content were still presence even after oxidation and this also complement with XRD results.

Subsequently, the thermal behaviors of decarbonated oil shale were comparatively studied by TGA/DSC. As shown in **Figure 35** the weight loss peak from the decomposition of carbonates disappears in the decarbonated TGA profile which further supports complete removal of carbonates in the original oil shale.

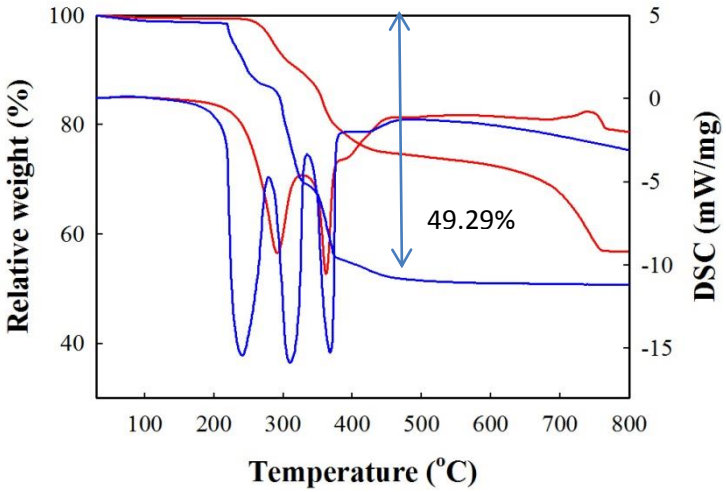

Figure 35 TGA/DSC curves of extracted oil shale (red) and decarbonated oil shale (blue) in air atmosphere at a Heating rate of 10 ^{o}C/min**.**

The surface area for the decarbonated sample increased and the pore volume for the HCl treated however also increased and thus makes the kerogen more accessible to reaction.

This however support the three exothermic peak observe from the decarbonate sample which signifies the conversion of the organic matters into products at 250,300 and 380 ^{o}C with an equivalent energy release of -15 J/(s*g) of decarbonate kerogen.

Moreover, the exothermic peaks of the decarbonated oil shale shift down lower temperature than those of the original oil shale. During the HCl treatment of extracted oil shale, some pores were created and thus the decarbonated-kerogen has more accessible kerogen surfaces to be exposed to air atmosphere, facilitating the conversion of kerogen. Therefore, combining FTIR and TGA helps to identify the organic matter while FTIR and XRD help in classifying the inorganic matter. Also, the comparing the FTIR with XRD proves that the inorganic matter peak of quartz and carbonates are available in original and TGA residue after oxidation.

4.3.3 Energy release and weight loss profile of organic matters in oil shale

To understand the effects of acid dissolution on the organic matters in an oil shale, the extracted bitumen, the DCM and HCl treated samples were compared. The atmosphere used was oxidative to promote total combustion of the organic matters. The overall mechanism for oil shale oxidation can be group into distillation of water, moderate temperature oxidation (MTO) and higher temperature oxidation (HTO). The first stage is moisture discharge, which

relates to the release of water vapor from the mineral layer, ends during the pre-heating of sample around 100 ^{o}C (±15 C) and the release of free hydrocarbon around (200 ^{o}C). Subsequently, some volatile hydrocarbons and kerogen start surfacing and remain up to 540 ^{o}C (±10 C) and further increase in temperature promotes the gasification of the inorganic matter [69].

In **Figure 36** the difference in the observed steps from the TGA profile and the complete oxidation of the bitumen provide enough grounds for the comparison. The distillation stages from room temperatures to 200 ^{o}C represent loss of moisture and some interlayer water from oil shale. The MTO region from 200-600 ^{o}C indicates the stage where most organic matters oxidize. The HTO region represents inorganic matter oxidation. This is made up of the burning of calcite and quartz and other minerals which occurs at higher temperature. The summary of the mass loss at these regions are represented in **Table 8** and as reflected in **Figure 36**.

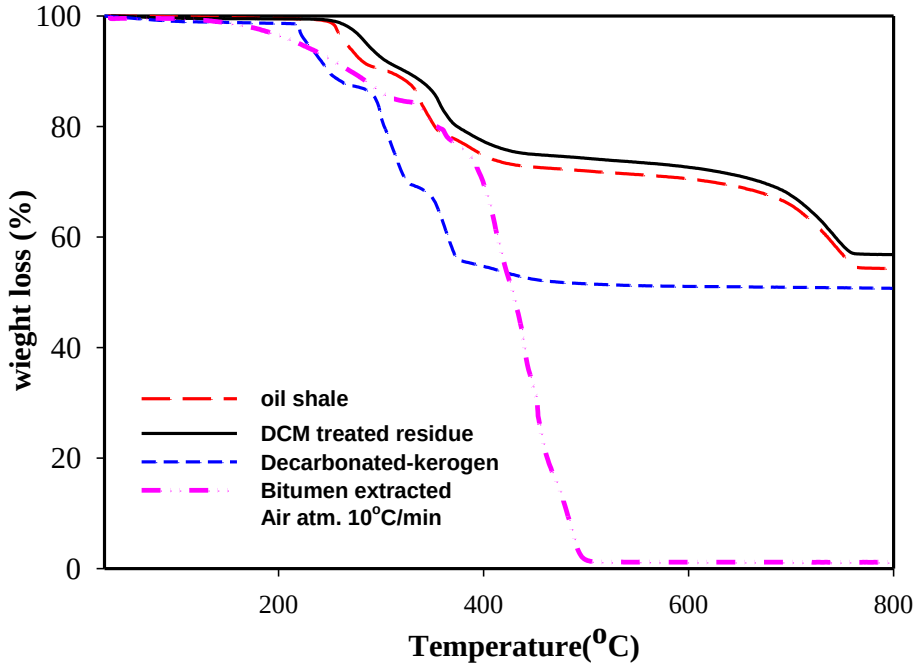

Figure 36 Comparative TGA profiles of the organic matters in oil shale: air atmosphere at a ramp rate of 10 ^{o}C/min

Table 8 Summary of relative weight loss profile of organic matters TGA,MTO (moderate temperature oxidation, HTO (high temperature oxidation): air atmosphere at a ramp rate of 10 ^{o}C/min

Sample	Water distillation (35-200 ^{o}C) Wt (%)	MTO (200-600 ^{o}C) Wt (%)	HTO (600-800 ^{o}C) Wt (%)
Original oil shale	0.44	29.17	15.92
DCM treated	0.59	26.78	15.77
Decarbonated-kerogen	1.23	47.15	0.72
Bitumen	4.78	93.45	1.49

The tabulated results suggests that TGA curve for the decarbonate sample has higher weight loss in the organic region (MTO) and negligible weight loss in the inorganic zone since its calcite and dolomite has been removed. Also, under oxidative atmosphere, the release of CO and CO_2 as seen in the reaction scheme **4, 5** and **6** may react with water to create an acidic environment such as carbonic acid which may decomposed into bicarbonate and Hydrogen ion which can destroy the mineral structure of the rock leading to autocatalytic cracking of the oil shale[70].

$$2C_nR + O_2 = 2CO + 2C_{n-1}R \quad \textbf{5}$$

$$2CO + O_2 = 2CO_2 \quad \textbf{6}$$

$$H_2O + CO_2 = H_2CO_3 = H^+ + HCO^-_3 \quad \textbf{7}$$

The water will be available due to its release in the first zone and will react with CO_2 to yield H^+ environment. The increased in weight loss at the organic region for the original oil shale sample correspond to weight loss from both bitumen and kerogen was ca. 29.17%. Also, both kerogen and inorganic matter (calcite and dolomite) are sources of CO_2 and their decomposition may lead to autocatalysis at the presence of water and hence little addition of oxygen in kerogen pyrolysis will be helpful for further auto-catalytic reaction.

This effect represented by the above reactions confirm the catalytic behavior of the minerals in the oil shale whose decomposition release a lot of CO_2. The energy required to activate the oxidation can also be observed. Moreover, the decarbonate sample has three endothermic

peaks in **Figure 37**. In this figure the DSC curves illustrate the energy release in seconds per gram of pretreated sample. The decarbonated kerogen sample has -15 J/(s*g) of energy release which may correspond to the conversion of organic matters to CO_2 and H_2O at three temperature regions in 250, 300 and 380 ^oC as seen in **Figure 37** as well as the MS peak in **Figure 39**. The thermal conversion of hydrocarbons in the kerogen sample differs from the bitumen oxidation. The bitumen as said before has higher temperature oxidation as compared with the original oil shale which has mineral matrix. The mineral matrix may have contributed auto-catalytically to reduce the temperature of oxidation of the original oil shale as well as low energy release of -10 J/(s*g). The bitumen has higher temperature oxidation around 500 ^oC and also releases the highest energy of -16 J/(s*g).

The energy released data may be helpful in modeling and simulation for topochemical reaction of kerogen in a high pressure fixed bed reactor.

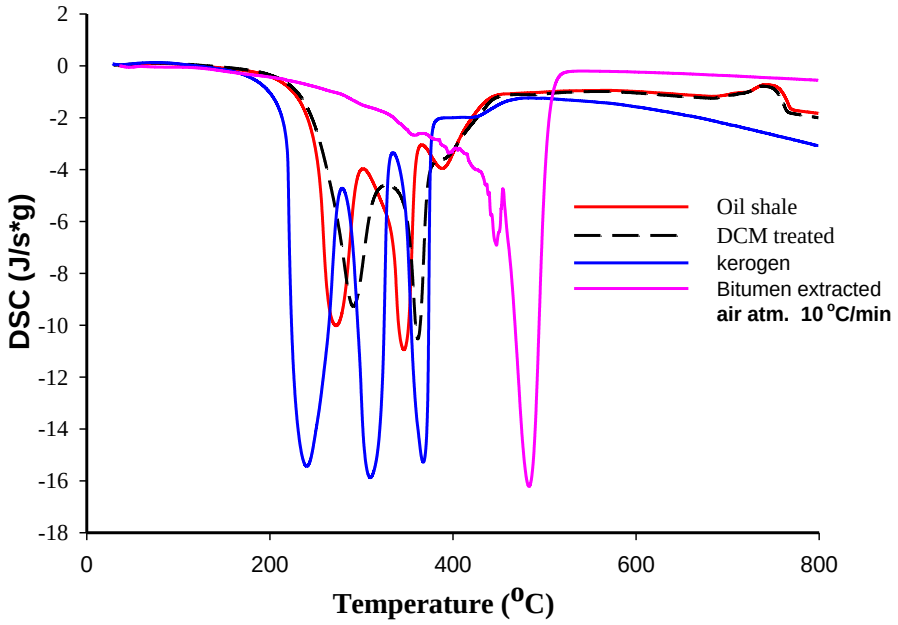

Figure 37 DSC curve of the compared organic matters in oil shale under air atmosphere, 10 ^oC/min

4.3.4 Deconvolution /$NaHCO_3$ decomposition

Deconvolution technique was applied to split peaks in the process of filtering a signal to compensate for unwanted convolution. In this case, the origin software is used to calculate the MS peaks area for standard $NaHCO_3$ compound. The response factor of 0.71 was found from the decomposition reaction (***eqt.8***) below and which has mole ratio of 1for H/C.

$$2NaHCO_3 = Na_2CO_3 + CO_2 + H_2O \qquad \mathbf{8}$$

The **Figure 38** shows the TGA/DSC-MS data for the pure $NaHCO_3$.The residue mass of 63.5% from the mass loss profile represent the ash content (Na_2CO_3) of the theoretical mass of 168 grams of pure $2NaHCO_3$ standard before the reaction. The theoretical value of the ash content correlate with the experimental value with an error margin of 0.64% and therefore the response factor is duly calibrated. The MS detected CO_2 and H_2O peaks and their area gave a response factor of 0.71 from the origin software.

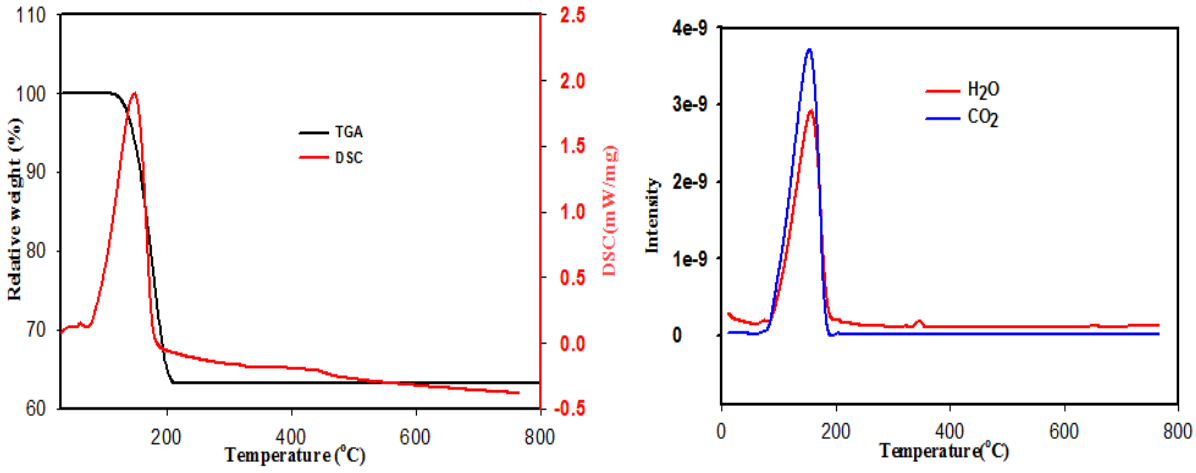

Figure 38 TGA/DSC-MS for pure $NaHCO_3$ used as standard for deconvolution analysis at air atm., heating rate 10 ^{o}C/min

4.3.5 H/C ratio of bitumen and decarbonated-kerogen

The product gases for the oxidation reactions were monitored by mass spectrometer as seen in **Figure 39** and based on the determined response factor the H/C ratio were calculated.

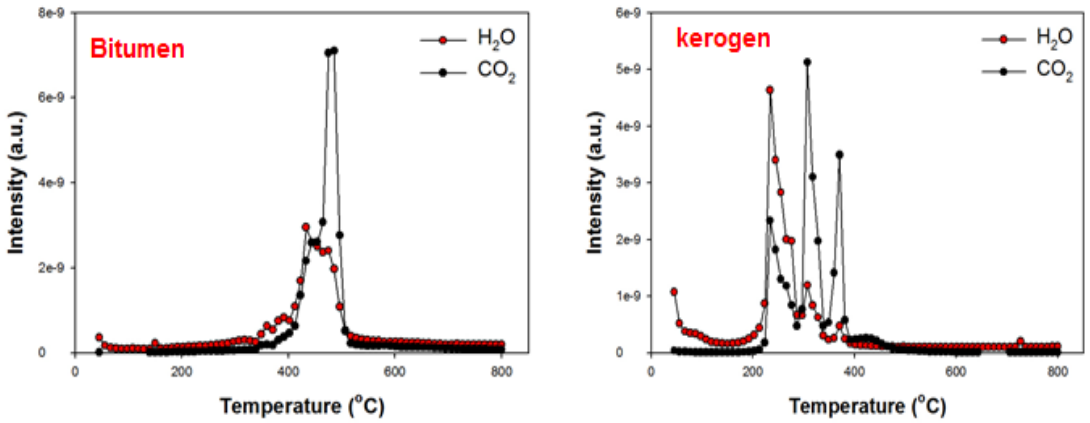

Figure 39 TGA-MS peak for bitumen and kerogen in air atm., heating rate 10 ^{o}C/min

The MS spectrum for the gaseous products from the oxidation of bitumen and HCl treated samples depicts the earlier explanation of product of oxidation from the organic matters. The bitumen sample has one narrow CO_2 peak around 500 ^{o}C and broad water peak on its base shoulder at ca. 450 ^{o}C. However, in the decarbonated-kerogen sample at ca. 200-450 ^{o}C, CO_2 major peaks were detected signifying the oxidation of the decarbonated-kerogen sample. The dominant peaks for CO_2 were found at temperature range of 200-450 ^{o}C at which three main water and CO_2 peaks were detected. The burning of the organic matter at this region could correspond to the kerogen and bitumen oxidation. Also, the disappearance of the CO_2 in the decarbonate sample after 600 ^{o}C is also confirmed as than already by other complementary characterization techniques such as the XRD and FTIR.

The determined response factor was used to calculate the H/C ratio in the bitumen and decarbonate-kerogen samples. The origin software was used to split the peaks and the ratio determined, as seen in **Table 9** the increased in H/C ratio shows in the kerogen shows the aliphatic natures.

Table 9 H/C ratio of bitumen and decarbonated-kerogen from Deconvolution analysis after MS peak splitting

Sample	n_H/n_C
Bitumen	1.87
Decarbonated-kerogen	1.90

This suggests that the oxidized products are linear hydrocarbons that could be made up of alkanes and alkenes (aliphatic). The homologous series for these hydrocarbons is ***–CH$_2$-*** for alkenes and **CH$_{2+n/2}$** for alkanes but as carbon number (n) increases both groups approaches **CH$_2$-** range as reflected from the analysis. This calibration strategy is useful to predict the hydrocarbon nature of the oil shale and was also confirmed by the Py-GC/MS analysis as well. The higher the H/C ratio the richer the source rock for petroleum generation.

4.4 Thermal upgrading of bitumen and kerogen to fuels (TGA/DSC)

The production of crude oil from oil shale by pyrolysis is applied in Enefit 280, Estonia, to process ca. 1.5 million barrels of liquid fuel per year as well as 40 million Nm^3 of high calorific retort gas [21]. In this process oil shale is heated in an inert atmosphere, the vaporized crude is then condensed and upgraded into liquid fuel. The Enefit 280 technology operates with no water, has lower CO_2 emissions as compared with other process where electricity is produced from oil shale and has ca. 1% organic matters in the waste (ash), and as such makes it environmentally benign [23]. However, the high temperatures involved in this process and the cost in reclamation of land in mining of the oil shale still makes the surface retorting process a high cost venture. The role of catalyst in conversion of the organic matters can reduce the high temperature pyrolysis process and as such pyrolysis with and without catalyst as well as energy release is studied with TGA/DSC. Sun et al., studied Huadian oil shale and concluded that the kerogen decomposed within 270-500 ^oC, although the samples are different as in this study an oil shale from Green River was employed but similar temperature range was observed in this study[70].

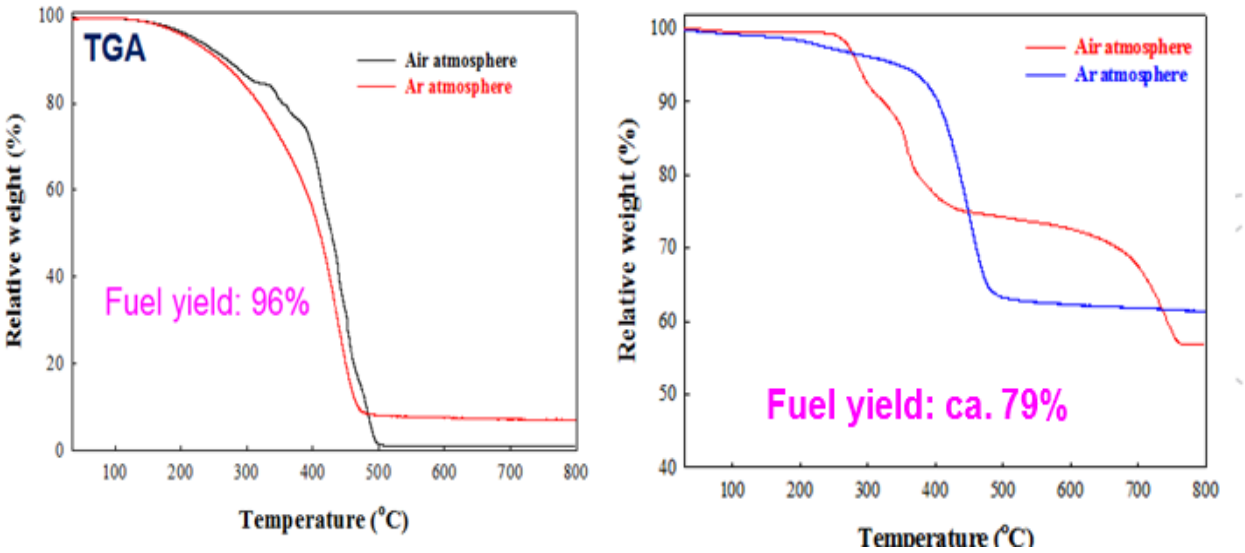

Figure 40 TGA- pyrolysis of bitumen (left) and decarbonated-kerogen (right) in Air and Ar atm. 10 °C/min

Table 10 Percentage of fuel produced by thermal process within the temperature range of 200-550 °C

Process	Bitumen (%)	Kerogen (%)
Pyrolysis	93.0153	38.712
Oxidation	98.8656	49.287
Fuel produced by thermal reaction	**94.083**	**78.544**

From **Figure 40** the decomposition of the organic matters is compared under inert and air atmospheres. The bitumen has maximum weight loss of 93% while kerogen decomposed with weight loss of 38.7%. However, in the oxidation condition different weight loss profile were observed due to the rigorous and exothermic nature of the reaction conditions, an increased weight loss was observed for both organic matters within the organic temperature combustion region form 200-550 °C in both atmospheres. In **Table 10** the overall preview of the conditions are presented.

Furthermore, from the initial source rock evaluation and the functional group characterization it was observed that the organic matters are located in the oil window and aliphatic natures respectively. This initial condition makes is valid to conclude that the decomposed weight loss leads to production of fuel and herein also confirmed by Py-GC/MS. The fuel yield is obtained by dividing pyrolysis condition by oxidation atmosphere and one can clearly see

that the kerogen produced 78.5% yield of fuel under only thermal upgrading. The bitumen although is soluble in organic solvent and is more matured for crude oil generation could not yield 100% due to the presence of some metal ions leading to ash residue after the oxidative atmosphere. The amount of ash presence was not determined but facial observation of Fe-like residue color was seen after both decomposition and oxidative atmospheres. However, from the TGA the remains of the weight loss after oxidation are about 1.13 wt% which could be ascribed as ash or inorganic matters content in the bitumen. The ash content of kerogen under the oxidative atmosphere is 50.7% and the organic content is 49.3% but 38.7% was decomposed. This data suggest that not all the kerogen is decomposed and **ca. 10.6% of organic matters is still remaining** in the residue under such high temperature, non-isothermal thermal upgrading.

The importance of this data suggests that only pyrolysis of kerogen has efficiency of ca. 78.5% fuel yield under very high accessible and pyrolysis atmosphere as results of the analytical procedures applied: A fine oil shale was used with particle size of 10 um, organic extraction with CH_2Cl_2 to increase the thermal accessibility for kerogen as well as the HCl treatment which also led to increase in the surface area and porosity of the kerogen.

4.4.1 Pyrolysis-GC/MS of bitumen and kerogen

Pyrolysis GC/MS (i.e., Py-GC/MS), is an efficient tool to identify and qualitatively and/or quantitatively analyze the pyrolysis products, in which the kerogen-containing sample is heated up to the right temperature to produce separable products that are separated by gas chromatography and detected using mass spectrometry. The evolved gas analysis (EGA)-MS of decarbonated oil shale was carried out. As shown in **Figure 41**, small amounts of volatile components are detected at 100-300 ºC, and fragment ions of hydrocarbons (HCs, m/z=41, 55, 69, and others) and tropylium ion (m/z=91) are observed in the averaged MS spectrum at 360-550 ºC. This indicates that most of the pyrolyzates are hydrocarbons. According to **Figure 41**, the pyrolysis temperature of 550 ^{o}C was chosen to investigate the pyrolysis of decarbonated oil shale. Volatiles/pyrolyzates were cold-trapped using micro jet cryo-trap (MJT) unit and liquid N_2, and the products were assigned by F-search and NIST libraries by kind curtsey of Frontier laboratory in Japan. The T_{max} of 460 ^{o}C was obtained for kerogen pyrolysis.

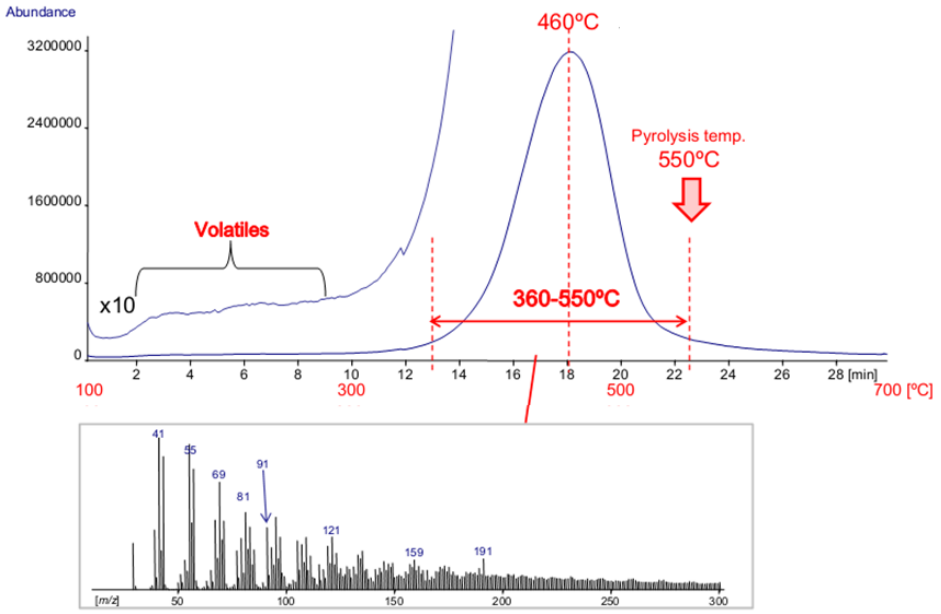

Figure 41 EGA-MS results of decarbonated oil shale.

The extracted ion chromatogram from EGA in **Figure 42** displays major hydrocarbon fragments ions such as m/z of 41, 43,55,57,69, 71 and other characteristics fragment ions such as 191, 159,119 and 91. Moreover, bitumen and Kerogen were further investigated with Py-GC/MS to quantitatively discover their product distribution.

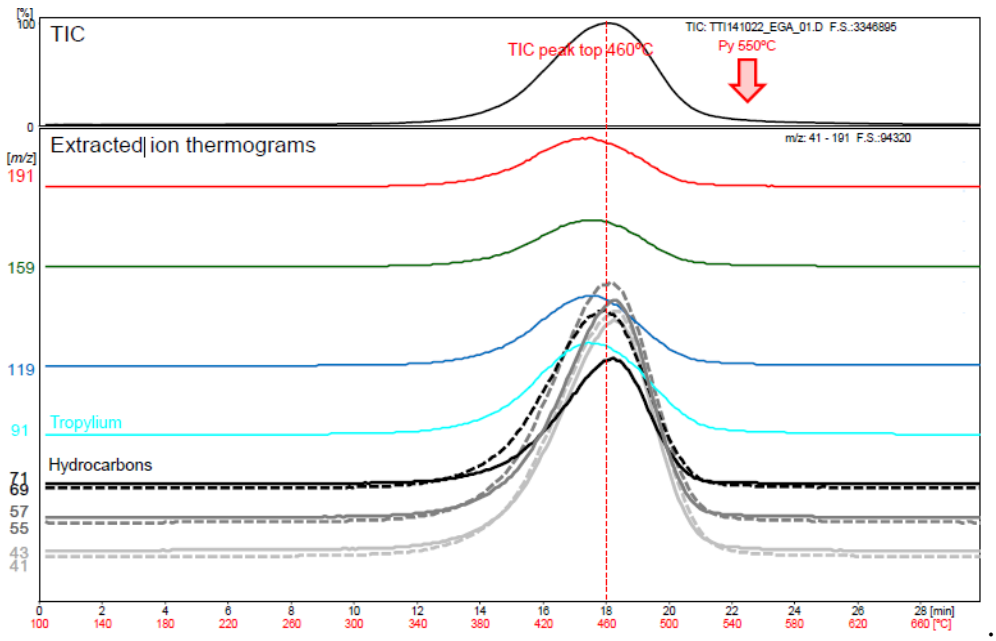

Figure 42 Two-dimensional-display of EGA thermograms obtained by F-Search. It is shown that the EGA TIC peak consists of major hydrocarbon fragment ions (m/z = 41, 43, 55, 57, 69 and 71) and some characteristic fragment ions (m/z=91, 119, 121, and 191).

The total ion chromatogram from Py-GC/MS of extracted bitumen at 550 ^{o}C is show in **Figure 43.**

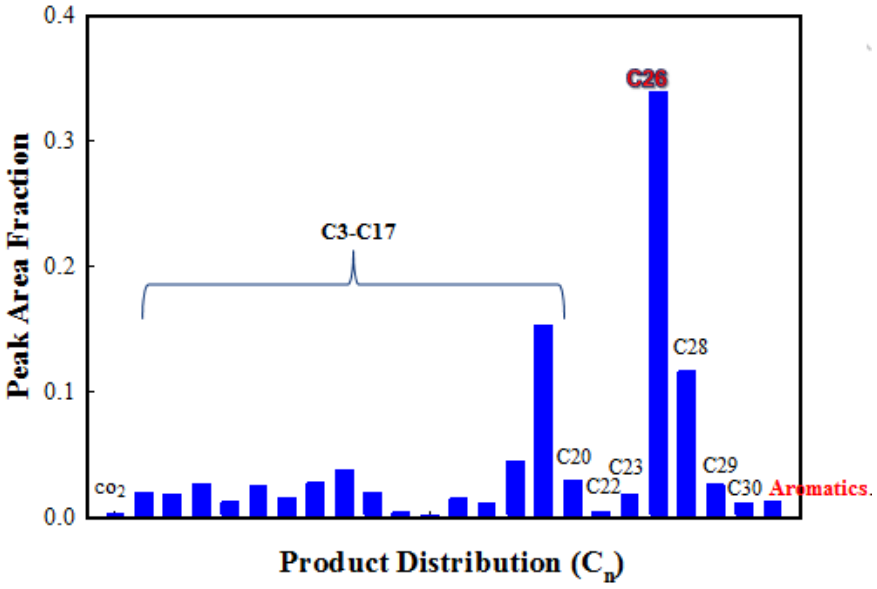

Figure 43 Product distribution of extracted bitumen

The peak area from the integrator function was employed to determine the area fraction of the product distribution of bitumen. The product characteristics are dominated by the homologous series of alkenes/alkanes from C_3 to C_{30}. The Carbon numbers represent the various alkenes and alkane's fraction found at varied retention times and sum together.

The peak assignment after C_{28} has low matching and probabilities from the NIST database and as such background subtraction method from the spectrum was used. The chromatogram of aliphatic olefin and alkane peak at C_9 and C_{10} shows maxima from the first 10 carbon numbers. The alkenes dominate among the homologous series although saturated hydrocarbons were also observed, notably among them were C_{17} and C_{20}. The aromatic such as toluene component is very insignificant and is not surprising that other complementary methods could not identify aromatics. The m/z ratio of C_{17} and C_{28} is found **Figure 44** and clearly hydrocarbon ion fragments are observed. The m/z ratio of 57($C_4H_{10}^{+1}$) has 100% abundance followed by 43 ($C_3H_8^{+1}$) and others. Moreover, in C_{28} the abundance fragment ion is $C_{14}H_{30}^{+7}$ but the matching of polycyclic compounds such as this makes the analysis of the products after C_{28} a bit difficult.

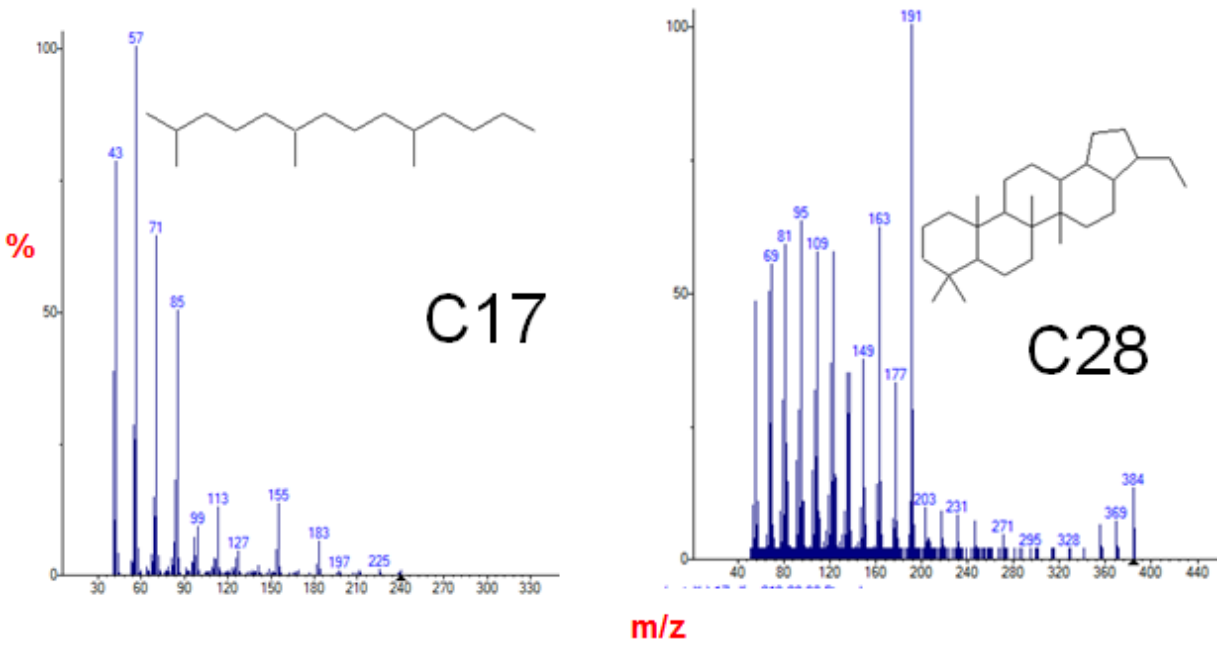

Figure 44 Typical structure of C_{17} and C_{28} and their characteristics fragments ions

These polycyclic structures were not considered to be part of the aliphatic groups and as such ignored but makes the analysis very challenging and as such different approach is required to complement this method.

The product distribution of the bitumen pyrolyzates display in **Figure 45** has hydrocarbons as the major product fraction. The value represents both olefin and saturated hydrocarbon and purely dominated by isomers of aliphatic hydrocarbons.

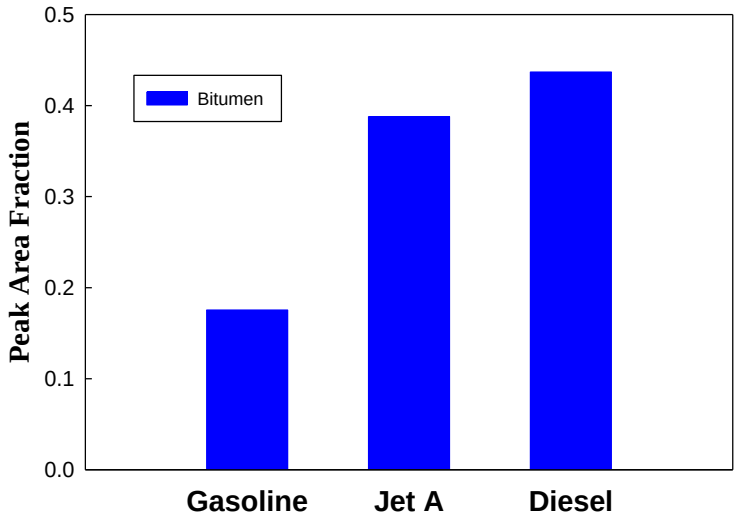

Figure 45 Fuel produced from the pyrolyzates of bitumen from Py-GC/MS at 20 ^{o}C/ min for 550 ^{o}C in Helium atm.

The fuel classification was done based on the petroleum fractions within carbon ranges: **the gasoline (C_4-C_{12}), Jet A (C_8-C_{18}), diesel (C_8-C_{24}).** The gasoline yield has the least peak fraction while the maximum yield of diesel was observed from the bitumen pyrolysis. Also aviation fuel class, Jet A, was found in between the two fuel yields. The dominance of alkene in the pyrolyzates is expected as the hydrocarbon product from bitumen pyrolysis has hydrogen shortage due to bond cleavage and hence there will be a need for subsequent upgrading by hydrogenation to produced stable fuel for the transport usage.

The pyrogram of decarbonated-kerogen and the corresponding magnified pyrogrames are shown in **Figure 46** and **Figure 47.** Obviously, linear hydrocarbons (C_3-C_{35}), hydrogen sulfide, hydrogen chloride, aromatic fragments such as benzene, toluene and xylene (BTX) and naphthalenes as well as characteristic biomarker compounds such as prist-1-ene and hopanes are observed, and the linear hydrocarbons are the major pyrolyzates.

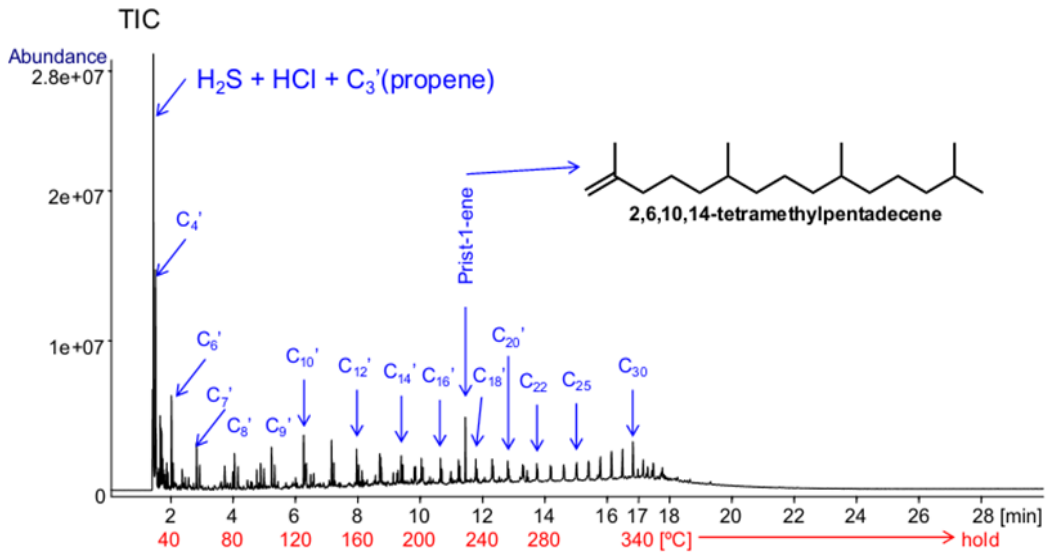

Figure 46 Pyrograme of decarbonated oil shale at 550 ^{o}C

This strongly indicates that this type of oil shale is a promising precursor for the production of crude oils. It is worth mentioning that the hydrogen chloride observed is most likely from the residue of decarbonation of oil shale using HCl treatment.

The n-alkenes and alkanes changing ratios and overlapping peak behaviors in the pyrolyzates of organic matters have been reported in Coburn et al. They reported that the ratio of alkenes to alkanes increases with carbon numbers [71]. The presence of prist-1-ene may indicate that the product is from algae source. Larter et al[72, 73] and Hold et al[72, 73] reported that algae material flash pyrolysis has greater matching for the occurrence of prist-1-ene and its source

is attributed to the phytyl side chain of chlorophyll. Other biomaker observed was hopanes which helps to predict the carbon skeleton of the kerogen evolution. The fact that these biomakers were not found in the bitumen indicates that they were bound to the kerogen core.

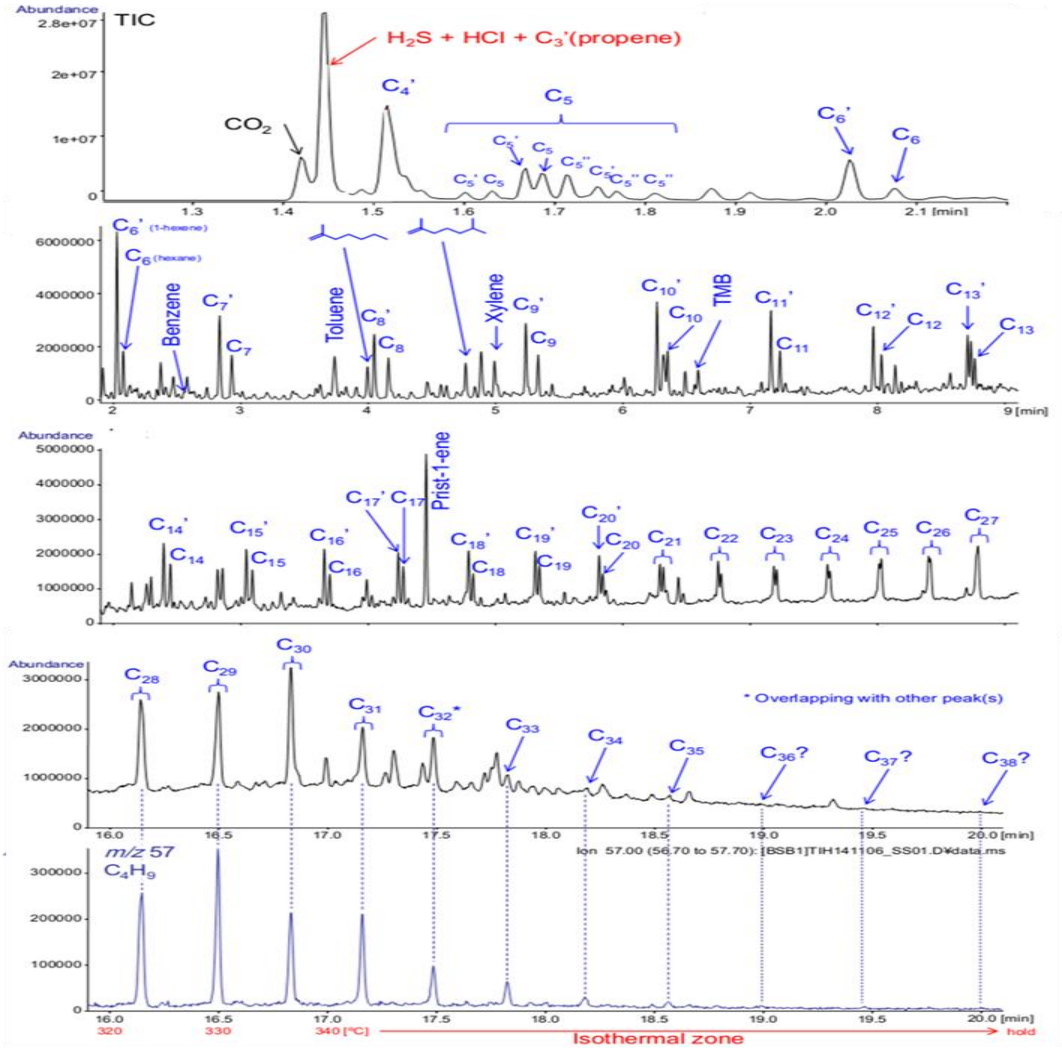

Figure 47 Magnified pyrograms of **Figure 44**

The product distribution (**Figure 48**) displays highest peak area fraction for C_{17} hydrocarbons with peak area ca.0.1. The C_{10} hydrocarbon has the greatest pool fraction pyrolyzates area and an increased in distribution as compared to the bitumen fraction from C_3-C_{10} in comparison with **Figure 45**. Furthermore, the aromatics fraction was also observed as seen in **Figure 47,** benzene, xylene and toluene were observed. Oil prone source rock (Green River oil shale) has been reported by [74] as having higher concentration of hydrocarbons after C_{11+}. This result is also seen in the product distribution plot in **Figure 48**. In contrast gas prone

source rock has greater proportion of its pyrolyzates within C_1-C_4 and some higher contributions from aromatics but the pyrolyzates shows that the kerogen is oil prone. The characteristics full spectrum from C_3-C_{35} from Py-GC/MS also supports the oil richness of the source rock. In determination of the peak area, some carbon numbers whose peak area is less than 1 % of the total peak area were omitted and a typical example is C_{23}.

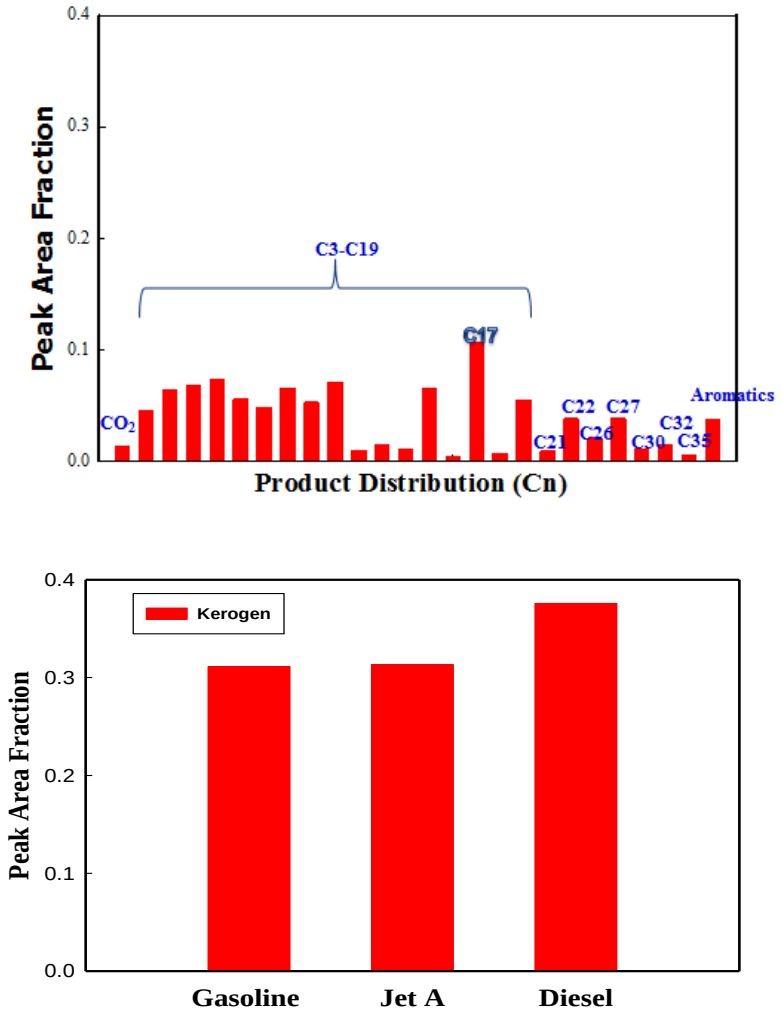

Figure 48 Peak area fraction (up chat), fuel yield (down chat) of kerogen pyrolyzates: Py-GC/MS at 20 ^{o}C/ min for 550 ^{o}C in Helium atm : the gasoline(C_4-C_{12}), Jet A(C_8-C_{18}), diesel(C_8-C_{24}).

The fuel categories of the kerogen were also determined from the similar classification as in bitumen sample: the gasoline (C_4-C_{12}), Jet A (C_8-C_{18}), diesel (C_8-C_{24}). Clearly, **gasoline** and **Jet A** pool show similarities. This indicates that the kerogen has greater fraction of low carbon number range as compared to the bitumen. The bitumen has higher molecular weight of aliphatic hydrocarbons as compared to the kerogen in **Figure 48**. Also observed from the fuel pool are the low quantities from C_{13}-C_{18} which provides the addition from the gasoline to

Jet A fuel. This lower amount makes the Jet A and gasoline chat looks similar. It was also observed that some portion of the hydrocarbons do not formed part of the fuel pool categories due to their higher carbon numbers. The C_{25+} fraction is not captured in these fuel pool chats.

4.5 Catalytic thermal upgrading of kerogen

The thermal upgrading of kerogen gave ca. 79% fuel production yield and ca. 11% of organic matters did not undergone pyrolysis. The organic matters yet to be decomposed are still too high notwithstanding the high temperatures employed. Oil shale structure is non-porous and has flake like features but kerogen employed in this analysis has more exposed surface due to the removal of carbonates and bitumen thus higher yield was expected. The experimental plan makes the up scaling of the catalytic studies a challenge. The particle size distribution is too fine for industrial up scaling however 100% product yield was not achieved. Therefore, in situ conversion of kerogen might require the coupling of catalyst into the process to reduce the high temperatures and promote the product stability to prevent gum formation and polymerization in the subsurface. Several catalysts such as inorganic acids, in-situ formed metal oxide and metal chlorides salts were tested.

Catalyst screening was done based on low temperature shift in the EGA and TGA profile. Lower temperature shift, cost, toxicity, thermal stability and solubility in water were the main factors considered for the catalyst selection. The optimization was done based on loading effects and changing of ramping rate. Also, synergetic effects were tested by initial mineral acids etching and pre-conditioning of kerogen by hydrogen donor.

4.5.1 Active phase identification

The identification and screening of catalyst active phase for this thesis was done mainly by trial and error method. This is because to the best of our knowledge no publication work has been done on the catalytic conversion of kerogen and as such common catalytic principles were employed to screen some potential catalytic materials.

4.5.1.1 Acid catalyst

In **Figure 49**, the effects of phosphoric acid catalyst are compared with decarbonated sample. The pure phosphoric acid decomposed with total mass loss of ca. 36.8% within organic matters pyrolysis temperature region. The sample alone has residual decomposition mass percent of ca. 31.5% and with catalyst the relative mass loss value was ca. 35.2%.

Considering the fact that 10 wt% catalysts were impregnated and 36.8% were decomposed then the residual mass for the catalytic sample should be greater than 36.8%..

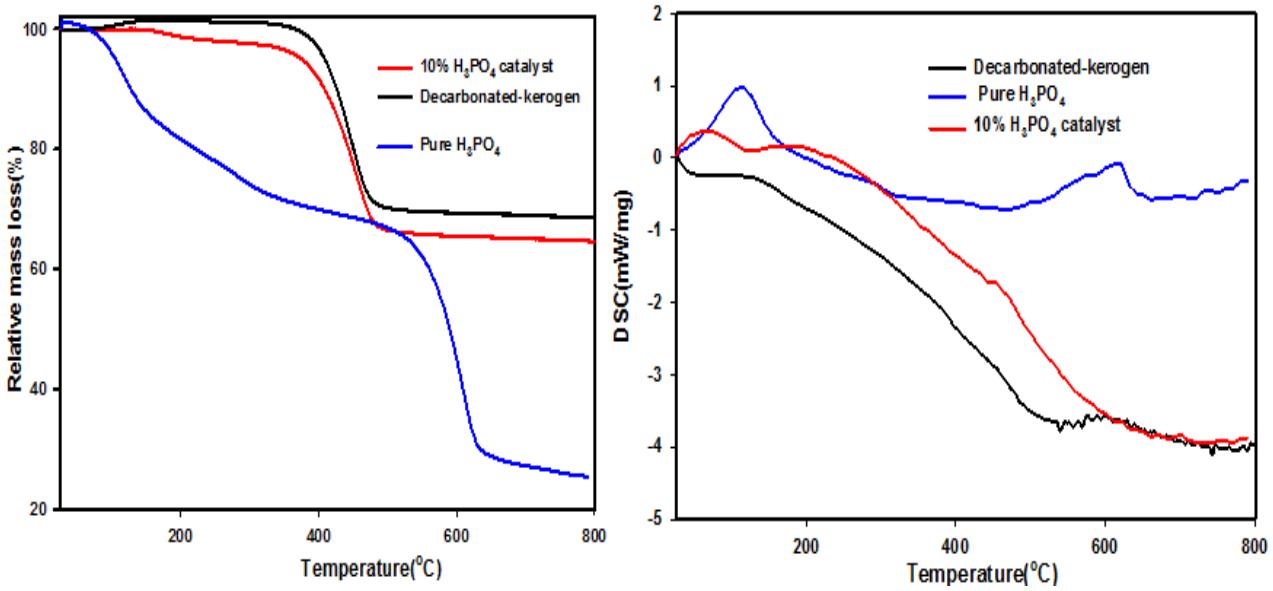

Figure 49 TGA/DSC curve for Phosphoric acid catalyzed decarbonated-kerogen sample: ar atm. 10 ^{o}C/min

The greater portion of the acid decomposed within the kerogen pyrolysis region and is responsible for the lower temperature shift in the catalytic sample. The difference between with and without catalyst residual mass is mainly due to pure acid decomposition on the sample and thus the promotional ability of the phosphoric acid catalyst towards kerogen conversion is insignificant. The decomposition temperature of the acid is from 200-500 ^{o}C and the kerogen decomposition temperature is also within the same zone. The DSC curve clearly supports this fact and the shift in TGA curve with the catalyst is due to the decomposition of the acid and not the residual kerogen organic matters decomposition. Also, from DSC before 200 ^{o}C the endothermic peak for the pure phosphoric acid is also observed. This decomposition is due to crystalline water decomposition of the acid.

The thermal instability of sulphuric acid within the kerogen pyrolysis temperature zone was also observed in **Figure 50**. The change in mass percent of the pure acid is ca. 95.52% from 200 ^{o}C to 550 ^{o}C with a residual content of ca. 4.5%. The catalytic sample has a mass loss of ca. 38.20 % while the blank sample has mass loss of 31.54%. The difference between the catalyzed and un-catalyzed sample is 6.66%. However, in reference to the catalytic loading of 10% onto the sample and incase all the acid decomposed within this region then the mass

loss expected should be greater than ca. 42%. In contrast 38.2 % were observed and considering the residual mass of 4.5% of the pure acid then clearly no promotional effects was observed. The shift in low temperature is due to the decomposition of the pure acid ($H_2SO_4 \rightarrow H_2O + SO_3 + 0.5O_2$).

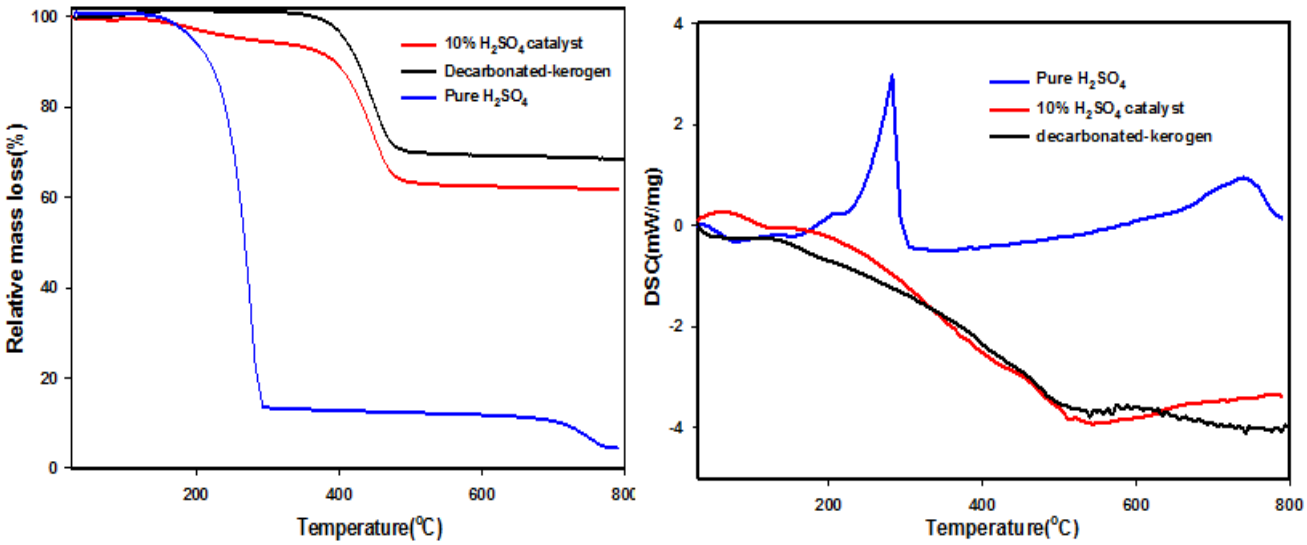

Figure 50 TGA/DSC curve for sulphuric acid catalyzed decarbonated-kerogen sample: ar atm. 10 °C/min

The DSC curve also confirms the endothermic reaction of inorganic content thus water in the pure acid within the organic matters zone at about 250 °C. The decomposition to SO_3 is seen at higher temperature from the DSC curve at which SO_3 decomposed to SO_2 [75].

It is worth to mention that the organic matter decomposition show a continuous decline curve in negative energy release segmental zone as seen in the kerogen sample. A similar characteristic is observed in the catalyzed reaction but no promotional effects are observed from the acids catalyst.

4.5.1.2 In-situ formed metal oxide

Cobalt oxide (CoO) was formed from in-situ decomposition of $Co(NO_3)_2.6H_2O$ precursor. From **Figure 51** the precursor decomposed by the reaction ($Co(NO_3)_2 6H_2O \rightarrow CoO + 2HNO_3 + 5H_2O$) to form the in-situ cobalt oxide [76]. The thermally stable form of the precursor is CoO which is linear at ca. 250 °C to 950 °C. The molecular weight of the precursor is 291.03 g/mol and 25.47% represent the residual mass of the precursor from the

TGA profile. Therefore, the calculated final mass from the experimental value of 25.47% of 291.03 is 74.12 g/mol corresponds to the CoO which has a molecular mass of 74.93 g/mol.

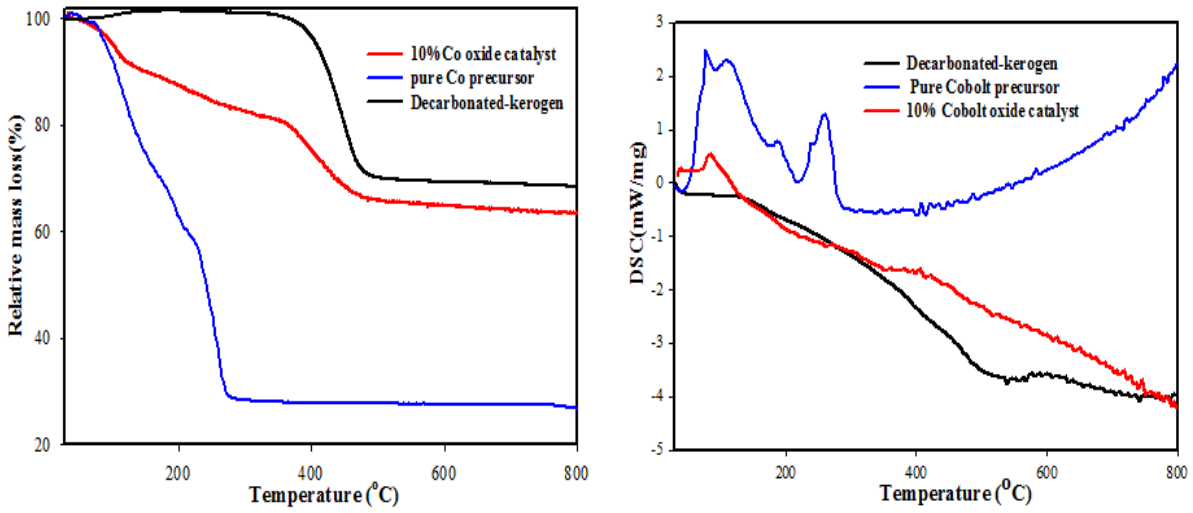

Figure 51 TGA/DSC curve for cobalt oxide (CoO) catalyzed decarbonated-kerogen sample: ar atm. 10 ^{o}C/min

The catalytic performance of the in-situ formed CoO was tested in decarbonated-kerogen sample. The decomposed kerogen in the un-catalyzed reaction was 31.534 %. Considering 74.58 wt% mass loss of the precursor and the initial catalyst load of 10 wt%, the catalytic kerogen sample is expected to have final a mass loss of greater than ca. 38% but the observed mass loss of the catalytic sample was 36.51%. Since the temperature of the organic matter begins after the in-situ formed oxide, it is likely that some of the kerogen was covered by the in-situ formed oxide and not all the kerogen converted. Hence, the shift in lower temperature from the catalyzed sample is due to the decomposition of the precursor and as such no promotional effect was observed from the CoO catalyst.

Also, $Ni(NO_3)_2 6H_2O$) precursor was tested to produce in-situ formed nickel(IV)oxide and according to[76] the precursor decomposed by series of reactions. The final thermally intermediately formed oxide is in the form of NiO_2 which is formed at ca. 250 ^{o}C and stays up-to 400 ^{o}C and higher. Final decomposition of $NiO_2$to NiO was observed from XRD[76]. Similar decomposition profile was observed from the TGA profile for the pure nickel precursor. From the profile, clearly the precursor mass loss is ca. 67.4 % with a residual mass of 32.6%. The molecular mass of the precursor is 290.81 g/mol and 32.6% of it gives calculated value of 94.80 g/mol which is almost equal to the theoretical mass

of $NiO_2(90.6\ g/mol)$ and hence the in-situ oxide is closed to Ni^{4+} than NiO (74 g/mol) oxide. The in-situ formed oxide, Ni^{+}, was tested in an impregnated kerogen sample. The final mass loss of the catalytic sample was 70.22% which is less than un-catalyzed sample mass loss. Hence, no catalytic performance from the in-situ nickel oxide was observed.

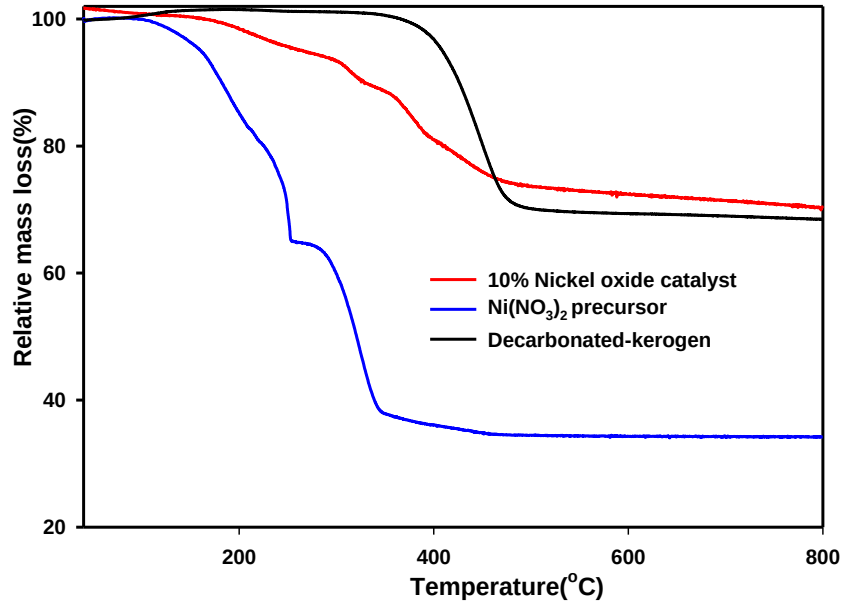

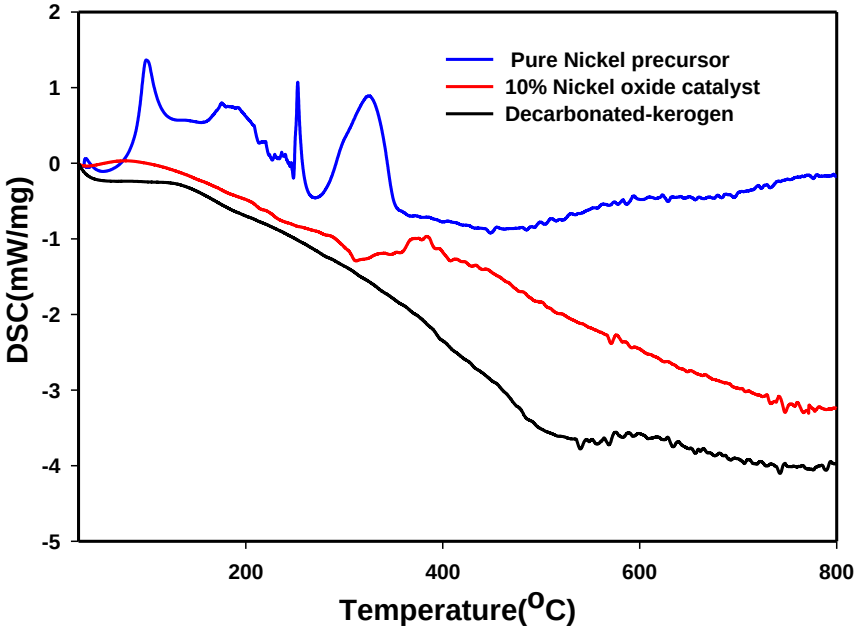

Figure 52 TGA/DSC curve for Nickel (IV) oxide catalyzed decarbonated-kerogen sample: ar atm. 10 ^{o}C/min

The kerogen sample was covered with the oxide and hence no promotional effects were observed from the catalyst.

4.5.1.3 Reducing agent catalyst

Subsequently, hydrogen donating compound was tested to promote hydrogenolysis and hydrogenation for the cleavage of C-C bond to yield olefin and paraffin from the complex heterogeneous kerogen compound. From **Figure 53** the TGA and DSC profile of the pure tetralin is observed. It is clearly seen that the tetralin decomposed before the kerogen decomposition temperature zone. The residual mass of 0.198% is seen from the pure tetralin. It is however expected that enough hydrogen might have produced to promote the hydrogenolysis and hydrogenation of kerogen decomposition to fuels. Moreover, the tetralin treated sample has a final mass loss of 39.21% while the un-catalyzed sample has a mass loss of 31.54%. Considering 10 wt% loaded tetralin on the kerogen sample and almost 100% decomposition of the pure tetralin, it is however unexpected to have final mass loss of less than ca. 41 wt% catalyzed sample. Therefore, the low temperature shift and steadily change in slope is due to decomposition of pure tetralin and thus no significant catalytic effects were seen.

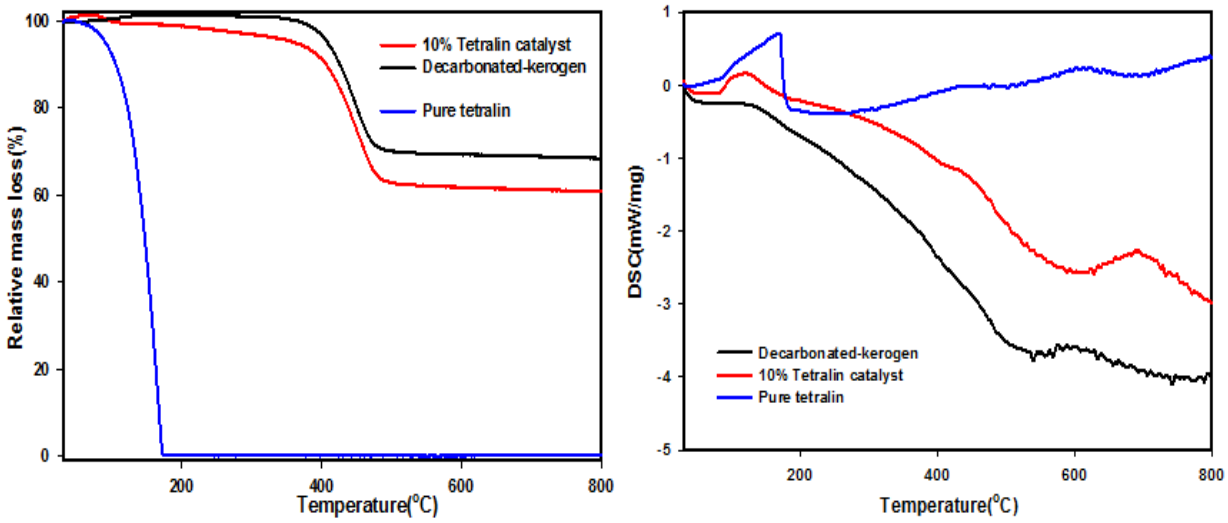

Figure 53 TGA/DSC curve for Tetralin catalyzed decarbonated-kerogen sample: ar atm. 10 ^{o}C/min

The observed mass loss of the catalyzed reaction is 39.21 % and hence the shift in low temperature is due to the decomposition of pure tetralin and no promotional effect was observed from the reducing agent catalysis.

4.5.1.4 Metal chlorides

Chlorides metal ions are thermally stable within the kerogen decomposition region. Cu^{2+}, Fe^{2+}, V^{2+} and Mn^{2+} have decomposition temperatures of 992, 1023, 1506, and 1200^{o}C respectively. An initial 10 wt % catalyst loading was tested on decarbonated-kerogen samples. From **Figure 54** the TGA profile of the metal ions is compared.

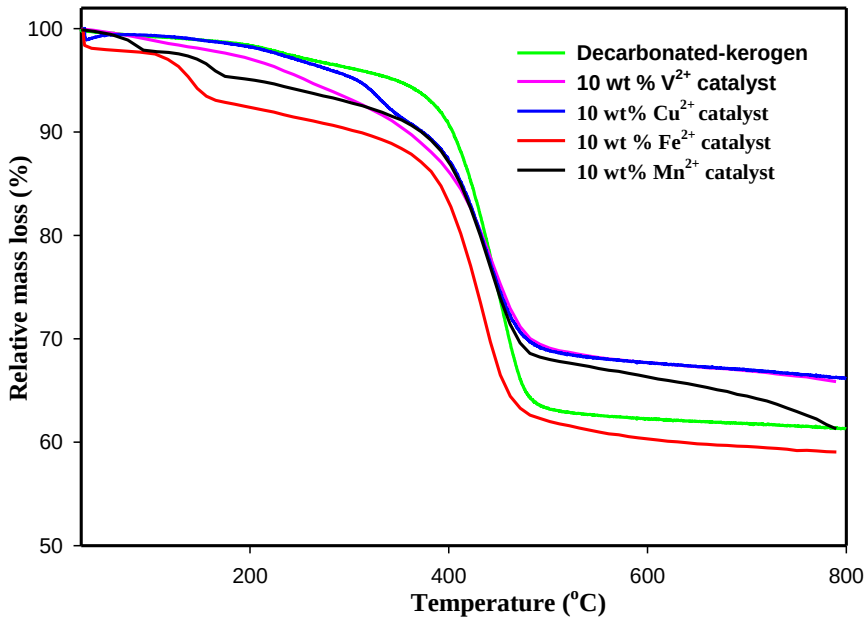

Figure 54 TGA curve for metal chlorides catalyzed decarbonated-kerogen sample

The Mn and V have initial shift in lower temperature from the decarbonated-kerogen sample. Fe also recorded the highest shift in lower temperature from the profile. However, $CuCl_2 \circ 2H_2O$ catalyzed shows **credible low temperature shift** in slope in the kerogen decomposition region from **250-500 ^{o}C**. Almost all the thermally stable chloride catalyst sample tested, started decomposing before the actual kerogen decomposition region with the exception of Cu^{2+}.

It is however, difficult to understand why the $FeCl_2$, VCl_2 and $MnCl_2$ catalyst decomposed before their original decomposition temperatures. The DSC curve in **Figure 55** illustrates the energy release profile and clearly at ***point A*** decomposition of crystalline water was observed

Thus, the shift in lower temperature of these catalysts before the kerogen decomposition zone is due to crystalline water decomposition. The anhydrous form of these metal ions might have affected their reaction with water during their preparation although they were dried in a vacuum oven to remove water. The crystalline water might have been formed during the catalyst preparation and it is however not clear not clear about their states and formation. The similitude between the kerogen sample and Cu treated sample in terms of energy and TGA profile indicates some catalytic role of Cu^{2+}. The final mass loss of the copper catalyst was not significant but the lower temperature shift makes this catalyst a credible one to study.

The active phase of the catalyst was also tested to identify whether the cation and/ or the anion has catalytic effects. The initial study seen **Figure 54** and **55** is a based on the 10 wt% loading of the cation. Therefore, 10 ***wt% of Cl ion*** was impregnated onto the kerogen sample to identify the catalytic effects of the anion. From **Figure 56** the potassium chloride treated sample was compared with kerogen sample. The TGA profile shows that no promotional mass loss was observed from the catalyzed reaction. The final mass loss of the catalyzed reaction is less than the sample and as such no effects from the chloride ion was observed.

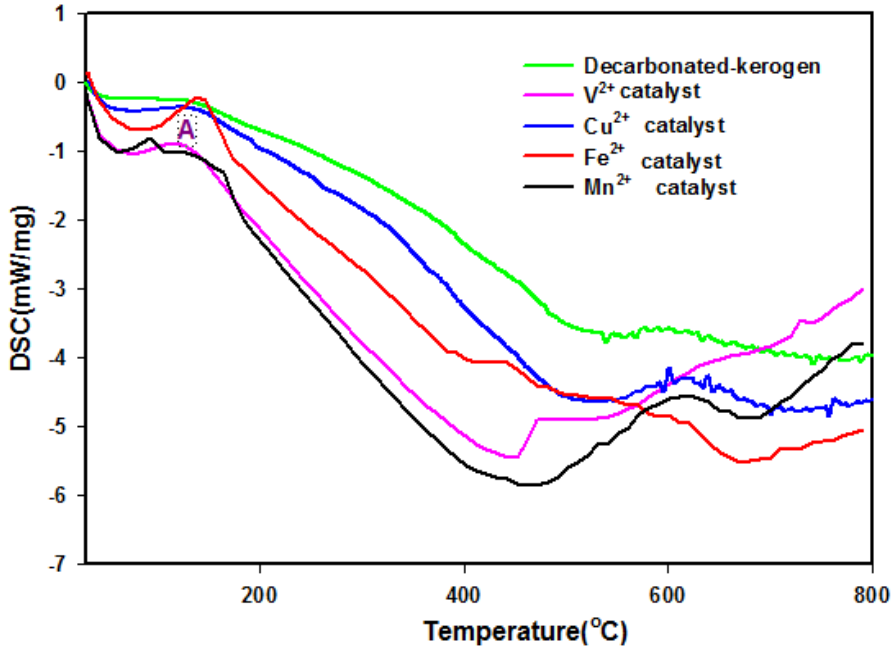

Figure 55 DSC curve for metal chlorides catalyzed decarbonated-kerogen sample, (A= point of crystalline water decomposition)

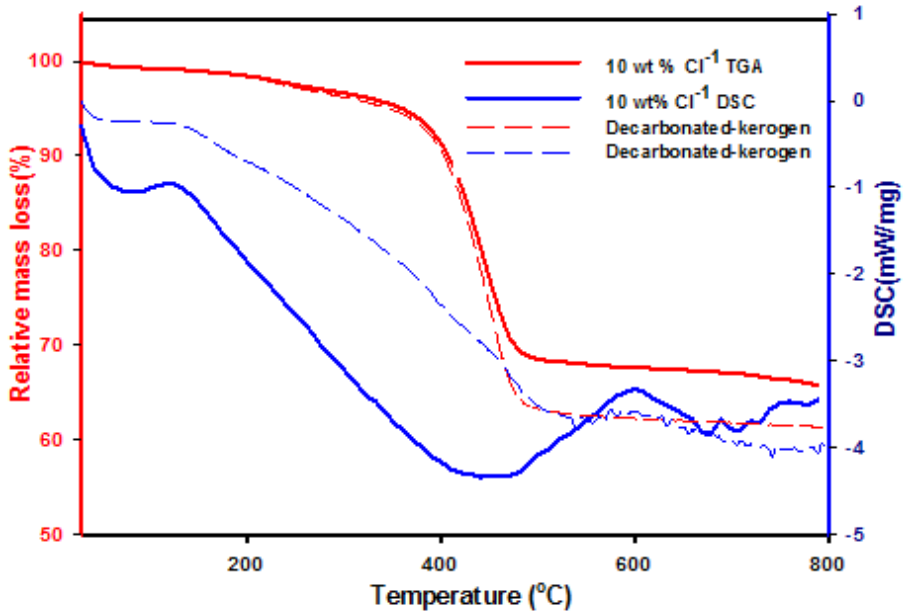

Figure 56 TGA/DSC curve for potassium chloride (KCl) catalyzed decarbonated-kerogen sample

4.5.2 Optimization

Cu^{2+} catalyst was selected and optimized based on variable loading and heating rate.

4.5.2.1 Effects of Cu^{2+} loading

Variable Cu^{2+} catalyst loading were tested. Figure 57 shows the TGA/DSC profile of comparison.

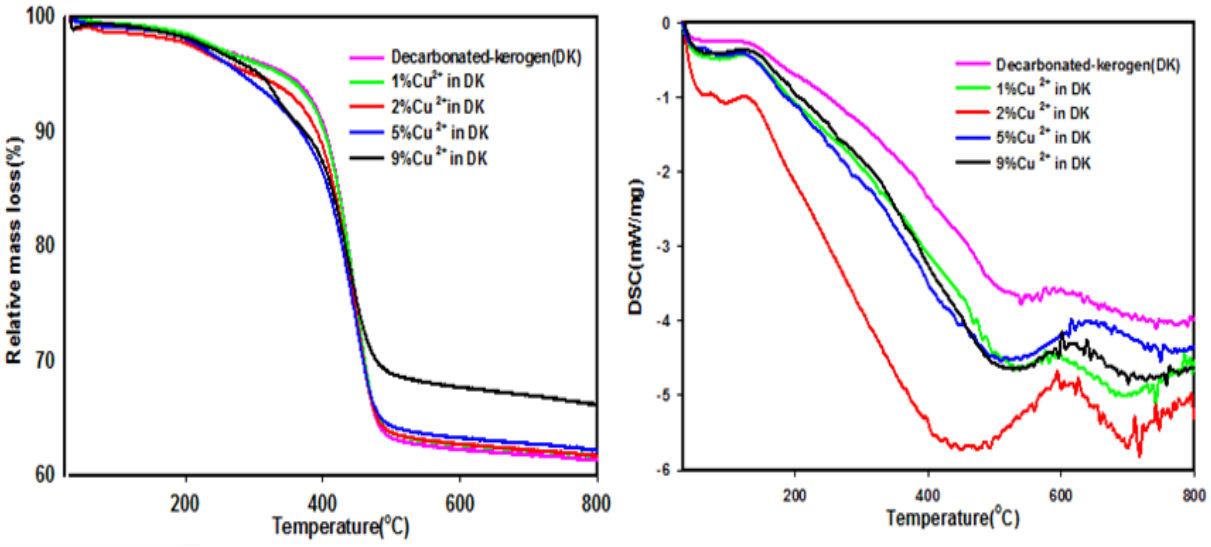

Figure 57 TGA/DSC profile for optimization of $CuCl_2 \circ 2H_2O$ catalyzed pyrolysis of kerogen

It was observed that 9 wt% shows less mass loss and it could be possible that some catalyst covered the kerogen surface and hindered thermal reaction but shifted more to lower temperature than 1 and 2 wt %. 1 and 2 wt % loading has less promotional effects in low temperature shift but its overall mass loss is similar to the decarbonated-kerogen. The 5 wt% Cu^{2+} catalyst loading was seen to be optimum loading since it has the highest shift in lower temperature.

The lower loading was further compared in EGA shown in **Figure 58**. Clearly, 1 and 2 wt % is seen to exhibit lower temperature decomposition at ca. 150 ^{o}C and 240 ^{o}C respectively. The decomposed lower temperature peak might be due the conversion of kerogen to fuel since the decarbonated kerogen sample did not show such a lower temperature peak.

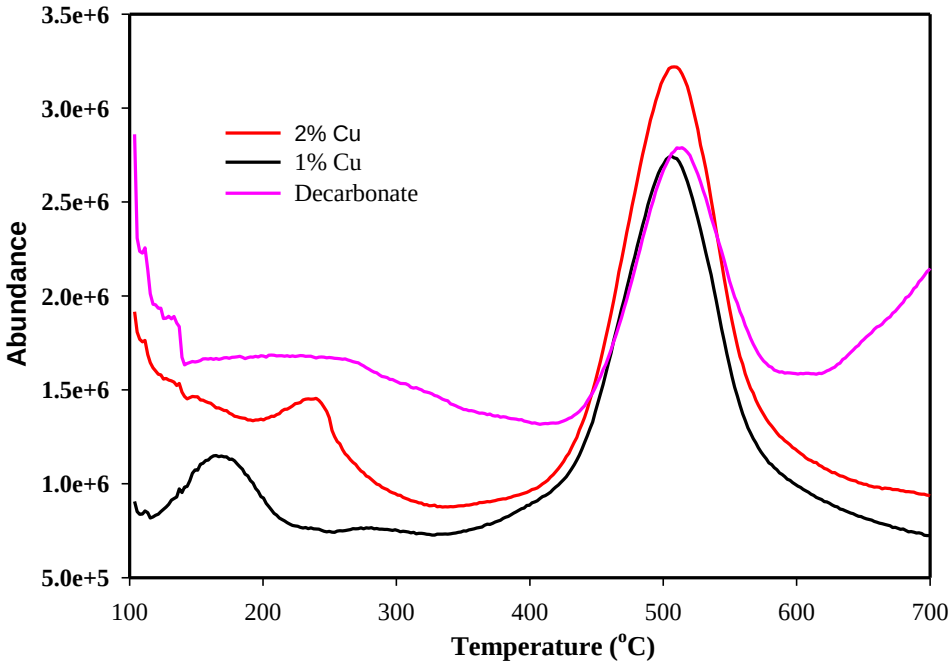

Figure 58 EGA pyrograms of the lowest Cu^{2+} catalyst loading

With 5 wt % Cu loading clearer shift in lower temperature was observed. In Figure 59 **a lower temperature shift in 30 °C was seen from the highest intense pyrograms.** The catalyst sample shows a shift in lower temperature and an in optimum two characteristics peaks were seen, each peak correspond to decomposition of organic matters. It is however; worth to mention that the impact of the 5 wt% catalyst was significant as a decrease in temperature of 30 °C may have substantial cost reduction in industrial scale, although detail cost estimates was not done. In conclusion, comparing TGA and EGA similar catalytic effects were observed and any equipment's complement each other.

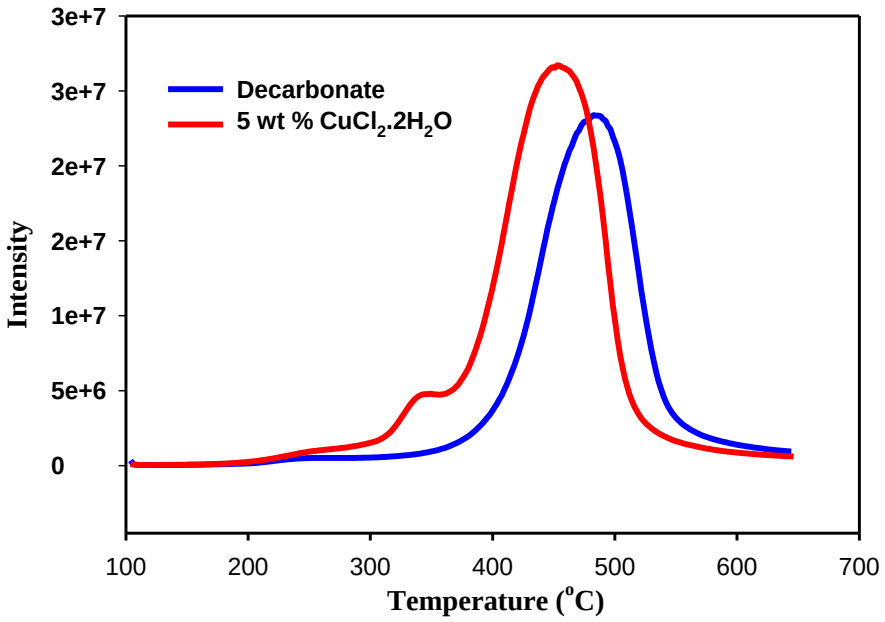

Figure 59 Optimized loading of 5 wt% Cu^{2+}: Ar atm. 25°C/min

4.5.2.2 Effects of variable ramping rate on selected catalyst

The 5 wt% of the selected Cu^{2+} catalyst was further optimized in variable ramping rate. This was done to visualize the effects of the changing the non-isothermal conditions. In practice it is desirable to apply non-isothermal techniques as constant heating rate are less demanding as compared to constant temperature process and most especially in exothermic reactions. Also, because of known heating rate the time of experiment is also reduced and mostly is easy to upscale to the constant heating rate procedures as applied in industrially ex-situ process [69]. In Figure 60 the results of the kerogen analysis during pyrolysis with variable heating rates were compared. The profile has three zones, moisture release, and devolatization and char formation. A linear curve was observed in the moisture release zone in the entire heating rates up to 250 °C at which the kerogen decomposition started and ended at 450 °C for the Cu^{2+} catalyst samples. Also, observed was a shift in lower temperature for the lowest heating rate. In 2 °C/min, a clear shift in lower temperature was seen in the kerogen decomposition zone and remains flat after the pyrolysis reaction. Furthermore, 5 and 10 °C/min also exhibited a shift in slope from the 10 °C/min decarbonated-kerogen sample. The kerogen sample in comparison with the catalyst sample at same heating rate demonstrated a difference in slope. The catalyst sample at 10 °C/min has lower temperature shift as compared to the un-catalyzed

sample. The overall pyrolysis reaction occurs much slowly at lower heating rate and much char was formed. At higher heating rate the several secondary pyrolysis reactions may occur and which led to lower mass loss profile in the TGA results. Although lower heating rate recorded the highest shift in temperatures the overall mass loss was smaller as compared to higher heating rate in the kerogen decomposition zone.

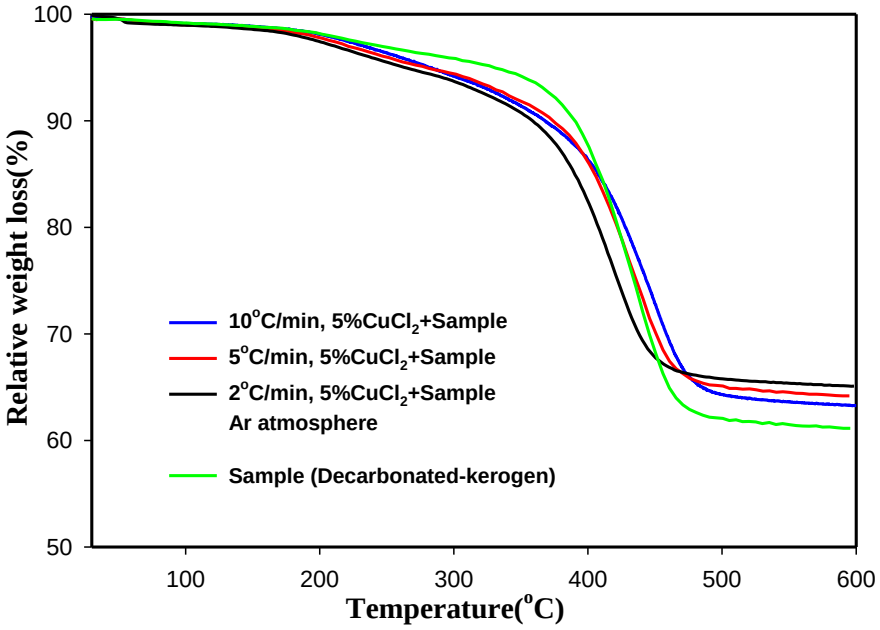

Figure 60 (TGA profile) effects of variable ramping rate on selected catalyst: 10 ^{o}C/min in Ar atmosphere for sample

Therefore, there is an existence of a tradeoff between lower temperature shift and extent of organic matters conversion. Lastly, all the heating rates have no influence in the char formation as stable profile was observed from 500 ^{o}C- 600 ^{o}C.

4.5.3 Synergistic effect

Acid and reducing agent catalyst alone were not active and were however combined with the selected metal chloride to see if any combined effect will lead to any promotional catalytic effects. The synergy effects as applied in several catalyst studies were tested on the decarbonated-kerogen sample.

4.5.3.1 Acid conditioning

The H_2SO_4 catalyst alone as discussed before a have no effect. The combination of the acid with 5 wt% Cu^{2+} was tested on kerogen samples. In **Figure 61** the pure acid has mass loss of

95.5% and the sample alone has a mass loss of 31.46. The catalyst sample had a mass loss of 38.2 with a percentage increase in mass loss of ca. 7 %. However, considering the initial catalyst loading, 9.5 wt % loss was observed from the catalyst and as such the catalytic sample should have a mass loss greater than ca. 40% but catalyst alone gave ca. 38.2%. Meanwhile, the addition of Cu^{2+} catalyst led to a mass loss of 49.50% and as Cu^{2+} is thermally stable within the kerogen decomposition region the increase in mass loss and shift in lower temperature is due to synergistic effects of Cu^{2+} and H_2SO_4.

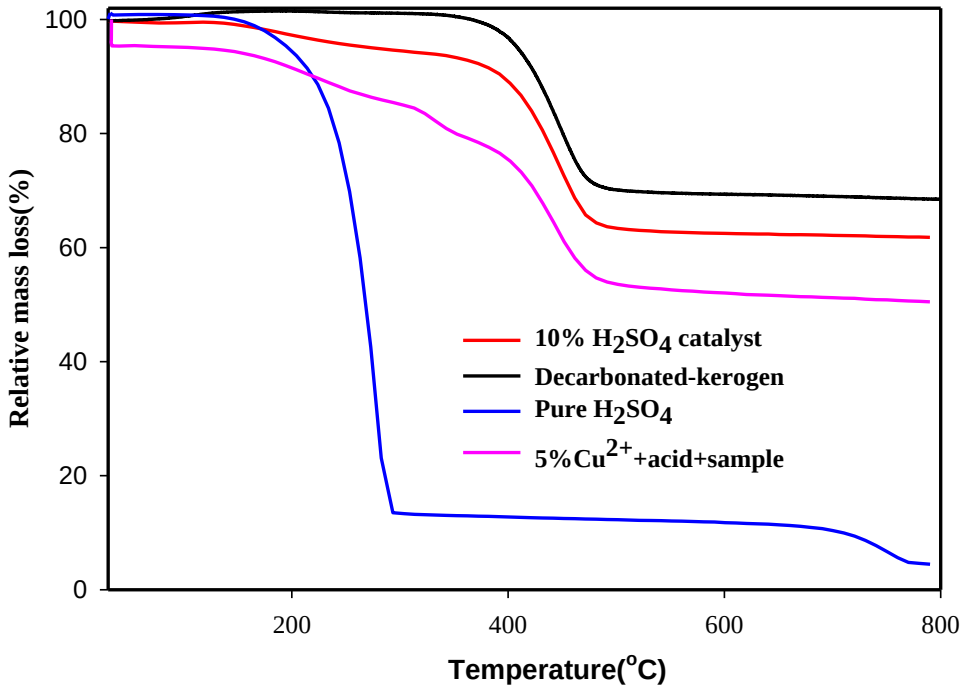

Figure 61 Synergistic effects from H_2SO_4 and Cu^{2+} catalyst: TGA profile at 10 ^{o}C/min in Ar atmosphere

In addition, from Figure 62 the synergy of H_3PO_4 and Cu^{2+} catalyst were investigated. The acid alone decomposed in the kerogen decomposition zone with a mass loss of 36.8% but with the combination of Cu^{2+} catalyst the mass loss was 35.9% as seen in Figure 62. The expected mass loss should be greater than ca. 39%. However, the inclusion of the Cu^{2+} catalyst, the mass loss profile was unchanged but is however difficult to assigned the shift in the low temperature to synergistic effects.

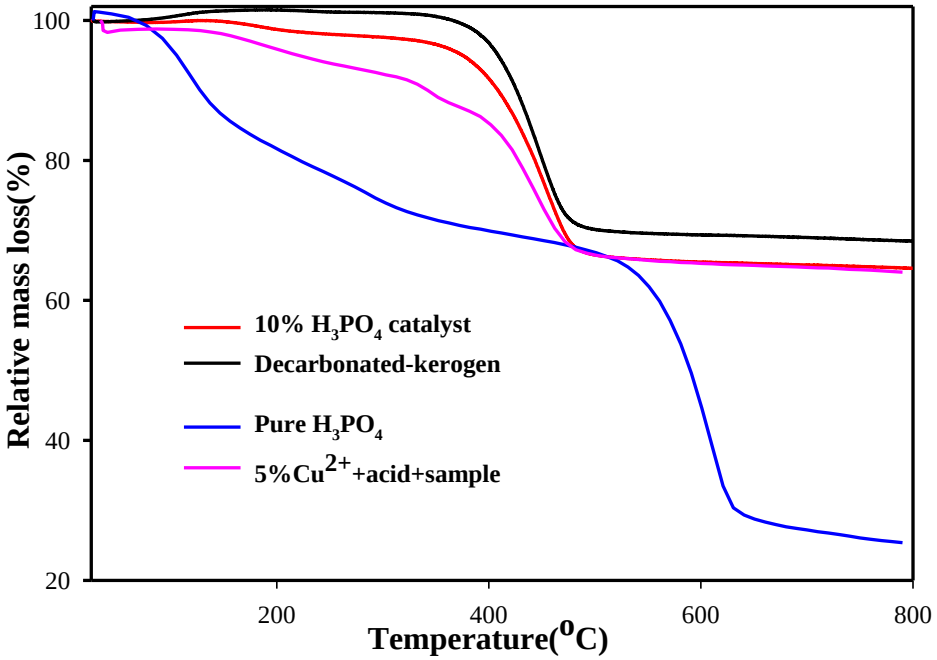

Figure 62 Synergistic effects from H_3PO_4 and Cu^{2+} catalyst: TGA profile at 10 ^{o}C/min in Ar atmosphere

4.5.3.2 Hydrogen donating compound

Subsequently, the combined effects of tetralin and Cu^{2+} catalyst were also probe. The tetralin is hydrogen donating compound and could initiate hydrogenation reaction to break the complex kerogen structure. As seen in Figure 63 the tetralin decomposed with mass loss of 99.9% before the kerogen decomposing region. The kerogen sample alone decomposed at a mass loss of 31.54 % and the catalytic sample also decomposed to 39.21%. Considering the mass loss of pure tetralin in 10 wt% loading a final mass loss greater than 41% is expected but 35.75 was observed. This indicates the extent of conversion of the kerogen was not enhanced but however the shift in lower temperature and the nature of the slope could suggest catalytic effects.

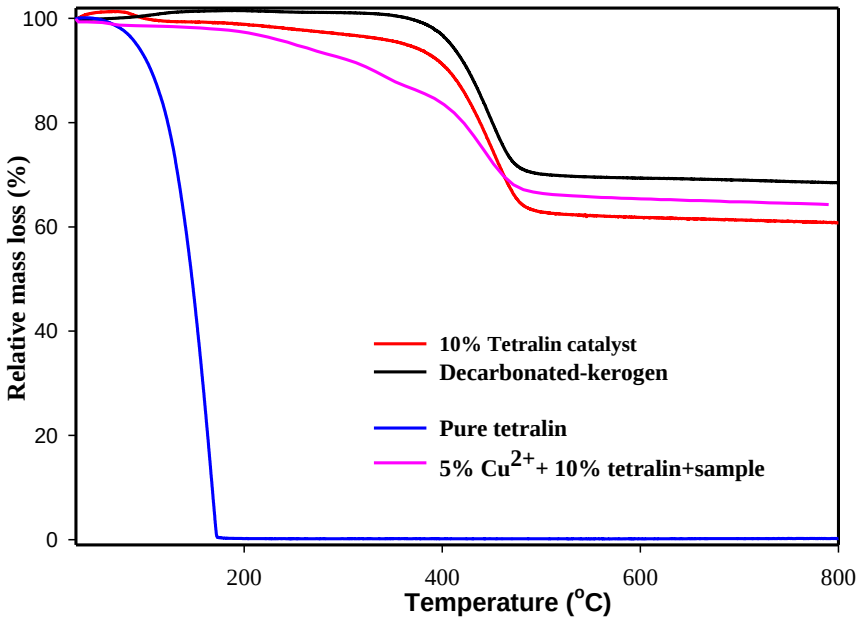

Figure 63 Synergistic effects from tetralin and Cu^{2+} catalyst: TGA profile at 10 ^{o}C/min in Ar atmosphere

4.6 Fuel produced from 5 wt % Cu $^{2+}$ catalysts

The pyrolyzates of Cu^{2+} optimized sample is seen in **Figure 64**. Clearly aliphatic hydrocarbons peaks were observed. The total ion chromatogram has products from C_4-C_{21} with products whose peak areas are less than 1 % of the total threshold is rejected from the integrator. Also, the background subtraction method was applied to obtain all products. One can visibly see that the higher carbon obtained was C_{21}. The kerogen sample already has higher carbon numbers up to C_{35} but with the use of a catalyst the carbon number reduced to C_{21}. This indicates the promotional effects of the catalyst to cleave the higher carbon numbers to smaller ones. The aromatics content peak area also increases and as such the catalyst might have facilitated aromatization reaction but this effect needs further investigations. The highest carbon number pyrolyzates was C_{17} and with no significant peak area coverage from the C_3.

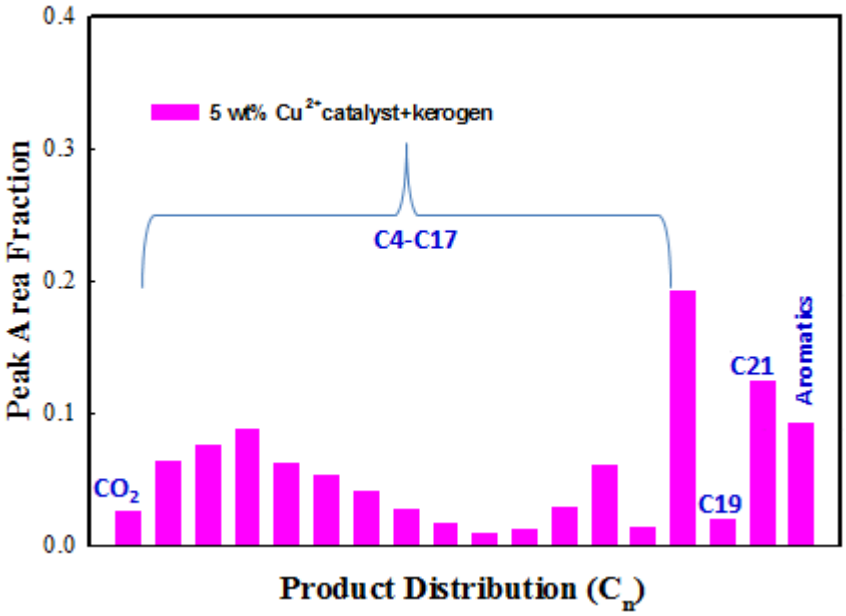

Figure 64 Fuel products from Cu^{2+} catalyst impregnated on Kerogen sample: Py-GC/MS 10 ^{o}C/min in Helium atmosphere

Furthermore, the fuel classifications of the catalyst and kerogen sample are compared in **Figure 65.** The fuel yield of the catalyst sample shows increases in peak area fraction for the Jet A and diesel pool and reduction in gasoline pool. The catalyzed-kerogen sample has similar fuel categories as the bitumen sample.

The mechanism of oil shale conversion to oil and gas has been proposed by Allred., (1966) as two series of reaction that leads to kerogen conversion to bitumen and bitumen further cracked to oil, gas and char. The result from the catalytic reaction is not far from current literature about kinetics of oil shale pyrolysis which has been proposed by several researchers [76]. The catalyst first shifted the product distribution towards bitumen and as such upgrading of the bitumen is required to obtained usable fuel products for commercial transport purpose.

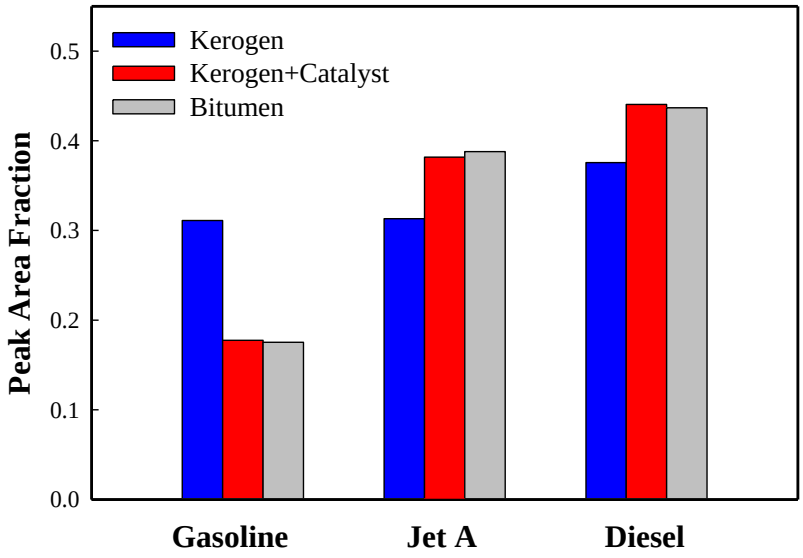

Figure 65 Compared fuel products **[(gasoline (C_4-C_{12}), jet A (C_8-C_{18}), diesel (C_8-C_{24})]** produced from the Cu^{2+} catalyst + kerogen sample: Py-GC/MS 20 ^{o}C/min in Helium atmosphere

4.7 Kinetic parameters

Kerogen is the solid organic material in the bitumen separated and decarbonated oil shale sample. The entire kinetic studies were done in a solid phase reaction. The mass transfer and gas diffusion were not excluded although smaller particle size of 10 um of kerogen sample were used as well as high gas velocity of 75 mL/min of Ar gas were applied in the TGA analysis. However, since TGA only measures the overall reaction data and not individual reaction scheme is difficult to know what specific reaction scheme activation energy is measured and as such E_a determined is apparent activation energy.

The pyrolysis of kerogen to produce fuel and char undergoes two reaction steps as proposed by Thakur and Nuttall (1987) [77].

$$kerogen \rightarrow bitumen + gas$$

$$bitumen \rightarrow oil + gas + char$$

Following the thermal decomposition of kerogen, each event during pyrolysis of kerogen is given as ***eqt.9***[77]

$$\frac{dX}{dt} \rightarrow K\,(1\text{-}X)^{n} \qquad \mathbf{9}$$

X is the extent of conversion, **t** is the final weight and **K** is the specific rate of constant and **n** is the order of reaction.

$\boldsymbol{X_t}$ is the weight loss at time t and $\boldsymbol{X_x}$ being the final weight

$$X = \frac{X_t}{X_x} \qquad \textbf{10}$$

The temperature dependence of the rate constant is seen in Arrhenius equation:

$$K = A\, e\frac{-E}{RT} \qquad \textbf{11}$$

Where A is the pre-exponent factor, E is the activation energy, T is the temperature and R is the Universal gas constant, to simplify the equation the order of the reaction is assumed as 1.

$$\beta = \frac{dT}{dt} \qquad \textbf{12}$$

A linear relationship between time and temperature is expressed as β

$$\frac{dX}{1-X} = \frac{A}{\beta}\, e^{\frac{-E}{RT}}\, dt \qquad \textbf{13}$$

inserting the above ***eqt.11*** and **12** into ***eqt. 13*** give the final form ***eqt. 17*** after rearrangement and differential method

This method is used to evaluate A and E at non isothermal conditions.

$$\int_0^x \frac{dX}{1-X} = \frac{A}{\beta}\int_{T_0}^{T} e^{\frac{-E}{RT}}\ \text{dt} \qquad \textbf{14}$$

Taking natural log of both sides

$$\ln\left(\frac{1}{1-X}\,\frac{dX}{dT}\right) = -\frac{E}{R}\frac{1}{T} + \ln\frac{A}{\beta} \qquad \textbf{15}$$

But, $\qquad \frac{dX}{dT} = \frac{X_{t2}-X_{t1}}{T_2-T_1} \qquad \textbf{16}$

A plot of ***y-axis*** against ***x-axis*** $(\frac{\mathbf{1}}{\boldsymbol{T}})$ and least square regression analysis is applied to get E_a and A

$$ln\left(\frac{1}{1-X}\left(\frac{X_{t2}-X_{t1}}{T_2-T_1}\right)\right) = -\frac{E}{R}\frac{1}{T} + ln\frac{A}{\beta} \qquad 17$$

In **Figure 66** the Arrhenius plot and regression analysis of the original oil shale were studied to determine the apparent kinetic parameters of the oil shale. The scattered data from the oil shale did not show a clear trend of straight line as known by Arrhenius plot. This has been reported by Syed et al.,(2011)[69] to be because of the unity order of reaction used [68]. Therefore an iterative approach is always desired to determine the order of reaction but in this case was not done but the regression analysis gave a correlation of 99.4% with an error estimate of 0.18. The regression plot gave a polynomial, from which the slope and the intercept were used to calculate the activation energies and pre-exponential factors within organic matters pyrolysis temperature range of 250-500 ^{o}C.

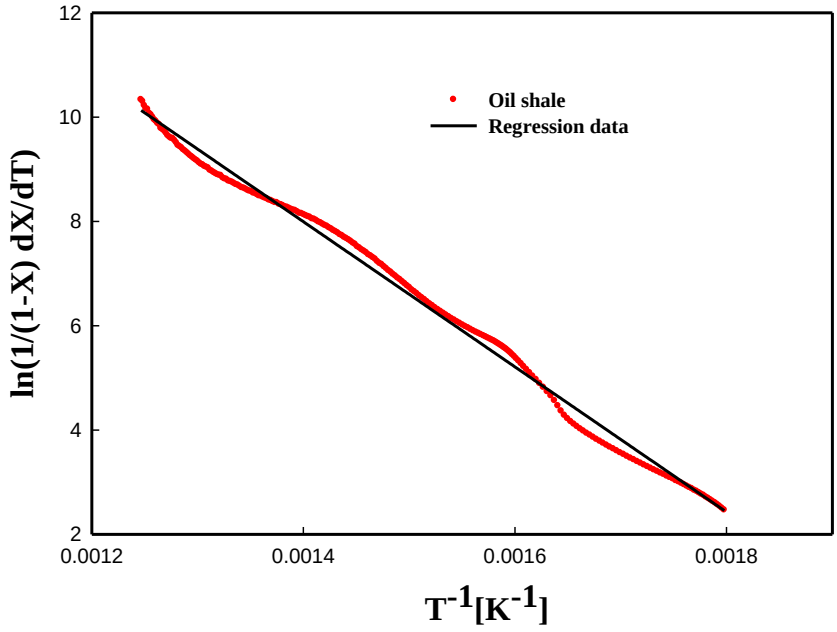

Figure 66 Arrhenius plot for original oil shale pyrolysis at 10^{o}C/min with its corresponding linear regression data plot: temperature range **(250 -500 ^{o}C)**

The trend of the Arrhenius plot clearly exhibit the difficulty of the original oil shale pyrolysis and several transition states could be identified. The apparent E_a and A of **115.7 kJ/mol** and **1.43e+28 sec^{-1}** were determined at **10 ^{o}C/min** heating rate. However, Reynolds and Burnham,(1994)[78] use Coats-Redfern analysis to determine discrete activation energy for Green River oil shale at which was found to be ca. **238.5 kJ/mol.**

The deviation in these two results looks very large although different models were applied but the concept of activation energy is expected to be similar. In this light, activation energy was determined at variable heating rate. For industrial application the decarbonated-kerogen sample conversion to fuel must occur at lower heating rate and as such the kerogen sample was tested in several heating rate and as seen in **Figure 67.** A two weight loss decomposition stages are observed in the TGA profile and all the heating rates shows a similar trend with linear trend towards char formation after 500 ^{o}C.

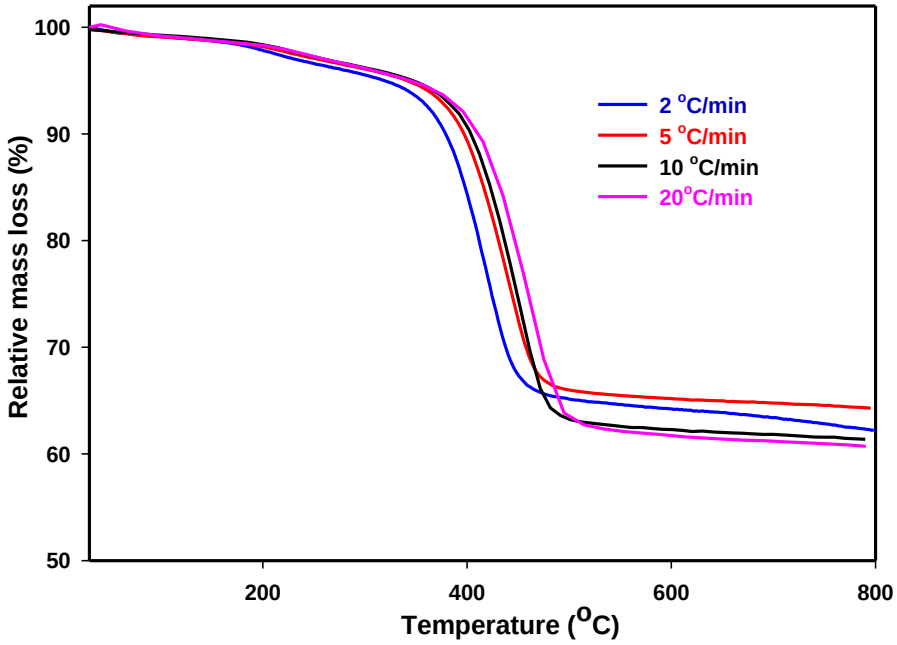

Figure 67 TGA for decarbonated-kerogen pyrolysis at different heating rates

A lower temperature shift was seen in lower heating but as heating rate is increased the residence time of kerogen to pyrolysis atmosphere is reduced and higher mass loss were observed. This indicates that the kerogen has less coke formation at higher heating rate as seen in the linear part of the profile after 500 ^{o}C. Although, the heterogeneity and complex natures of the kerogen structure makes its reaction scheme too difficult to model however knowing that several consecutively chain reactions steps might occur has made it a bit possible to understand the pyrolysis reactions of kerogen. In particular, it is obvious that the following reactions might occur: the decomposition of kerogen to heavy oil, light oil, hydrocarbon gas, hydrogen, carbon dioxide and char. Also, heavy oil may further undergoes

cracking into light oil, hydrocarbon gas, hydrogen and char as the light oil may also be cracked into hydrocarbon gas, hydrogen and char. The hydrocarbon gas may also be further cracked into hydrogen and char. All these reactions may have different product distribution and reaction mechanism. The aromatization of alicyclic compounds, dehydrogenation and combination of aromatics rings and coke formation are reactions that have higher activation energies. All these reactions were proposed by [79] in oil shale symposium, Colorado School of Mines, as possible oil shale pyrolysis reactions with higher apparent activation energies. In considering a group of several reactions occurring simultaneously in pyrolysis of kerogen, it is appropriate to model the reaction in the form of apparent activation energy.

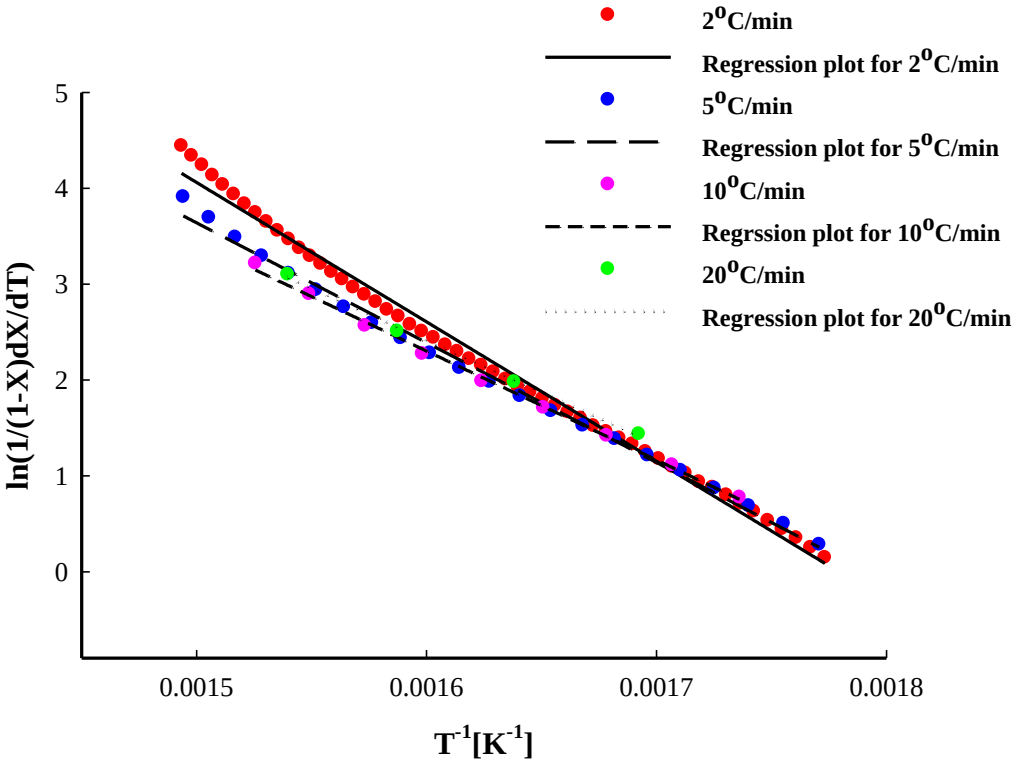

Figure 68 Arrhenius plot for decarbonated-kerogen pyrolysis at different heating rate with their corresponding linear regression plot: temperature range **250-380 °C/min**

The direct Arrhenius plot for the variable heating rates is seen in **Figure 68**. At 5, 10, 20 °C /min a clear and almost similar trend was observed

The activation energies obtained from TGA data are apparent activation energies because TGA gives the overall reaction kinetics from several reaction data rather than individual reactions. The influence and magnitudes of these individual reactions and their dominion occurrence might affect the apparent activation energy. Although the heating rates are different but the similitude of the Arrhenius plot support the concept of activation which is

only altered by the introduction of catalyst. However, since these heating rates are bit higher the reaction will also be faster and possible overlapping behaviors in the cracking reactions at these different heating rates might occur.

Table 11 Kinetic parameters (apparent E_a and A) for pyrolysis of kerogen at various heating rates using direct Arrhenius plot method: temperature range **(250- 380^{o}C)**

Heating rate (^{o}C/min)	**Events**	**Ea (kJ/mol)**	**A (s^{-1})**	**R^2 (%)**
2	Kerogen pyrolysis	121	3.6e+26	99.2
5	Kerogen pyrolysis	104	1.3e+23	99.5
10	Kerogen pyrolysis	95	1.5e+21	99.7
20	Kerogen pyrolysis	90	2.9e+20	99.6

Moreover, with critical look at **Table 11** and since a tested single regression plot fits well into the three heating rates (5, 10, 20 ^{o}C /min). The Arrhenius plot from the three data points looks similar and was not surprised a single regression plot also fits very well and upon which the kinetics parameters were determined based on their separate linear regression plot. The pre-exponential factor shows a slight difference since it's is a function of heating rate. The apparent E_a of the decarbonated kerogen of ca. **104, 95** and **90 kJ/mol** were calculated for **5, 10** and **20 ^{o}C/min** respectively. However, at **2 ^{o}C/min** a deviation in the E_a was observed but is not clear why such a difference was observed. The change in the E_a may be due to the fact that the determined activation energy at such low heating rates where several reactions occurs. At low heating rate, the kerogen is exposed to pyrolysis temperature for 6.6 hours in the range of 30-820^{o}C, slow reaction and coke formation was dominant. Also, observed was high coke formation for lower heating rate as has been postulated by[79] in oil shale symposium in Colorado School of Mines as a cause for higher apparent activation energy. Again the following reaction steps: dehydrogenation, rupture of heterocyclic compounds, combination of aromatic rings and coking reaction were all stated as causal agent for high apparent E_a. Looking at these reaction mechanisms it is clear to note why **2 ^{o}C/min** shows higher activation energy since slow reaction of kerogen led to coke formation and cracking of branched aliphatic chains. Aliphatic ring hydrocarbons are the major components from the pyrolyzates of the kerogen and the most precursors for oil and gas generations. The cleavage of C-C bond requires series of reactions and considering the structure and molecular

arrangement of the kerogen is not clear what kind of reactions are dominion.

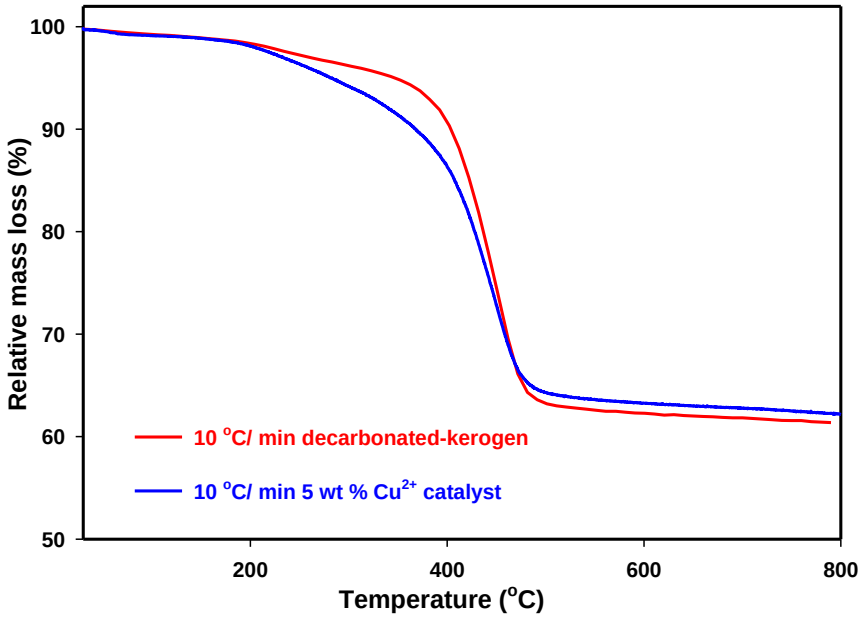

Figure 69 TGA for kerogen pyrolysis at same heating rates (10 °C/min) for Cu^{2+} catalyst and un-catalyst kerogen sample

Figure 69 is a compared TGA profile for catalyzed and un-catalyzed pyrolysis of kerogen. The catalyst reaction has a clear shift in lower temperature and the activation barrier is expected to be reduced. The final mass loss towards coke formation looks similar. Subsequently, the TGA data were used to determine the kinetic parameters for the decomposition reactions in different heating rate.

In **Figure 70** the direct Arrhenius plot is observed for the catalyzed, un-catalyzed and bitumen sample pyrolysis as well as their linear regression plot at 10 ^{o}C/min. It was very difficult to achieve a liner Arrhenius plot for the bitumen and catalyzed samples and as such a fixed temperature range of 290-350 ^{o}C were selected were a linear plot was achieved to determine the slope and the intercept for higher correlation and similitudes.

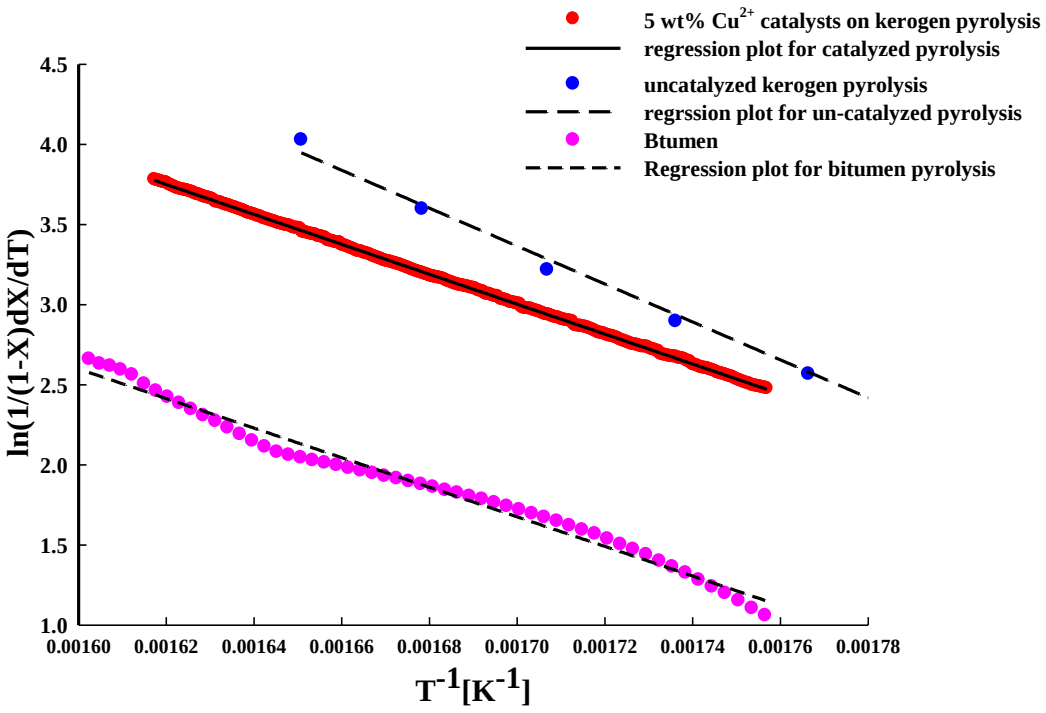

Figure 70 Arrhenius plot for catalytic-kerogen and bitumen pyrolysis at10 ^{o}C/min: temperature range **(290-350^{o}C)**

The apparent activation energies and pre-exponential factors were determined based on the slope and intercept from the linear regression. The bitumen recorded less activation energy and almost similar to the catalyzed reaction within the temperature range selected. In **Table 12** the calculated E_a and A is recorded. The bitumen and catalyzed-decarbonated-kerogen has E_a of **77** and **78 kJ/mol** respectively and shows similar outlook in both kinetic and fuel yield.

Table 12 Kinetic parameters (apparent E_a and A) for 5 wt % Cu^{2+} catalytic pyrolysis of kerogen at 10 ^oC/min using direct Arrhenius plot method: temperature range **(290-350^{o}C)**

Heating rate(10^{o}C/min)	Events	Ea (kJ/mol)	A (s^{-1})	R^2(%)
Cu^{2+}catalyst + kerogen	Kerogen pyrolysis	78	3.6e+19	99.9
Un-catalyzed kerogen	Kerogen pyrolysis	98	1.4e+24	98.9
Bitumen	Pyrolysis	77	1.1e+18	98.3

Djurcic, et al., proposed that the oil shale pyrolysis reaction with low activation E_a is due to split of weak chemical and closed ring bonds as well as C-O and C-S bonds. They further suggested that the cleavage of branched functional groups in kerogen long molecular structure have weaker bonds. This is because the release of H_2O, CO_2, H_2 and H_2S has low rupture energy. Also, medium activation energy may be due to the cleavage of β-site of aromatics and decomposition of large molecular weight normal alkane. The results from the **Table 12** suggest that within same temperature range the catalyst reduced the activation energy by ca. **20 kJ** for every mole of molecule formed. The pre-exponential factor, which is a function of temperature and rate constant, determines how often the molecules are collided and formed. Moreover, with assumption of first order of the reaction the A is considered as the frequency factor and the catalyzed reaction has exponential magnitude of A of **3.6e+19** while the un-catalyzed pyrolysis has power of **1.4e+24**. The bitumen collision is faster as in every second **1.1e+18** molecules collide but their orientation is not studied in this case. This means that the molecular collision and formation is faster in catalyzed reaction than un-catalyzed. The determined E_a and A for the catalyzed reaction may be due to the decomposition of large molecular weight normal aliphatic pyrolyzates. The product distribution from the pyrograms for the catalyzed reaction has the maximum C_{21} while that of un-catalyzed reaction has maximum C_{35}. The reductions in carbon number as the results of catalyst suggest that the dominion reaction step is the decomposition of large molecular weight aliphatic hydrocarbons and rearrangement of molecules. Finally, it was also observed that the bitumen and catalyzed pyrolysis product distribution has similar outlook and was not surprised that within the temperature range selected similar kinetic parameters were observed with much correlation and similitude within acceptable error margin.

In Table 13 the standard error of estimates for the kinetic parameters is tabulated. The root mean square error for the various heating rates and samples shows negligible error margin 0.5% to 11%. The catalyst sample has almost 100% precision.

Table 13 Results of standard error of estimate for the kinetic method

	Kerogen-pyrolysis				Catalyst	bitumen	Un-catalyzed pyrolysis
Heating rate ^{o}C/min	**2**	**5**	**10**	**20**	**10**	**10**	**10**
Standard Error of estimate	0.11	0.08	0.04	0.04	0.005	0.055	0.066

The determined kinetic parameters can be used to simulate the weight loss profile for the decarbonated and catalytically upgraded kerogen. Also, the rate of reaction and rate constant could all be determined based on the E_a and A values from the direct Arrhenius method derivation. These parameters if well investigated thoroughly would guide the design and operations of pyrolysis reactors for kerogen studies.

4.8 Design of fixed bed reactor

The thermal conversion of kerogen in Py-GC/MS should be compared with the fixed bed reactor for easily up scaling and pilot studies. This will be of much importance in modeling industrial ex-situ and in-situ pyrolysis of kerogen. The reactor configurations for ex-situ catalytic process still needs much research since smaller particle size reactors are still not in operation. The fixed bed reactor has been designed and installed but was not tested due to time constraints. In this method specific temperature and time of reaction could be tested as well as the proposed catalyst. The fixed bed could also monitor the gaseous product (C_1-C_3) during decomposition. Although the kerogen is found to be oil prone but quality and quantity of the gaseous product will be much needed. The proposed reactor scheme is found in **Figure 68** with some suggested operation conditions. The reactor is connected with GC-FID for analyzing the gaseous product results. The gaseous product especially methane was not identified from the Py-GC/MS and as such the fixed bed reactor is expected to measure it. The liquid product will be liquefied and analyzed in Py-GC/MS. The bed will contain a catalyst and kerogen either impregnated or deposited on the isolated kerogen.

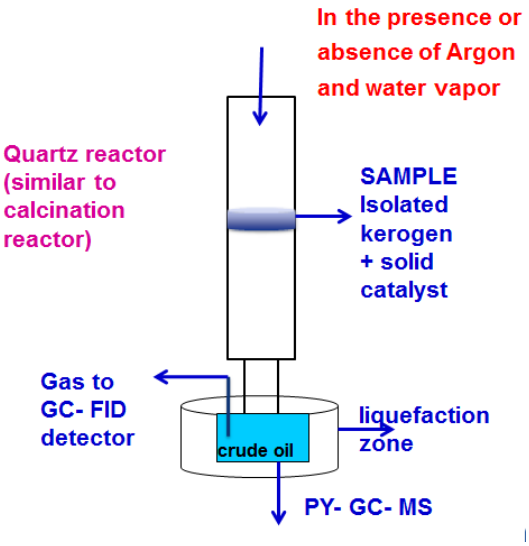

Figure 71 Proposed reactor scheme for fixed bed reactor for catalytic pyrolysis of kerogen

5. Conclusions

In this study, extensive characterizations and experiments of oil shale from Green River Formation was carried out. On the basis of the qualitative and/or quantitative analyses, a better understanding on the physico-chemical properties of the oil shale has been obtained. Some of the main findings are summarized as follows.

(i) The raw oil shale from Green River Formation mainly consists of dolomite, calcite, analcime, Fe-doped SiO_2, bitumen and kerogen. The total organic carbon (TOC) value of oil shale is 24.6 wt%. The type of kerogen is type I, which is oil prone and shows excellent maturity with a thermally upgraded fuel yield of ca. 85%.

(ii) The extraction experiments of bitumen using DCM (CH_2Cl_2) as extractant in the Soxhlet extractor show good reproducibility, and the content of bitumen is determined to be ca. 3.67%. The present HCl treatment conditions almost guarantee the removal of carbonates. The decarbonated kerogen shows a shift to lower temperature than the extracted oil shale, owing to the more exposed accessible kerogen surfaces of the former sample and has a content of 27.56%.

(iii) Bitumen shows aliphatic nature, and has wide temperature range in the TGA profile, which overlapped with kerogen. Separation of bitumen and removal of carbonate enhanced the exposed kerogen surface area as well as preventing the interference of inorganic carbon from calcite and dolomite, and organic carbon from bitumen.

(iv) The pyrolysis products of bitumen and kerogen mainly consist of linear hydrocarbons (C_3-C_{35}) indicating that this type of oil shale is a promising precursor for the production of fuel. Furthermore, the thermal upgrading of bitumen and decarbonated-kerogen gave a fuel yield of ca. 96% and 79% respectively.

(v) Various catalysts such as mineral acids, metal oxides and metal chlorides were tested for the kerogen conversion. Among the chlorides, $CuCl_2 \circ 2H_2O$ was the most active, acids and metal oxide had no obvious promotional effects. The optimized loading of $CuCl_2 \circ H_2O$ was 5 wt% and showed a low temperature shift of 30^oC.

(vi) Fuel produced by 5 wt % $CuCl_2 \circ H_2O$ catalytic reaction shifts towards the diesel yield and is slightly higher than the bitumen yield.

(vii) The apparent activation energies and pre-exponential factors for catalyzed and un-catalyzed reaction of kerogen were determined to be ca.**78 kJ/mol**; 3.6e+19sec^{-1} and **98**

kJ/mol; 1.4e+24sec^{-1} respectively within a kerogen pyrolysis temperature range of 290-350 ^{o}C.

6. Perspectives

In future studies, fixed-bed reactor in the absence or presence of catalysts could be used to study the gaseous products in the decomposition of kerogen. The liquefied product could be analyzed in the Py-GC/MS. The reactor together with the TGA-MS could be used to study the kinetics and catalysis of kerogen conversion. The reactor has been installed and the pyrolysis of kerogen in different residence times such as 24 hours, 2 week and 1 month etc. could be investigated.

Catalytic hydro-conversion of kerogen in high-pressure reactor could also be studied and the focus should be on quantitative analyzes of products. This would guide the fundamental understanding of kerogen depolymerization in hydrothermal systems.

Also, several 3D transitional metal chlorides have been bought and were not tested but could be done in future catalyst testing. The following catalyst is still yet to be tested $ZnCl_2$, $CoCl_2$ $NiCl_2$ and $SnCl_2$.

Finally, homogeneous catalyst for kerogen conversion could also be tested that may unlock the difficulty in regeneration of the proposed catalyst in this thesis. Since catalyst is not consumed in the reactions their regeneration is of key importance but with the current design is still not clear how to achieve that goal.

References

1. *BP Statistical Review of World* Energy *June 2014*. March 12, 2015; Available from: http://www.bp.com/content/dam/bp/pdf/Energy-economics/statistical-review-2014/BP-statistical-review-of-world-energy-2014-full-report.pdf.
2. *OPEC share of world crude oil*. 2013; Available from: http://www.opec.org/opec_web/en/data_graphs/330.htm.
3. Sun, Y., Bai, Fengtian., Liu, Baochang., Liu, Yumin., Guo, Mingyi., Guo, Wei., Wang, Qiuwen., Lü, Xiaoshu., Yang, Fang.,Yang, Yang.,, *Characterization of the oil shale products derived via topochemical reaction method.* Fuel, 2014. **115**(0): p. 338-346.
4. *Retorting Enefit280*. 2015 [cited 2015 16.04.2015]; Available from: https://www.enefit.com/retorting-enefit280.
5. *BP energy outlook 2030*. 2014; Available from: http://www.bp.com/fr_ch/switzerland/medias/communiques-aux-medias/pm-energy-outlook-2030-2013.html.
6. *Alternative Transport Fuels*. 2014; Available from: http://www.world-petroleum.org/index.php?/Technology/alternative-transport-fuels-courtesy-of-aip.html.
7. James T. Bartis, T.L., Lloyd Dixon, D. J. Peterson, Gary Cecchine, *Oil Shale Development in the United States.*
8. *crude oil and commodity price*. [cited 2015 4/16/2015]; Available from: http://www.oil-price.net.
9. Suleimenova, A., et al., *Acid demineralization with critical point drying: A method for kerogen isolation that preserves microstructure.* Fuel, (0).
10. Tissot, D.H.W.B.T., *Petroleum formation and occurrence*. 1984, Berlin Heiddberg New York Tokyo: Springer-Verlag.
11. Speight, J.G., *Chapter 3 - Kerogen*, in *Shale Oil Production Processes*, J.G. Speight, Editor. 2012, Gulf Professional Publishing: Boston. p. 75-92.
12. Vandenbroucke, M. and C. Largeau, *Kerogen origin, evolution and structure.* Organic Geochemistry, 2007. **38**(5): p. 719-833.
13. Durand, B., Espitalie', J, *Evolution de la matie're organique au cours de l'enfouissement des sediments.* compte rendus de l'Academie des Sciences (Paris), 1973.
14. You-Hong Sun, F.-T.B., Xiao-Shu Lü, Qiang Li, Yu-Min Liu, Ming-Yi Guo, Wei Guo & Bao-Chang Liu, *A Novel Energy-Efficient Pyrolysis Process: Self-pyrolysis of Oil Shale Triggered by Topochemical Heat in a Horizontal Fixed Bed*. 2015, Scientific Report.
15. James T. Bartis, T.L., Lloyd Dixon, D.J. Peterson, Gary Cecchine, *Oil Shale Development in the United States* P.a.P. Issues, Editor. 2005.
16. Dell, R.M.M., Patrick T. Rand, David A. J., *Chapter 3 - Unconventional Fuels*, in *Towards Sustainable Road Transport*, R.M.M. Dell, Patrick T. Rand, David A. J., Editor. 2014, Academic Press: Boston. p. 86-108.
17. Energy, D.o., *Strategic Significance of America's Oil Shale Reserve.* 2004.
18. *Oil and gas geology*. 2014; Available from: http://oilandgasgeology.com 16/11/2014.
19. Mclver, R.D., *Composition of kerogen. Clue to its role in the origin of petroleum.* seventh world petroleum congress proceedings, 1967. **vol.2**.
20. Williams, P.F.V., *Oil shales and their analysis.* Fuel, 1983. **62**: p. 756-760.
21. ; Available from: http://www.eia.gov/analysis/studies/worldshalegas/ 16/11/2014.

22. Guo, H., et al., *Effect of minerals on the self-heating retorting of oil shale: Self-heating effect and shale-oil production.* Fuel, 2014. **118**(0): p. 186-193.
23. *Oil shale* 2015 [cited 2015 21-03-2015]; Available from: https://www.enefit.com/en/usa.
24. *Oil Shale* 2015; Available from: https://www.enefit.com/oil-shale.
25. Durand, B., *kerogen insoluble organic matter from sedimentary rocks*. Editions Technip paris ed. 1980: Technip paris.
26. *Oil Shale Reource in USA*. 2015 [cited 2015 03/20/2015]; Available from: http://instituteforenergyresearch.org/topics/encyclopedia/oil-shale/.
27. James T. Bartis, T.L., Lloyd Dixon, D. J. Peterson, Gary Cecchine, *Oil Shale Development in the United States*.
28. Allix-Total, P. *What is Total doing on oil shle* 2008 [cited 2015 29/04/2015]; Available from: http://www.ceri-mines.org/documents/28thsymposium/presentations08/PRES_2-3_Allix_Pierre.pdf.
29. *Oil Shale*. 16-11-2014; Available from: http://instituteforenergyresearch.org/topics/encyclopedia/oil-shale/ 16-11-2014.
30. *Chevron and Los Alamos Jointly Research Oil Shale Hydrocarbon Recovery*. [cited 2015 20-03-2015]; Available from: http://www.greencarcongress.com/2006/09/chevron_and_los.html.
31. Brown, S.D., Sirkecioglu, O., Snape, C.E., Eglinton, T.I.,, *Speciation of the organic sulphur forms in a recent sediment and type I and II-S kerogens by high pressure temperature programmed reduction.* Energy & Fuels . 1997. **11**.
32. Peters, K.E., Walters, C.C., Moldowan, J.M.,, *The Biomaker guilde,*. cambrigde university press, 2004. second edition.
33. Huc, A.Y., *Origin and formation of organic matter i recent sediments and its relation to kerogen.* Durand, B. Edition Technips, Paris 1980.
34. Henrich, S.M., *Early diagenesis of organic matter.* organic Geochemistry,, 1993(Plenum press, New York).
35. Deming, J.W., Baross, J.A.,, *Early diagenesis of organic matter: bacterial activity* Organic Geochemistry, 1993(Plenum Press, New York).
36. Tyson, R.V., *Sedimentary organic matter.* Organic Facies and Palynofacies, 1995(Chapman and Hall, London).
37. Mayer, L.M., *Organic matter at sediment wat interface.* Organic Geochemistry, 1993. Plenum Press, New York.
38. Van Krevelen, D.W., *Coal: Topology*-. Chemistry and physis -constitution 1993. 3edition, elsevier, the Netherlands.
39. Tissot, B., Durand, B., Espitalie, J., Comba, A.,, *Influence of nature and diagenesis of organic matter in formation of petroleum.* American Association of Petroleum Geologists 1974. Bulletin 58.
40. Down, A.G., Himus, G.W.,, *A preliminary study of the chemical constitution of kerogen.* journal of the institute of petroleum 27, 1941.
41. Van Krevelen, D.W., *Coal: Topology.* chemistry and physis -constitution, 1961.
42. Kevin McCarthy, K.R., Martin Niemann, Daniel Palmwski, Kenneth Peters, Arthur Stankiewicz, *Basic Petroleum Geochemistry for souce Rock evaluation*. summer 2011.
43. *Total organic carbon*. Available from: http://spec2000.net/11-vshtoc.htm 16/11/2014.
44. Anita M. Orendt, I.S.O.P., Shyam R. Badu, Mark S. Solum, Ronald J. Pugmire, and Julio C. Facelli, *Three-Dimensional Structure of the Siskin Green River Oil Shale Kerogen Model: A Comparison between Calculated and Observed Properties.* Energy & Fuels . 2013(27): p. 702-710.

45. Bushnev, D.A. and N.S. Burdel'naya, *Kerogen: chemical structure and formation conditions.* Russian Geology and Geophysics, 2009. **50**(7): p. 638-643.
46. Ishiwatari, M., et al., *Thermal decomposition behavior of oil shale kerogens observed by stepwise pyrolysis—gas chromatography.* Journal of Analytical and Applied Pyrolysis, 1993. **24**(3): p. 273-290.
47. SISKIN M., a.K.A.R., *Reactivity of Organic Compounds in Hot Water: Geochemical and Technological Implications.* Science, 1991. **vol.254**: p. 231-237.
48. Snape, C.E., Lafferty, C.J., Eglinton, G., Robinson, N., Collier,R.,, *The potential of hydropyrolysis as a route for coal liquefaction.* International Journal of Energy Research 18, 1994.
49. Joll, C.A., Couton, D., Heitz, A., Kagi, R.I., , *Comparison of reagents for off-line thermochemolysis of natural organic matter.* Organic Geochemistry 35,, 2004.
50. Schaeffer-Reiss, C., Schaeffer, P., Putschew, A., Maxwell, J.R.,, *Stepwise chemical degradation of immature S-rich kerogens from Vena del Gesso (Italy).* Organic Geochemistry., 1998. **29**.
51. Ho¨ld, I.M., Brussee, N.J., Schouten, S., Sinnighe Damste , J.S.,, *Changes in the molecular structure of a type IIS kerogen (Monterey Formation, USA) during sequential chemical degradation.* Organic Geochemistry., 1998. **29**.
52. al, H.J.e., *Influence of pyrolysis condition and transition metal salt on the product yield and characterization via Huadian oil shale pyrolysis.* Journal of Analytical and Applied Pyrolysis, 2015: p. 6.
53. Robinson, W.E., *Kerogen of Gree River Formation.* Organic Geochemistry, 1969. Springer-Verlag, Berlin, Germany.
54. McCollum, J.D., Wolff, W.F.,, *chemical beneficiation of shale kerogen.* Energy fuels 1990.
55. anderson, Y.C., Gardner, P.M., Whitehead, E.V., Anders, D.E., Robinson, W.E.,, *The isolation of steranes from Green River oil shale.* geochemical et Cosmochemica Acta 33, 1969.
56. Anders, D.E., Doolittle, F.C., Robinson, W.E.,, *Polar constituents isolated from Green River oil shale.* geochemical et Cosmochemica Acta 39, 1975.
57. Anders, D.E., Robinson, W.E.,, *Cycloalkanes constituents of the bitumens from Green River oil shale.* geochemical et Cosmochemica Acta 35, 1971.
58. Saxby, J.D., *Technique for the isolation of kerogen from sulflde ores.* Geochimica et Cosmochimica Acta, 1970. **34**(12): p. 1317-1326.
59. *Rock-Eval Parameters*. 2015 [cited 2015 22.03.2015]; Available from: http://www.dcnr.state.pa.us/topogeo/econresource/oilandgas/marcellus/sourcerock_index/sourcerock_quantity/sourcerock_rockeval/index.htm.
60. *X-ray Diffractometer and X-ray Flaw Detector*. Available from: http://www.angstrom-advanced.com/index.asp?page=IntroXRD.
61. *Scanning Electron Microscopy (SEM)*. Available from: http://serc.carleton.edu/research_education/geochemsheets/techniques/SEM.html 17/11/2014.
62. *ATR-FTIR procedure*. Available from: http://www.kirj.ee/public/oilshale_pdf/2012/issue_4/Oil-2012-4-344-356.pdf 17/11/2014.
63. *TGA Instrumentation*. [cited 2015 22.03.2015]; Available from: http://www.slideshare.net/nimmidalwadi5/tga.
64. *Multi-Functional Pyrolysis System*. 2015 [cited 2015 22-03-2015]; Available from: http://www.frontier-lab.com/product/.

65. Zhang, Z., et al., *Flash pyrolysis of kerogens from algal rich oil shales from the Eocene Huadian Formation, NE China.* Organic Geochemistry, 2014. **76**(0): p. 167-172.
66. Robert J. Klingler, R.E.W., Darren R. Locke, Marcus O. Wigand, Mark D. Looney, , *Preparation and use of nano-catalysts for in-situ reaction with kerogen*. 2011: USA. p. 1-12.
67. Forsman, J.P. and J.M. Hunt, *Insoluble organic matter (kerogen) in sedimentary rocks.* Geochimica et Cosmochimica Acta, 1958. **15**(3): p. 170-182.
68. H. Ganz, W.K., *Application of infrared spectroscopy to the calssification of kerogen types and evaluation of source rock and oil shale potentials.* Fuel, 1986. **66**: p. 708-7010.
69. Syed, S., et al., *Kinetics of pyrolysis and combustion of oil shale sample from thermogravimetric data.* Fuel, 2011. **90**(4): p. 1631-1637.
70. Sun, Y., et al., *Characterization of the oil shale products derived via topochemical reaction method.* Fuel, 2014. **115**(0): p. 338-346.
71. T. T. Coburn. , R.E.B., J. E. Clarkson. , J. H. Campbell.,, *Correlation of shale oil 1-alkene/n-alkane ratios with process yield.* Analytical Chemistry, 1978. **50**: p. 958-962.
72. Larter, S.R., Solli, H., Douglas, A. G., de Lange, F., de Leeuw, J. W., , *Occurence and significance of Prist-1-ene in kerogen pyrolyzates.* Nature, 1979. **279**: p. 405-408.
73. Hold, I.M., Schuten, S., Van der Gaast, S.J., Sinninghe Damste, J.S.,, *Origin of prist-1-ene and prist-2-ene in kerogen pyrolysates.* Chemical Geology, 2001. **172**: p. 201-212.
74. HARRY DEMBICKI. JR., B.H., THOMAS T. Y. HO;, *Source Rock Evaluation by Pyrolysis-Gas Chromatography.* American Association of Peteroleum Geologist Bulletin, 1983. **67**: p. 1094-1101.
75. *Decomposition of Sulfuric Acid to Produce Sulfur Dioxide and Oxygen in Is Cycle*. [cited 2015 2015.05.15]; Available from: https://aiche.confex.com/aiche/2006/techprogram/P62286.HTM.
76. Wolfgang Brockner., C.E., Mimoza Gjikaj.,;, *Thermal decomposition of nickel nitrate hexahydrate, Ni(NO3)2·6H2O, in comparison to Co(NO3)2·6H2O and Ca(NO3)2·4H2O.* Thermochimica Acta 2007. **456** p. 64-68.
77. Deepak S. Thakur., H.E.N.J., *Kinetics of pyrolysis of Moroccan oil shale by thermogravimetry.* Ind Eng Chem Res 1987. **26**(7): p. 1351-6.
78. Reynolds, C.o.K.A.o.S.R.a.K.C.b.B.a., *Comparison of Kinetic Analysis of Source Rocks and Kerogen Concentrates.* Organic geochemistry, 1994. **23**(1): p. 11-19.
79. Ein, O.S.A.-A.a.S.Q.A., *Variable Activation Energy to model oil shale pyrolysis kinetics,* in *oil shale symposium* 1971: Colorado school of mines.

Appendix

A) XRD pattern for oil shale

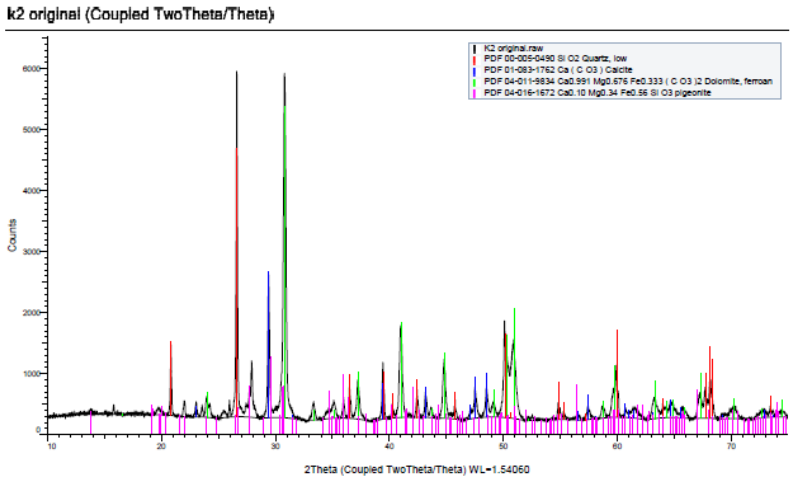

B) XRD pattern for HCl treated sample

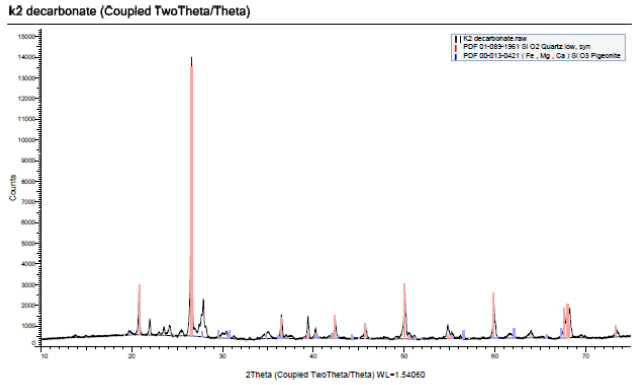

C) Calculation of HCl concentration used in decarbonate experiment

From molarity;

$$C_f V_f = \frac{\%\text{purity} * \rho_{HCl} * V_i}{Mw_{HCl}}$$

$$C_f = \text{final concertration} = 6M$$

$$\mathrm{Mw_{HCl}} = \text{molecular weight } = 36\ \mathrm{g/mol}$$

$$\rho_{\mathrm{HCl}} = \text{density of HCl} = 1.19\mathrm{g/cm\hat{}3}$$

$$\mathrm{V_f} = \text{final volume } = 100\mathrm{ml}$$

$$\%\text{purity} = 37\%$$

$$\mathrm{V_i} = \text{initial volume} = ?$$

D) Calculation of catalyst loading

Water adsorption volume is determined by dissolving a known oil shale mass in in distilled water until all becomes wet and the volume is used to dissolve the metal salts and catalyst precursors.

$$\boldsymbol{Mass\ of\ metal\ ion}\ (\boldsymbol{M}) = \frac{\%\ \text{loading (X)} * \text{mass of oil shale sample}}{(1 - \mathrm{X})}$$

$$\text{Mass of metal salt/ precursor (W)} = \frac{\text{Molecular wieght of metal salt} * \text{Mass of metal ion}}{\text{Molecular weight of metal ion}}$$